Henrik H. Øvrebø

Lifting sustainable food science from lab to industry: An experimental study and development of a Soluble Gas Stabilisation (SGS) flow concept using low-cost off-the-shelf components

Master's thesis in Mechanical Engineering
Supervisor: Anna Olsen
Co-supervisor: Martin Steinert and Sara Esmaeilian
September 2023

Master's thesis

NTNU
Norwegian University of
Science and Technology

TROLL LABS

Henrik H. Øvrebø

Lifting sustainable food science from lab to industry: An experimental study and development of a Soluble Gas Stabilisation (SGS) flow concept using low-cost off-the-shelf components

Master's thesis in Mechanical Engineering
Supervisor: Anna Olsen
Co-supervisor: Martin Steinert and Sara Esmaeilian
September 2023

Norwegian University of Science and Technology
Faculty of Engineering
Department of Mechanical and Industrial Engineering

NTNU
Norwegian University of
Science and Technology

Abstract

Sustainability issues are important for design stakeholders. Food safety is crucial for human health and a significant contributor to climate change. Food waste and packaging usage are problems in today's food industry. A potential technology to reduce food waste and use less packaging material is the implementation of Soluble Gas Stabilisation (SGS). SGS is a development of Modified Atmosphere Packaging (MAP) seen in stores today, where bacteriostatic CO_2 is dissolved into a food product to increase shelf life. Lab-scale, early-phase research has been done to verify the microbiological effectiveness of SGS. However, the research is limited to the biological aspect and does not explore the real-world implications and optimization this technology has the potential to become. E.g, MAP achieves bacteriostatic properties after a few days, and lab-scale SGS achieves this after a few hours, while no research has tried to use as little time as possible, e.g. 5 minutes at high pressures. Therefore, in this thesis, an experimental early-phase prototype SGS flow chamber has been developed, prototyped and tested. The work done in this thesis is the start of two publications going to be submitted to Design 2024 and the Journal of Food Engineering. The experiment conducted in this thesis is a comparison experiment with existing static SGS research. The results suggest some more development is needed before proper amounts of data are able to be collected. The thesis concludes that the flow chamber design may help researchers develop and optimize a way for the SGS technology to be widely adopted in the food processing industry.

Sammendrag

Bærekraftsspørsmål er viktige for designinteressenter. Mattrygghet er avgjørende for menneskers helse og en betydelig bidragsyter til klimaendringer. Matsvinn og emballasjebruk er problemer i dagens matindustri. En potensiell teknologi for å redusere matsvinn og bruke mindre emballasjemateriale er implementeringen av Soluble Gas Stabilization (SGS). SGS er en utvikling av Modified Atmosphere Packaging (MAP) som er i butikker i dag. Her løses bakteriostatisk CO_2 opp i et matprodukt for å øke holdbarheten. Tidlig-fase forskning i labratorier i har blitt gjort for å verifisere den mikrobiologiske effektiviteten til SGS. Forskningen er imidlertid begrenset til det biologiske aspektet og utforsker ikke de virkelige implikasjonene og optimaliseringen denne teknologien har potensial til å bli. For eksempel oppnår MAP bakteriostatiske egenskaper etter noen dager, og laboratorieskala SGS oppnår dette etter noen timer, mens ingen forskning har forsøkt å bruke så lite tid som mulig, f.eks. 5 minutter ved høyt trykk. Derfor, i denne oppgaven, har en eksperimentell tidligfase prototype strømningskammer for SGS blitt utviklet, prototypet og testet. Arbeidet i denne oppgaven er starten på to publikasjoner som skal sendes til Design 2024 og Journal of Food Engineering. Testresultatene i denne oppgaven er et sammenligningseksperiment med eksisterende statisk SGS behandling. Noe mer utvikling er nødvendig og Strømningskammerdesignet kan hjelpe forskere med å utvikle og optimalisere en måte for at SGS-teknologien blir tatt i bruk i næringsmiddelindustrien.

Table of Contents

List of Figures

List of Tables

1 Introduction

This chapter outlines the problem statement derived from existing research and the subsequent objectives and the approach to achieving this, while the chapter ends with an overview of the thesis structure.

1.1 Problem statement

In recent years, sustainability in all areas of society has become a very prevalent issue (Giovannoni and Fabietti 2013; Ruggerio 2021). Many urge a reduction of consumption of, e.g. energy, travel and consumption to reach the UN sustainability goals (Olabi et al. 2023; Reisch et al. 2013). Food is a topic of significant attention because it is crucial for human survival while contributing significantly to climate change and ecological degradation (Wieben 2017; Willett et al. 2019). By the year 2050, the global population is projected to approach 9.7 billion people, while the demand for food worldwide is anticipated to increase by as much as 60% (Nations 2017).

According to the Food and Agriculture Organization of the United Nations (FAO), roughly a third or 1.3 billion tons of food produced for human consumption worldwide is either wasted or lost (Wieben 2017). Technologies specifically targeting the causes of domestic food waste have yet to be adequately explored in research, together with the role of different packaging (Brennan et al. 2021).

Therefore, there is potential for increasing sustainability by reducing the amount of waste and packaging usage in the global food system through the use of better food processing. We face the dual challenge of feeding a growing population while wealthy countries throw out an alarming amount of food (Poyatos-Racionero et al. 2018; Stenmarck et al. 2016; Wieben 2017).

Food processing transforms raw agricultural products into safe, nutritious, and marketable food products (Knorr et al. 2020). These products are also known as higher-value food products (Wang 2014). In 2013, the food processing industry in the European Union was responsible for 28% of the entire food sector's energy utilisation, while the food sector as a whole contributed to 17% of the total energy consumption (Atuonwu and Tassou 2021; Monforti et al. 2015). In this context, developing and adopting sustainable food processing equipment is one solution to address these challenges and promote a more sustainable and responsible food industry. A strategy to develop this technology involves elevating current food science from a low technology readiness level (TRL) to a more advanced stage. This transition hinges on turning scientific discoveries into practical, adaptable technologies. Amplifying the potential of such technologies requires inventive design coupled with the creation of technical scale prototypes, setting the stage for rigorous validation (Ebert and Aganovic 2022).

An area where technology can contribute to minimising wasted food while people do not change their behaviour is to increase the shelf life of produced food (Brennan et al. 2021). Seafood is a nutrient-rich product with a relatively short shelf life (Olatunde and Benjakul 2018). Soluble gas stabilisation (SGS) is a technology that can increase the shelf life of such a product, reducing waste and using less packaging material (A. N. Jakobsen et al. 2022). SGS dissolves CO_2 into the product to decrease bacterial activity and keep the food fresh longer by putting the salmon in a high-pressure CO_2 atmosphere (M. Sivertsvik and Birkeland 2006). A fillet of salmon uses 2.6 kg CO_2 equivalents per kg product (Ellingsen et al. 2009). SGS is a technology that can increase all types of meat's sustainability (Al-Nehlawi et al. 2013; Morten Sivertsvik and J. S. Jensen 2005). The word meat implies all types of eatable animal tissue (Boler and Woerner 2017). Specifically, this thesis will investigate salmon fillets.
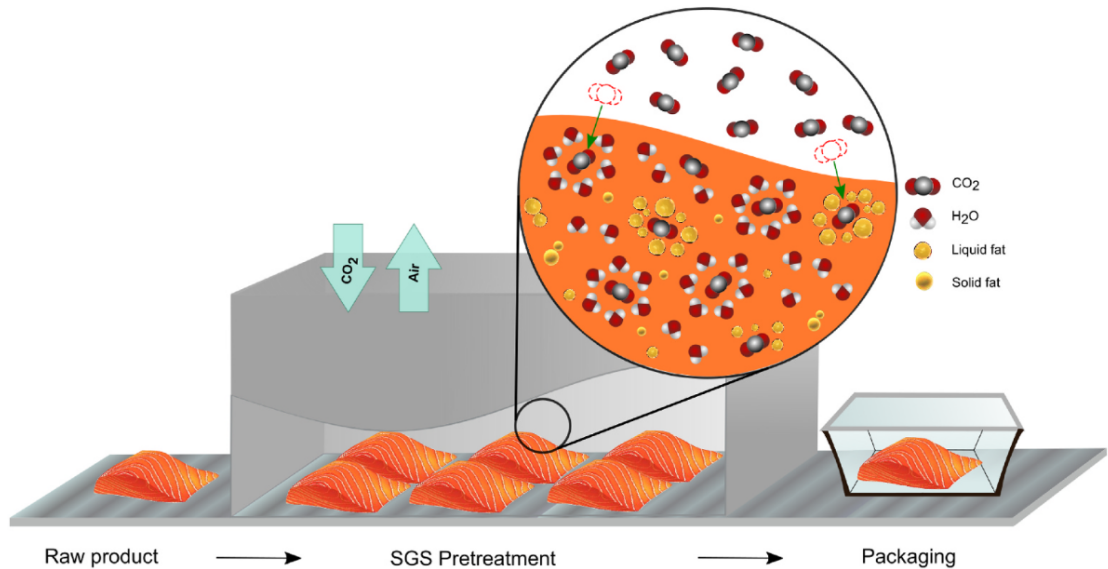
Figure 1: Overview of the SGS technology (Esmaeilian et al. 2021)

1.2 Research question

SGS is a technology that is very much in a research state, and little investigation has gone into researching and developing the full-scale industrial implementation of this technology (Esmaeilian et al. 2021). Therefore, the research question is, "How can one make an SGS design, and use this data to make simulation models, to be adopted by the industry?". This thesis tackles the first part of the research question.

1.3 Objectives

In order to investigate, research and improve SGS design, the following objectives were set:

- Analyse the existing experiment design and research done.

- Finalise the static chamber experiment setup by making the chamber air-tight

- Modify and finalise the design of the flow test chamber for SGS.

- Develop electronics able to measure flow and diffusion data.

- Establish a FEM model of the chamber.

- Establish experimental test methods to validate CO_2 dissolution.

- Propose future research on the topic

This thesis explores the concept of CO_2 flow in SGS to decrease the time required for sufficient CO_2 dissolution in the salmon fillet to gain the benefits of increased shelf life while also being practical to adopt in the industry.

1.4 Approach

This thesis uses a multidisciplinary approach due to the cross-linked complexity of the problem. The baseline of the research is a solid foundation in food science. In order to design and develop

such a design, an understanding of the principles of the technology and the products being used is essential in order to understand the boundary conditions between food science and industry.

To translate these scientific principles into concrete design, an understanding and experience in mechanical engineering is needed. This domain ensures that the theoretical constructs are translated into real-world applications. Activities such as the design of the flow test chamber, the development of electronics for data acquisition, and the formulation of a FEM model of the chamber are encompassed in this discipline, working with the practical viability of the solutions. Also, by understanding the principles of processing equipment, the experiments become better.

Since there are also limited previous designs and theories on the subject, an iterative process of refining a solution suited for industry adoption is needed. These product development strategies of working fast and making the right decision at the right time are essential throughout the work done in this thesis, which is similar to previous product development work done on low-cost, open-source equipment design applied to research (Øvrebø et al. 2023).

Working interdisciplinary, bridging food science with engineering principles, positions the findings as theoretically robust and practically implementable, ensuring relevance and applicability in the broader food industry context.

1.5 Thesis structure

The thesis follows an IMRAD structure.

The first chapter presents the problem statement and objectives, while the background theory for why the SGS concept is investigated in this thesis and what future work can be conducted with the solutions presented in this thesis is established in the second chapter.

The third chapter presents an in-depth description of how the concept was prototyped and developed. This chapter encompasses all the prototypes, iterations, and insights gained throughout the development process.

In Chapter Four, the preparations and method for the experiments conducted and their equipment are presented together with how post-experiment analysis was done. Chapter Five presents the final flow chamber, its design and the subsequent results from the experiments done to investigate the CO_2 absorption.

Chapter Six discusses the prototyping, the experiment results and design improvements. Furthermore, the seventh chapter outlines potential future research avenues and future design work arising from ongoing developments and lessons learned in this thesis.

Chapter eight presents two abstracts for the two upcoming research papers based on the work done in this thesis. The concluding chapter nine presents a summary, highlighting the key findings derived from the research conducted in this thesis.

2 Theory and background

This chapter presents an overview of essential theories for the methodology used to develop the SGS flow chamber. First, a background summary of food processing equipment is presented before describing salmon biochemistry. Next, carbon dioxide (CO_2) dissolution theory is reviewed. Lastly, a presentation of the current state of SGS and the subsequent concept that laid the groundwork for this thesis is presented.

2.1 Background

The increasing global demand for making the food industry more sustainable means more effort should be focused on improving food processing operations' efficiency, productivity, and environmental performance (Atuonwu and Tassou 2021; Monforti et al. 2015; Nations 2017).

Technological advancements, such as automation, sensor integration, and machine learning, enable researchers with the tools to extract experimental data from a concept design in order to validate a concept's efficiency and viability (Iqbal et al. 2017; Murcek et al. 2021). Which afterwards can be optimised with simulation. By researching potential technologies in the early phase, the technology gets a higher probability of industry adaptation (Ebert and Aganovic 2022). In this thesis, such research and development has been conducted.

2.1.1 Examples of sustainable processing equipment

There are many examples of food processing equipment that have improved sustainability. Particularly regarding post-processing to increase shelf life, there is sous vide, microwave pasteurisation, conventional pasteurisation (Esmaeilian et al. 2021)

Another example of technology that increases sustainability, specifically related to packaging, is Modified Atmosphere Packaging (MAP). MAP is a technique used to extend the shelf life of perishable food products by altering the gas composition inside the packaging. MAP often involves reducing oxygen (vacuum) and increasing levels of gases like CO_2 to slow microbial growth and maintain product quality (Lambert et al. 1991; McMillin 2008; Al-Nehlawi et al. 2013). MAP can be seen in stores today where there is a headspace for an MA gas in a product's packaging, illustrated in Figure 2

Figure 2: Typical MAP product seen in stores. From https://landercn.com/modified-atmosphere-packaging-machine-tray-sealer/

2.1.2 Research to lift technologies for industrial adaptation

The state of adaptation of technologies is measured on a Technology Readiness Index (TRL) (Ebert and Aganovic 2022). TRL is a tool used to assess the maturity of a technology in the context of its development and readiness for practical application or deployment. Initially developed by NASA

in the 1970s to evaluate the readiness of technologies for space missions, the TRL framework has since been widely adopted across various industries and sectors as a valuable tool for technology assessment and decision-making.

The TRL scale consists of discrete levels, usually numbered from 1 to 9, each representing a specific stage in the technology's development and progression toward full-scale deployment. Certain critical aspects of the technology are evaluated at each TRL level, including theoretical feasibility, experimental validation, prototype development, and operational testing.

As technology advances through the TRL levels, its degree of maturity and readiness increases. At the lower end of the TRL scale (e.g., TRL 1-3), the technology is primarily at the conceptual or theoretical stage, with limited experimental evidence to support its feasibility. As it progresses to mid-level TRLs (e.g., TRL 4-6), the technology undergoes iterative development and testing, creating functional prototypes and an improved understanding of its capabilities and limitations. Finally, at the higher TRLs (e.g., TRL 7-9), the technology is subjected to realistic operational conditions and demonstrated in relevant environments, showcasing its readiness for integration into operational systems by the industry.

Many actors in the industry contribute to developing sustainable processing equipment; however, the industry is more focused on short-term development for a rapid return on investment by implementing higher TRL technology. Therefore this thesis and the surrounding research, like Esmaeilian's manuscript (in writing) (Esmaeilian 2023), focus on lifting food science technology from low TRL to high TRL through applied research in an effort between food science and mechanical engineering. Thus bridging the gap between research and application (Ebert and Aganovic 2022).

Previous examples of this are the conjoined efforts done in researching modified atmosphere packaging (MAP), where researchers found a technology potential in modifying atmospheres for food in 1821 (Robertson 2005). Experimental work was done to establish the potential for commercial use of MAP in the late 1950s and early 1960s (Blakistone 2012). The first patents on MAP came in 1985 (Myers 1985), while for SGS, there are no patents, meaning the technology is not ready for adoption. Today, Norwegian retail stores predominantly offer convenient vacuum-sealed or MA portion packages of filleted salmon products (Heide 2020).

2.2 Biochemistry of Salmon

The Norwegian-farmed Atlantic salmon (Salmo salar L.) is a very sought-after product (Sciencedirect 2023). In 2022, Norway, the leading producer of Atlantic salmon, exported 1.3 million tonnes valued at NOK 105.8 billion (B.-A. Jensen and Mutter 2022; Skaug 2023). The processing of Norwegian salmon was observed at a visit to both Salmar and Lerøy's slaughtering facilities at Frøya and Hitra, respectively, on the 1st of March 2023. This section describes the characteristics of salmon and their biology after slaughter.

Salmon flesh predominantly comprises water, protein, fat, and a small amount of minerals and vitamins. The proportions can vary based on the species, diet, and environmental factors. However, generally, the composition can be broken down to water content which is typically 65%, while about 22% and 12% are protein and fat, respectively (U.S. Department of Agriculture 2019). The protein in salmon is complete, meaning it includes all the essential amino acids the human body requires (Cervoni 2022). Salmon is particularly known for its high content of omega-3 fatty acids, which have been associated with various health benefits (Cervoni 2022).

2.2.1 Salmon post mortem

After the fish has been pumped into the slaughter factory and put down, the state of the fish meat post-mortem can be characterised into three biological stages.

The first stage is pre-rigour. This stage is the period immediately following a fish's death when fish are filleted, but bone removal is not possible by machinery without damaging the flesh (Thielemann 2014). Pre-rigour-processed salmon are considered ready-to-eat without the need for cooking or

additional processing to reduce or eliminate harmful microorganisms (A. N. Jakobsen et al. 2022).

The second stage is rigour mortis which occurs within 6-12 hours post-mortem, where the flesh stiffens considerably and is influenced by factors such as temperature, pre-mortem handling, and slaughtering procedures (A. N. Jakobsen et al. 2022). Rigour mortis occurs in muscles when the ATP process consumes all the oxygen available (Fremery and Pool 1960) and lasts up to 3-5 days for salmon (Thielemann 2014).

The last stage is post-rigour, when a fish is again flexible after a few days and bones are removed (Thielemann 2014).

2.2.2 Bacteriostatic effect in salmon

The ability to prevent the growth of bacteria is called the bacteriostatic effect (Pankey and Sabath 2004), illustrated in Figure 3. The ability to control this effect is important in preserving freshness and quality when processing food, e.g. salmon.
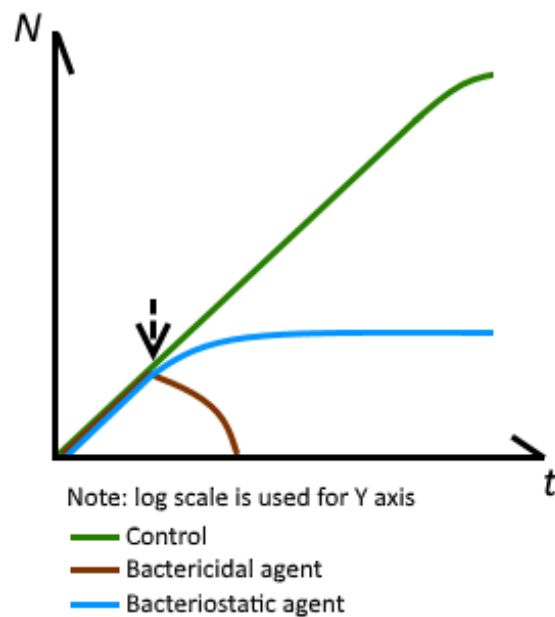
Figure 3: Representation of different growths of bacteria. When a bacteriostatic agent is introduced (arrow), the number of bacterias (N) do not increase over time t, while a bactericidal agent, like antibiotics, kills all bacteria, and the count returns to 0. From https://en.wikipedia.org/wiki/Bacteriostatic_agent#/media/File:Bacteriostatic_agent_and_bactericidal_agent_-_en.png

There are several ways to achieve a good bacteriostatic effect (Fusieger et al. 2023); however, in this thesis, the only focus will be applied to the effects caused by CO_2. The effect that CO_2 causes is a change in pH, which decreases the respiratory rate of microorganisms; however, this effect is not entirely understood (M. Lima et al. 2014). Nevertheless, the effect increases with increased amounts of dissolved CO_2 in the food (A. N. Jakobsen et al. 2022). The CO_2 dissolves into the product's liquid water and fat, forming carbonic acid (H_2CO_3). This acid can then break down into bicarbonate (HCO_3), carbonate (CO_3^{2-}), and hydrogen ions (H^+) (Esmaeilian et al. 2021; M. Lima et al. 2014). Because dissolution must happen with liquid water, freezing temperatures are inappropriate for SGS.

For decades, combining MAP and vacuum packaging with low temperatures has been employed to extend the shelf life of seafood, effectively countering the detrimental effects of microbiological

and endogenous enzymatic activity during storage (A. N. Jakobsen et al. 2022). However, this technology has limitations discussed in Section 2.5.

Achieving bacteriostatic effects in salmon without compromising its sensory qualities requires a balance between effective dissolution and retaining sensory qualities (Esmaeilian et al. 2021). In, e.g. SGS, high pressures can yield water loss, thus drying out the fillets, reducing quality (Esmaeilian et al. 2021).

It is also important to understand that CO_2 will not solve all problems because little oxygen (O_2) in a vacuum and MA packages can also facilitate certain bacteria's growth, while other bacteria are linked to seafood and can produce toxins even at low temperatures (≥ 3.3°C) (A. N. Jakobsen et al. 2022). Thus, keeping microbial growth to a minimum with low temperatures is important when designing a setup.

2.3 Dissolution of CO_2

The correlation between the concentration of absorbed CO_2 and changes in package volume in MAP is described by the model introduced by B. T. Rotabakk et al. 2007, (A. N. Jakobsen et al. 2022):

$$C_{CO_2}^{t=\infty} = \frac{1000 \times P(V_g^{t=0} - V_g^{t=\infty}) \times \text{MwCO}_2}{R \times T \times W} \tag{1}$$

,where $C_{CO_2}^{t=\infty}$ is the total CO_2 (ppm) absorbed by the product, P is absolute pressure (Pa), V_g is gas volume (m^3) at start, and at equilibrium, Mw_{CO_2} is the molecular weight of CO_2, R is the gas constant, T is the absolute temperature (K), and W is the weight of the product (kg). Generally, we see that the concentration of CO_2 is proportional to the pressure while inversely proportional to the temperature. This formula will be used to analyse the experiments in this thesis. Pressure has a much stronger effect on dissolution than temperature (M. Jakobsen and Bertelsen 2004). Additionally, solubility is not always inversely proportional to temperature because CO_2 dissolves in the liquid state of water and fat (Esmaeilian et al. 2021). Therefore, the solubility can increase with increasing fat content above 2 °C, while solubility decreases with high-fat content below 2 °C (M. Jakobsen and Bertelsen 2004). This temperature dependence should be investigated further.

Following Henry's law, when a sample reaches equilibrium with the surrounding gas, the quantity of CO_2 in the headspace is directly proportional to the amount of CO_2 absorbed by the sample (A. N. Jakobsen et al. 2022):

$$P_{CO_2}^{t=\infty} = H_{CO_2,p} \times C_{CO_2}^{t=\infty} \tag{2}$$

Where $P_{CO_2}^{t=\infty}$ signifies the equilibrium partial pressure of CO_2 in the headspace gas (Pa), and $H_{CO_2,p}$ represents the temperature-dependent Henry's constant for CO_2 within the sample (Pa/ppm). The dissolution of CO_2 and the corresponding Henry's constant is an empirical constant varying with the composition of the product and its temperature. Therefore decreasing temperature yields a higher potential concentration of CO_2 in the product. A model based on the experimental data a flow setup could provide, can help future researchers to get a better calculated constant and thus be able to predict the concentration. Similar to what is done for MAP in Equation 1.

2.4 Current state of soluble gas stabilisation (SGS) technology

Soluble gas stabilisation (SGS) technology combines all the mentioned concepts and aims to get a sufficient amount of CO_2 into the product as soon as possible. SGS's main potential lies in all the areas which MAP falls short.

Compared to MAP, where adequate CO_2 levels can take several days, SGS can use a few hours (Esmaeilian et al. 2021; A. N. Jakobsen et al. 2022). These few hours are still too long and

impractical for the industry to adapt into their process lines, which means that more research is needed to develop SGS technology for the industry.

Getting CO_2 faster into the product also means less spoilage occurs, and the product is fresher for longer compared to MAP. In addition, achieving the optimal effect of CO_2 in MAP typically requires a gas-to-product volume ratio of 2:1 or 3:1, using thick rigid plastic containers in order to facilitate enough headspace for CO_2 to penetrate into the product without package collapse, using both more plastic for packaging material and requires more shipping volume (A. N. Jakobsen et al. 2022). A promising and sustainable approach to meet consumer demand for high-quality fresh salmon products involves combining SGS technology and vacuum packaging (A. N. Jakobsen et al. 2022). From both environmental and financial perspectives, packaging usage and time of adequate bacteriostatic effect can be considered a disadvantage of MA packaging.

The research done so far has been focused on the verification that the SGS process has better bacteriostatic properties than MAP and that it is safe (Esmaeilian et al. 2021; A. N. Jakobsen et al. 2022; Al-Nehlawi et al. 2013; B. Rotabakk et al. 2008). However, there is limited data on how different temperatures and pressures affect the product. For example, most of the studies done on SGS use "100% CO_2" instead of pressure as one parameter for the experiment (Dang et al. 2020; A. N. Jakobsen et al. 2022; M. d. Lima et al. 2021; Al-Nehlawi et al. 2013; Bjørn T. Rotabakk et al. 2006). An industrial application would look into how the pressure of 100% CO_2 would affect solubility. Up to this point, the studies have been very much focused on the comparability of SGS and MAP with static chambers at low pressures while not seeing SGS as a stand-alone technology and trying to develop the technology out of the lab (Esmaeilian et al. 2021). The literature also states that SGS with vacuum packaging has a high industrial potential for value-added product development (A. N. Jakobsen et al. 2022). The literature provided can be used to verify that a specific concentration of CO_2 achieved in a certain amount of time yields safe products for consumption while also seeing trends in a setup, e.g. decreased temperatures and increased pressures improve the time of solubility (Esmaeilian et al. 2021). However, more data for appropriate SGS pressures must be determined to lift the technology from a low TRL level. Developing a modular, high-pressure chamber capable of static and flowing pressure hopes to contribute to advancing the field of food science through this product development.

2.5 SGS flow concept presentation

As mentioned, all current experimental research on SGS is done using a sealed chamber with varying pressures, where the gas inside is static. This static chamber will be referred to as a static chamber. A concept to increase the rate of CO_2 absorption by the use of pressured flowing CO_2 has been developed in Esmaeilian's PhD research, which concludes in a manuscript (Esmaeilian 2023). The concept is shown in Figure 4.

The concept is based on the idea that by changing the setup design of a traditional experiment, one can effectively dissolve a sufficient amount of CO2 into food in a short time (Esmaeilian et al. 2021). The idea is to use a continuous high-pressure CO_2 flow to accelerate the process. This idea would involve increasing pressure and lowering the temperature to dissolve CO_2 into a fish fillet.
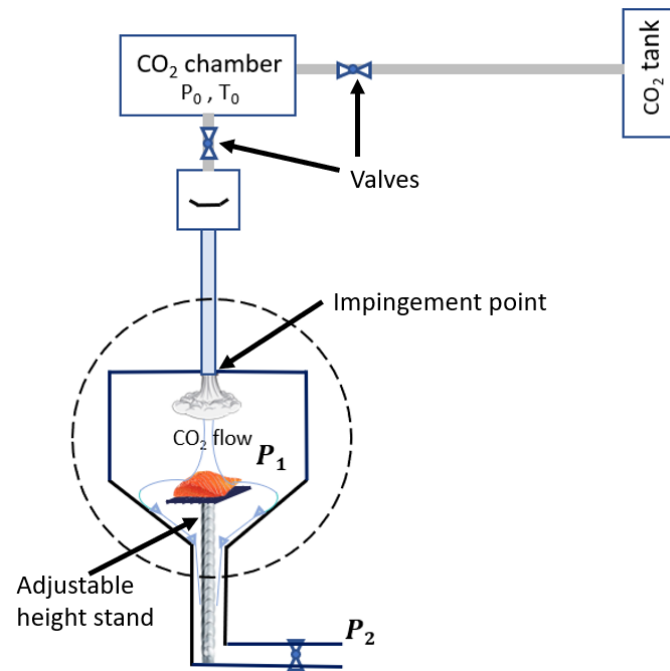
Figure 4: The SGS concept developed by Esmaeilian 2023. A CO_2 tank provides high-pressure gas to a chamber that keeps temperature and pressure at a nominal level. The CO_2 is flushed over the sample at a desired pressure. The flow is driven by a difference in pressure regulated by the valves

A main chamber with a nominal pressure P_1 is where the sample is placed and is supplied with CO_2 gas from a chamber where temperature and pressure are controlled. This CO_2 comes from a large outside tank. The gas goes through a flow control valve. Then, it is flushed through an array plate with orifices into the system like an impinging jet. The orifices can be turned on and off, and their number is also adjustable, depending on the case. The gas flow hits the salmon surface, surrounds it, and then goes to the outlet through a funnel-shaped area. Finally, it exits through a pressure control valve or pressure regulator to the outside at a lower pressure. The flow, therefore, comes from a pressure difference. The pressure regulator controls the pressure inside the main chamber (Esmaeilian 2023). A concept CAD has also been made and is shown in Figure 5.
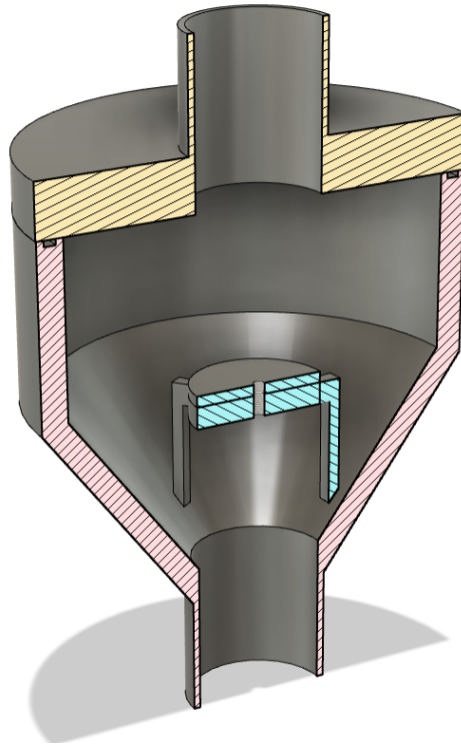
Figure 5: The SGS concept made into a preliminary CAD by Esmaeilian 2023. Shown section view with stand for the sample and O-ring in the chamber walls

To further develop the SGS technology, the concept has the following goals and constraints:

- Create a pressurised chamber that minimum holds 2 barG and up to 8 barG

- Create flow speeds over the sample up to 50m/s.

- Salmon sample of Ø65mm

- The flow pipe diameter is the minimum sample size, i.e. 65mm.

- Have a fully developed flow - Therefore, a pipe over the main chamber must have a length of around ten times the pipe diameter. This pipe length is based on the calculations done by Esmaeilian 2023.

- Valves to control input and output pressure

- Temperature control down to 1°C

- Being able to vary the distance between the sample and orifice point between 10-60mm.

- Get data on flow speed, force due to gas flow on sample, temperature and pressure.

- Made for food safety and HSE limitations.

Therefore, this thesis focuses on developing a dissolution solution through an experimental setup with practical parameters that realistically emulates the simulation based on the constraints above and gets data that can be validated and is a proof of concept for model validation. This is going to be done with cheap off-the-shelf components to rapidly test and prototype the setup in order to learn fast.

3 Prototyping and development

This section presents all the work and prototyping done to arrive at the final design of the flow chamber and its surrounding components. The design development is illustrated in Figure 6. This section focuses on the development process, lessons learned, and the decisions taken throughout the semester to arrive at the final design. This section is presented in chronological order. First, the early phase static chamber test is presented, followed by dimensioning and simulation of the flow chamber. The last section goes through all the prototyping stages to arrive at the final design used for the experiments, which is presented in detail in Section 5.1.
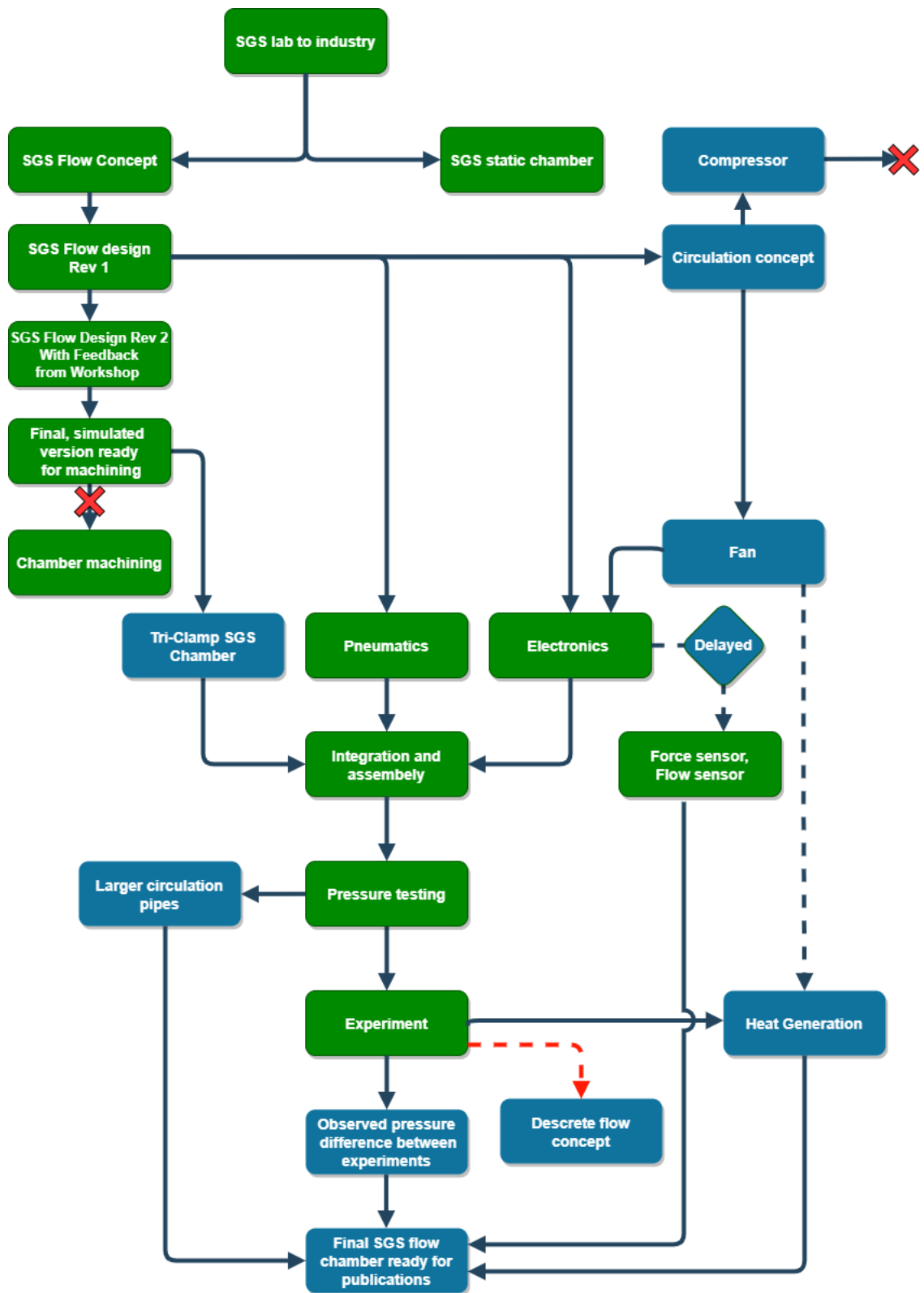
Figure 6: Flow chart showing all the developments made and how they relate to each other. The squares marked in green were a part of the initial plan, while the blue was generated throughout the process

3.1 Static chamber

The work in this thesis started with continuing the work previously done. In previous research, a custom pressure chamber was made to experiment with static SGS. A perfect chamber seal over, e.g., 24 hours, was necessary to continue and advance the literature. To verify simulations of the SGS process, one needed to see the only pressure reduction inside the chamber coming from the dissolution of CO_2 inside the salmon or water, and no leakage. Thus one can model based on an experimental Henry's Constant as described in Section 2.3. The initial tests done with this chamber showed a substantial pressure reduction of the static chamber, implying leakage.

3.1.1 Previously used Static chamber design

The design of the chamber previously used was an outer chamber, inner chamber and lid, shown in Figure 7. The inner chamber is placed inside the outer chamber, and the lid is screwed on with threads inside the outer chamber. The sealing of the chamber is the O-ring placed in the lid that presses on the top of the inner chamber when the threads are tightened. This method of sealing the chamber was not 100% tight as the pressure decreased with nothing inside after a few hours. The main reason suspected was that the threads were too coarse to achieve the required pressure on the O-ring to seal the chamber.
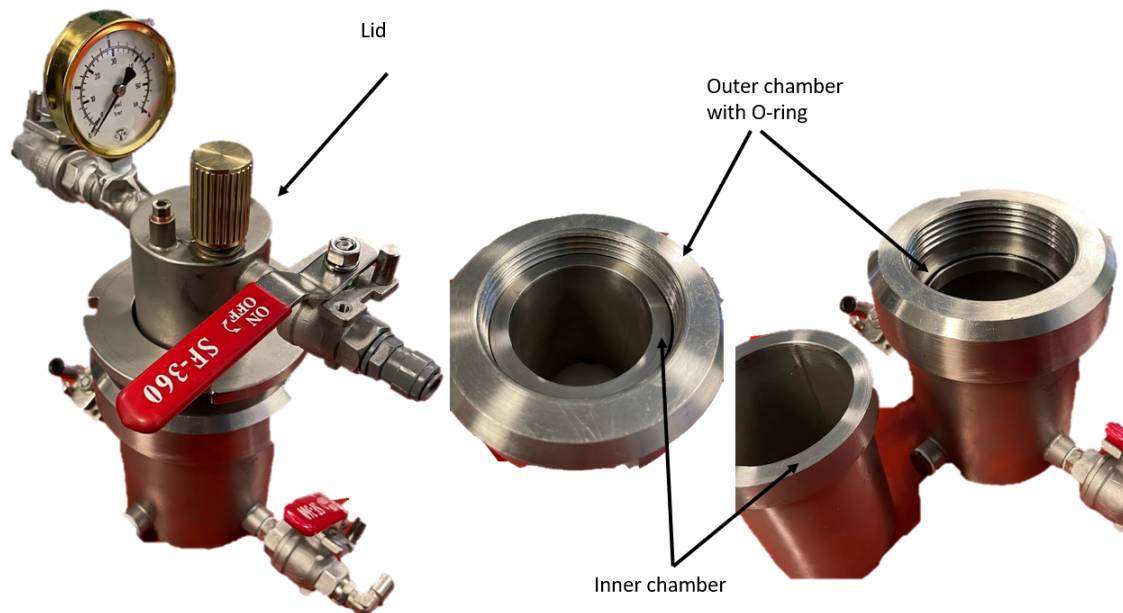
Figure 7: The original static flow chamber used for earlier experiments

It was decided that it was worth trying to change some aspects of the chamber to test for complete sealing. It was identified that the leak was coming from the threads, and thus, gas was escaping through the O-ring. First, the contact surfaces of the O-ring were machined to allow for better contact between the top of the inner chamber and the O-ring. After testing, the leak was still there.

It was discovered through measuring the O-ring groove that the dimensions were not optimised for the O-ring currently used using the Trelleborgs calculator (Trelleborg 2023). Therefore, based on the current grove, particular dimensions for the O-ring were required based on the calculator. An O-ring in a flexible filament material, TPU, was 3D-printed as a fun preliminary experiment. The subsequent test showed that a proper O-ring was needed. A customised O-ring, with a size of 72.62x3.53mm NPR70, was ordered from Gummi & Maskinteknikk AS and tested. This test was also unsuccessful. Therefore, the surfaces were machined to a recommended dimension with a standard O-ring size of 72.62x3.53mm NPR70. The final pressure test was also unsuccessful.

After this, several smaller tests were done using silicone sealing tape in the groves, vaseline on the O-ring and different degrees of tightening. Silicone tightening with Tec7 was also tried without luck. Tec7 is a modified silicone polymer sealant with good sealing capabilities. It has a pressure resistance of 1,19 N/mm² (Novatech 2023). All these unsuccessful tests meant that this chamber could not be used for the experiments wanted.

3.1.2 Final static chamber

Eventually, it was decided to purchase a new airtight chamber that proved to be successful. This chamber was used to establish a baseline for the static chamber model. The chamber for this will be presented in the methodology chapter.

3.2 Machined flow chamber development

A preliminary machinable flow design was made based on the initial concept design from Esmaeilian, presented in Section 2.5. Changes were made to simplify the chamber and reduce production costs. For example, a straight pipe was used for the main chamber, which would serve as the pressure chamber. To guide the flow, 3D-printed funnel structures (presented in Section 3.12.2) were added inside, which was a more affordable option than machining the chamber into a funnel shape. This design also aimed for quick assembly and disassembly, essential for changing the samples efficiently.
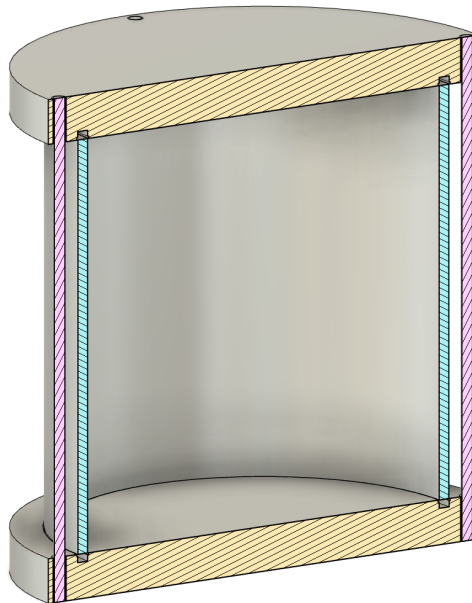
Figure 8: Early version two of the machined flow chamber

This design was presented to the workshop team; they offered feedback on its practicality for machining. It was discussed whether the best method to ensure a sealed pressure chamber was to weld the connecting pipes or use BSP/NTP screws. Given the large diameter of the connecting pipes (around Ø65mm), using screws was not practical due to their size and the effort needed to ensure a tight fit. While the idea of welding the pipes was considered, the decision was made to use a combination of welded pipes and KF-flanges. This allowed for flexible connections to the main chamber.

To ease mounting, continuous screws, shown in Figure 8 from the top lid to the bottom, were designed. However, thermal expansion could make the screws expand, reducing O-ring pressure, and thus changing the sealing capability of the lid. This was changed to regular bolts with nuts.

The flanges themselves were moved from being welded on the side of the pipe to being welded to the end of the pipe. This made welding easier because tolerances of fitting the circular flange on the outside of the pipe could be a problem. In addition, O-rings were moved from the flange (see Figure 5) to the lid because the flange had to be flattened after welding due to possible warping, while the lid does not need to be surfaced machined unless the O-ring is in the flange. This secures an entirely flat surface pressing against the O-ring with minimal machining.
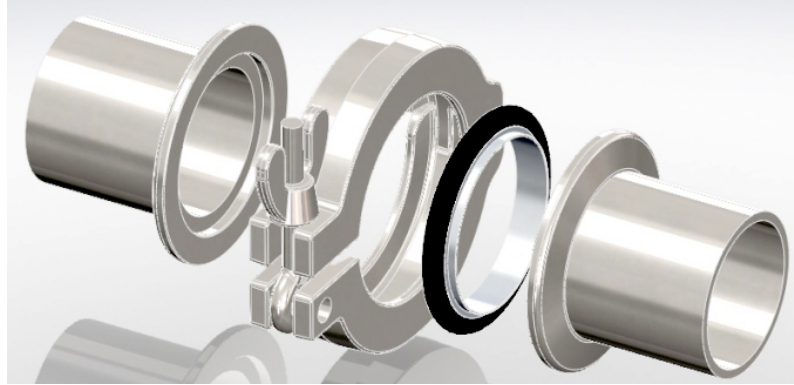
Figure 9: A KF-standard flange

As mentioned, KF flanges were suggested and is shown in Figure 9. KF-flanges are used in high-performance systems with quick assembly, e.g. vacuum (High Vac Depot staff 2020). These components, however, are expensive. A way cheaper option was Tri-Clamp systems made for brewing and distillation, shown in Figure 10. These have easy assembly and disassembly and come with the BS 4825 standard that specifies pressure rating and dimensions (Hygienic Stainless Steel 2023). The rated pressure for these components is 10 barG, which is perfect for this application.

Figure 10: A Tri-Clamp standard flange

The use of acrylic pipe for the main chamber pipe was also considered, but it was not deemed a requirement to be able to see the experiment, and it would make the chamber considerably more expensive.

The stand for the sample is made of a 3D-printed funnel with a stand where the area between the stand and the funnel is equal to the calculated necessary area for the exit hole.

The exit pipe only needs to be large enough to achieve sub-sonic speeds. The logic used is the conservation of mass and the limitation of how fast a gas can flow in a pipe. There are many factors at play here, but assuming a theoretical max speed of 0.9 of the speed of sound of CO_2 pressurised to 8barG at one °C, which is 257m/s, we get:

$$v = 257\,\text{m/s} \times 0.9 = 231.3\,\text{m/s} \tag{3}$$

Using this in the equation:

$$\dot{V} = A \cdot v \tag{4}$$

We get a minimum diameter of 34mm. Therefore this hole was set at the size of a 2-inch Tri-Clamp.

In addition, in a differential pressure system, choke occurs in a steady-state flow when the downstream pressure falls below a critical value p^*, assuming ideal gas behaviour. That critical value can be calculated from the dimensionless critical pressure ratio equation:

$$\frac{p^*}{p_0} = \left(\frac{2}{\gamma + 1}\right)^{\frac{\gamma}{\gamma - 1}} \tag{5}$$

where γ is the heat capacity ratio $\frac{c_p}{c_v}$ of the gas. CO_2 at 8 barG and 1 °C has $c_p = 0.900$ and $c_v = 0.6584$, we therefore find:

$$\gamma = \frac{c_p}{c_v} = \frac{0.900}{0.6584} \approx 1.367$$

$$p^* = 8 \times \left(\frac{2}{\gamma + 1}\right)^{\frac{\gamma}{\gamma - 1}} \approx 4.27 \text{ bar}$$

Here, p_0 is the total (stagnation) upstream pressure, which is 8 bar, and p^* is approximately 4.27 bar. Meaning if the top valve is set to 8 bar, the exit valve can, at the lowest, be 4.27 bar for choke not to occur, assuming steady-state conditions.

3.2.1   Final machined flow chamber design presentation

The main chamber consists of 4 customised machined parts, shown in Figure 11. The top lid is welded to a Tri-Clamp pipe. The main chamber is the main pipe; this is welded together with a top flange with bolt holes. To make welding easier, a machined lip gives an edge to fillet weld against. The same lip is made in the centre of the lids to weld the Tri-Clamp ferrule. Since the bottom does not need to be removed, this bottom lid is welded to the pipe. In the top lid, O-rings are dimensioned from Trelleborgs O-ring calculator (Trelleborg 2023). 6 bolt holes in the top lid are made with room for nuts next to the pipes.
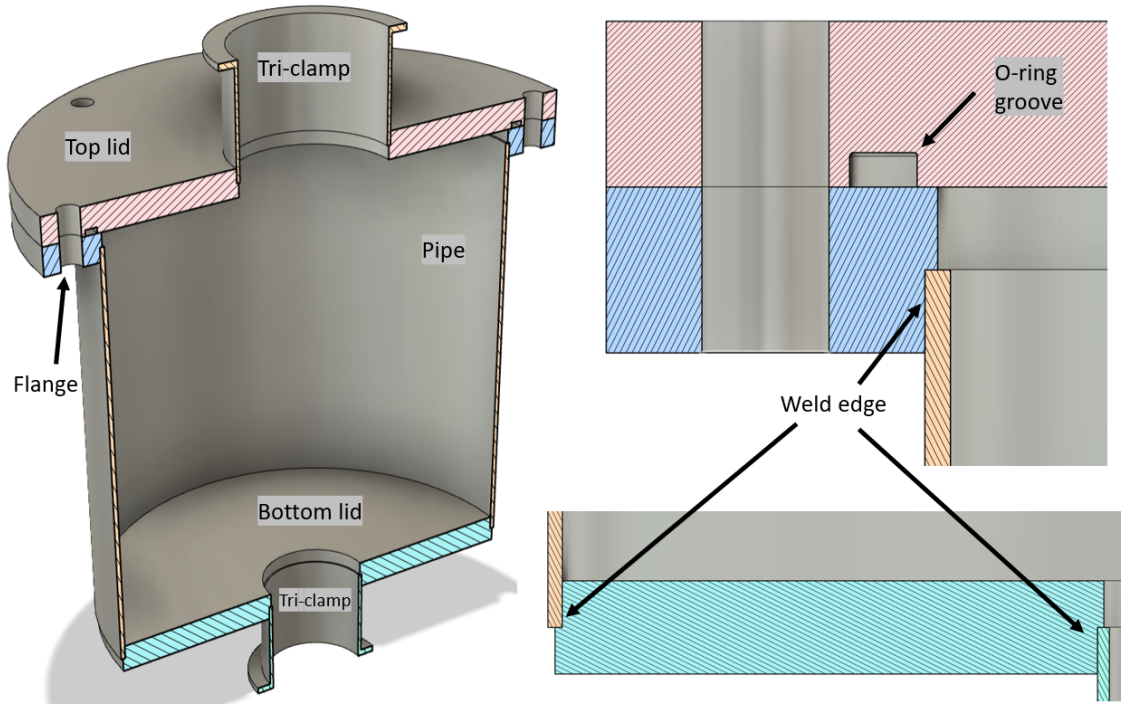
Figure 11: Final machined chamber

The inner pipe diameter is oversized at 200 mm to accommodate potential future experiments needing more room. The hole in the top flange is based on the dimensions for the 3-inch Tri-Clamp ferrule, while the bottom one is dimensioned for 2 inches.

3.2.2 Bolts, lid and pipe thickness calculation and simplification

A baseline analytical analysis was done on the chamber in order to dimension the chamber properly. This baseline calculation was done to be later verified with FEA simulation. It was also predicted that a simulation would yield stress concentrations and that this analysis would be a handy tool to analyse that.

Bolt calculation:

Formulas for a bolt in a flange on a straight pipe were used for this analysis (Collins et al. 2010).

$$F_{\text{radial}} = p \cdot A_{\text{tank}} \tag{6}$$

Where F_{radial} is the radial force component; p is the pressure acting on the given areas, and A_{tank} is the cross-sectional area of the tank/pipe where the pressure is applied.

This is not the only force a bolt experience because the flange is at the end of the pipe; the bolt experiences an additional axial force as the pressure pushes the end lids of the chamber. These two forces are, therefore, added together.

$$F_{\text{bolts}} = F_{\text{radial}} + F_{\text{lid}} = p \cdot A_{\text{tank}} + p \cdot A_{\text{lid}} \tag{7}$$

Where F_{bolts} is the total force exerted on the bolts; F_{lid} is the force exerted by the lid, and A_{lid} is the surface area of the lid where the pressure is applied.

Simplified with a pressure of 10 barG and the diameter of the tank and lid is 180mm, giving us a force of 50.9kN:

$$p = 1\,\text{MPa} = 10\,\text{bar}$$

$$A_{\text{tank}} = 90^2 \cdot \pi = 25\,434\,\text{mm}^2$$

$$A_{\text{lid}} = A_{\text{tank}}$$

$$F_{\text{bolts}} = 50.9\,\text{kN}$$

This simplification is a more conservative assumption as the actual force is probably smaller than the two added together. In addition to this force, O-rings in a system like this with hardness 90 require 2-4.5 kN of force to be sealed (Trelleborg 2023). It is assumed that these forces are baked into the 50.9kN. The force on one bolt is given by:

$$F_{\text{bolt}} = \frac{F_{\text{bolts}}}{n_{\text{bolts}}}$$

where n_{bolts} is the number of bolts. Together with:

$$\sigma_{\text{bolt}} = \frac{F_{\text{bolt}}}{A_{\text{M10 bolt}}}$$

where σ_{bolt} is the yield strength of a bolt, which for a 10.9 bolt is 800MPa (Engineering ToolBox 2023), representing the maximum amount of stress that the bolt can withstand while maintaining its shape and $A_{\text{M10 bolt}}$ is the cross-sectional area of an M10 bolt, which is 58 mm^2. Rearranging yields:

$$n_{\text{bolts}} = \frac{F_{\text{bolts}}}{A_{\text{M10 bolt}} \cdot \sigma_{\text{bolt}}}$$

With a factor of safety of 3, this yields a minimum of 4 bolts. See Appendix A for the Python code for solving these and the following formulas in this section.

Thin walled pipe calculations:

Assuming the main chamber is a thin-walled container, the stresses in the θ and z directions are defined by the equations (Collins et al. 2010)

$$\sigma_\theta = \frac{r \cdot p}{t} \tag{8}$$

and

$$\sigma_z = \frac{r \cdot p}{2t} \tag{9}$$

, respectively. Here, σ_θ represents the circumferential or radial stress, while σ_z denotes the axial stress. The variable r refers to the radius of the cylindrical vessel, p is the internal pressure acting within the system, and t is the wall thickness of the vessel. These equations are commonly used to analyse the stress distribution in thin-walled cylindrical pressure vessels subjected to internal pressure.

Using the Von Mieses criterion with no shear forces ($\tau_{xy} = 0$), (Collins et al. 2010), yields the following formula:

$$\sigma_{\text{yield}} = \sqrt{\left(\sigma_\theta - \sigma_z\right)^2 + \sigma_\theta \sigma_z} \tag{10}$$

Inserting Equation 8 and 9 into Equation 10, and solving for t yields:

$$t = \frac{\sqrt{3} \cdot p \cdot r}{2 \cdot \sigma_{\text{yield}}}$$

where σ_{yield} is the proof stress of SS316L steel which is 205 MPa (Matweb 2023).

Putting in the numbers given above yields a pipe thickness of 1.3 mm thick.

Solving Equation 10 with 1 mm thickness yields a max stress of 86.6Mpa. This equation was then verified with a simulation in Fusion, shown in Figure 12, where the stress of a 1 mm pipe is 86.35 MPa.
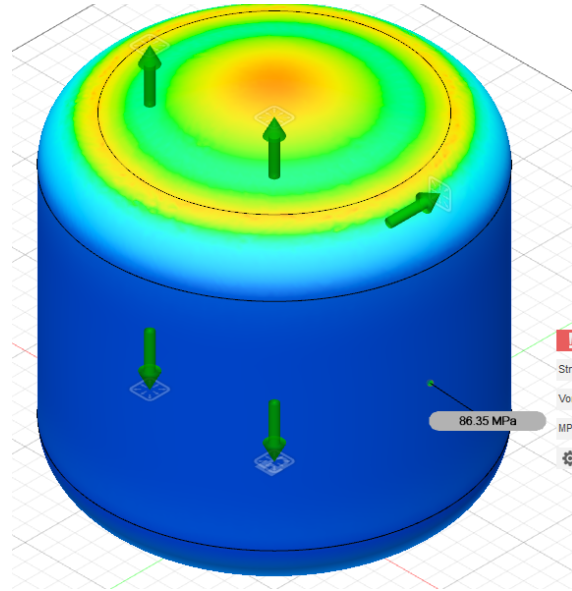
Figure 12: Simulation validation of the analytical model used. The stress in the pipe walls is 86.35 MPa

These dimensions, as well as a lid thickness of 10mm, were used in the subsequent simulation of the entire chamber, which is elaborated on in the next section.

3.2.3   Simulation of machined flow chamber

Based on the analytical analysis, the chamber was designed to these dimensions in Solidworks, and several static simulations were done. Based on early simulations, it was decided to use 6 bolts to get even pressure on the O-ring and avoid high lid displacement between the bolts. This simulation was done before a welded bottom lid was designed; however, it was decided that this did not affect the simulation in any meaningful way. Therefore the simulation was not redone. The simulation is shown in Figure 13 and Appendix F.
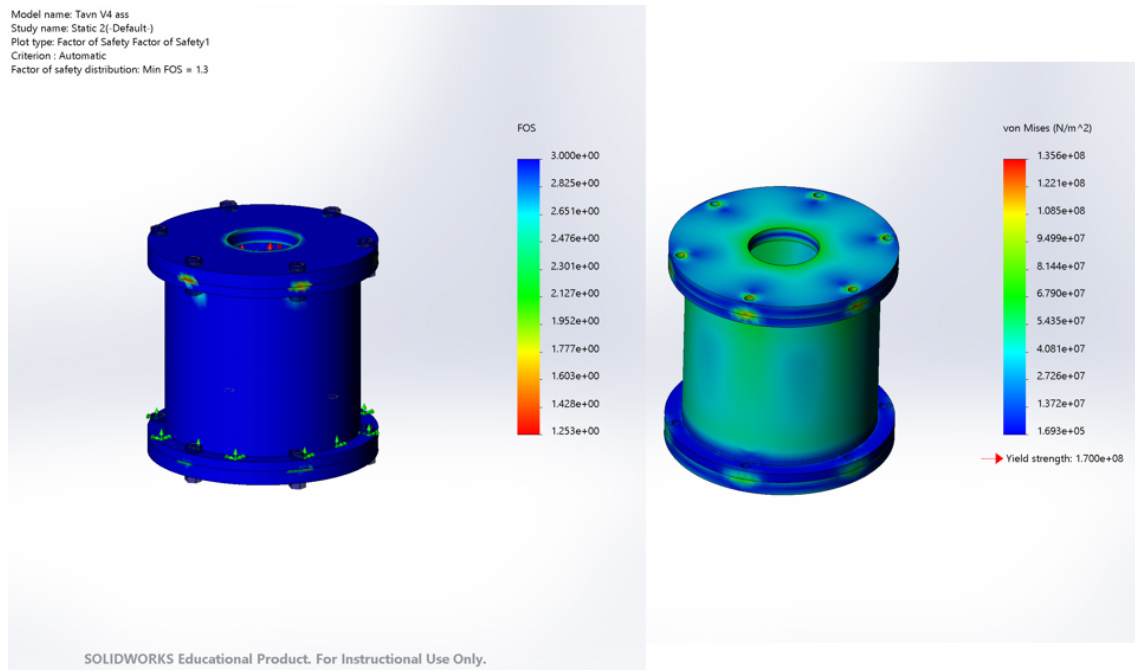
Figure 13: Final simulated machined chamber

The static simulation consisted of three parts: two lids and one connector pipe. The pipe had flanges fastened to itself like the final part after welding. SS316L was the material used for the simulations. Solidworks used its own standard yield strength of 170 Mpa. The assembly was fixed on the upper surface of the lowest flange on the pipe. This was because the bending here would not be different from the top, and if this was fixed instead of the bottom lid, the bottom lid could deform and get realistic forces. This simulation could also be simplified because of symmetry; however, since the pipes in and out were probably different, it was deemed necessary to simulate the top and bottom lid.

Inside the chamber, a pressure of 1 MPa was applied to the three faces. Since the simulation consisted of three parts, the two contact surfaces between the lids and pipe were set to "contact set", with no penetration contact pair. The parts could, however, move away from each other, and therefore it was modelled in 12 screws, 6 on each lid. These were modelled as "bolts" with a diameter of 10mm. A connection type distributed was used for the bolts, as this produces more realistic stress compared to rigid connection (Solidworks 2020). However, when using a realistic bolt pre-tension of a few kN, the simulation gave extremely unrealistic stress concentrations underneath the bolt head and nut. Therefore, it was decided that using 100N would mitigate this, even though a higher pre-tension force would be applied. In the simulation, each bolt on the bottom experienced an average axial force of 8.69 kN. This gives a total force on all the bolts equal to 52.1kN. 2.3% off the 50.9kN in the analytical analysis.

The simulation was run with a high mesh quality and an element size of 7.996 +-0.3998mm. After several simulations, it was concluded that a lid with a thickness of 13mm would have an acceptable safety factor, i.e. 3, and displacement.

Regarding pipe wall thickness; even though the analytically calculated wall thickness of 1.3 mm was used in the first simulation, several simulations, while having the yield criteria at 170 MPa for the simulation, yielded a final minimum wall thickness of 2.0 mm. The final simulation showed a sufficient safety factor and displacement. Therefore, the following minimum requirements were made for the machine shop.

- Pipe thickness minimum 2 mm

- Lid thickness minimum 13 mm

- Number of bolts per lid minimum 6 x M10.9 bolts

The requirements were a minimum, as if the machine shop had, e.g. a 15 mm plate in-house, a waiting period of, e.g. a week for a 13 mm plate would be avoided.

3.2.4 Validating with flange standard

Before machining, comparing the dimensions found for the end flanges to an industry standard for flanges was interesting. One standard one could use is EN 1092, based on the ISO 7005-1 standard(*EN1092 Flange standard* 2023). When using an outside diameter of 200mm and pressure of 10 barG (PN10), the thickness recommended by the standard is 20mm, using 8 M16 bolts.

While industry standards often provide robust and widely accepted solutions, they might occasionally be over-engineered for a specific application, leading to unnecessary costs. By contrast, when the flange is specifically dimensioned and simulated for a particular application, it can be tailored to meet only the essential requirements of that application, eliminating superfluous features or materials. This decision uses way less raw material, resulting in cost savings. However, it is crucial to ensure that this optimisation does not compromise the flange's integrity or functionality for its intended use. The analysis above is arguably enough to make the decision to use the thinner lid of 13 mm with 6 screws.

3.3 Using the simulations of the machined chamber to purchase Tri-Clamp parts

After validating the design of the chamber, mechanical drawings for the machine shop were made. To get accurate dimensions for the fastening of the Tri-Clamp connectors above the chamber, an investigation into accurate dimensions for the Tri-Clamps was done. Preliminary research showed a maximum of 2-inch Tri-Clamps being sold on Norwegian sites. Since the requirement for the setup was 60mm, i.e. 2.36 inches, international sites were researched. Here, 3-inch pipes were found in addition to 6-8 inch Tri-Clamp pipes. These pipes were also supplied with a machined standard certified to specific internal pressures. These pressures were above the requirements we had for the system.

As this setup was way cheaper than machining and welding together all components, it was decided to go with a setup based solely on Tri-clamps. This setup would also be way more modular and adaptable than a machined design. After a process of adapting the machined design to a setup with only Tri-clamps, the components were ordered. The final setup with Tri-Clamps is presented in Section 5.

3.4 Circulation concept

The starting concept for this thesis used continuously provided CO_2 from an outside tank to be sent through the system before being vented out to the environment. Calculations for CO_2 usage were therefore done. Using the equation for mass flow rate:

$$\dot{m} = \frac{m}{t} = \frac{\rho \cdot V}{t} = \rho \cdot \dot{V} = \rho \cdot A \cdot v \tag{11}$$

Here, $\dot{m}$ represents the mass flow rate, ρ is the density, $\dot{V}$ is the volumetric flow rate, A is the cross-sectional area, and v is the velocity. With a gas density of 16 kg/m^3 at 8 barG and 1 °C, and a flow speed of 50 m/s in Ø73mm pipe gives a mass flow rate of 12 tonnes of CO_2 per hour (Megawatsoft 2023). It was very evident that there needed to be developed a circulation concept for the CO_2.

This concept was developed in tandem with the dimensioning of the chamber described in the preceding sections.
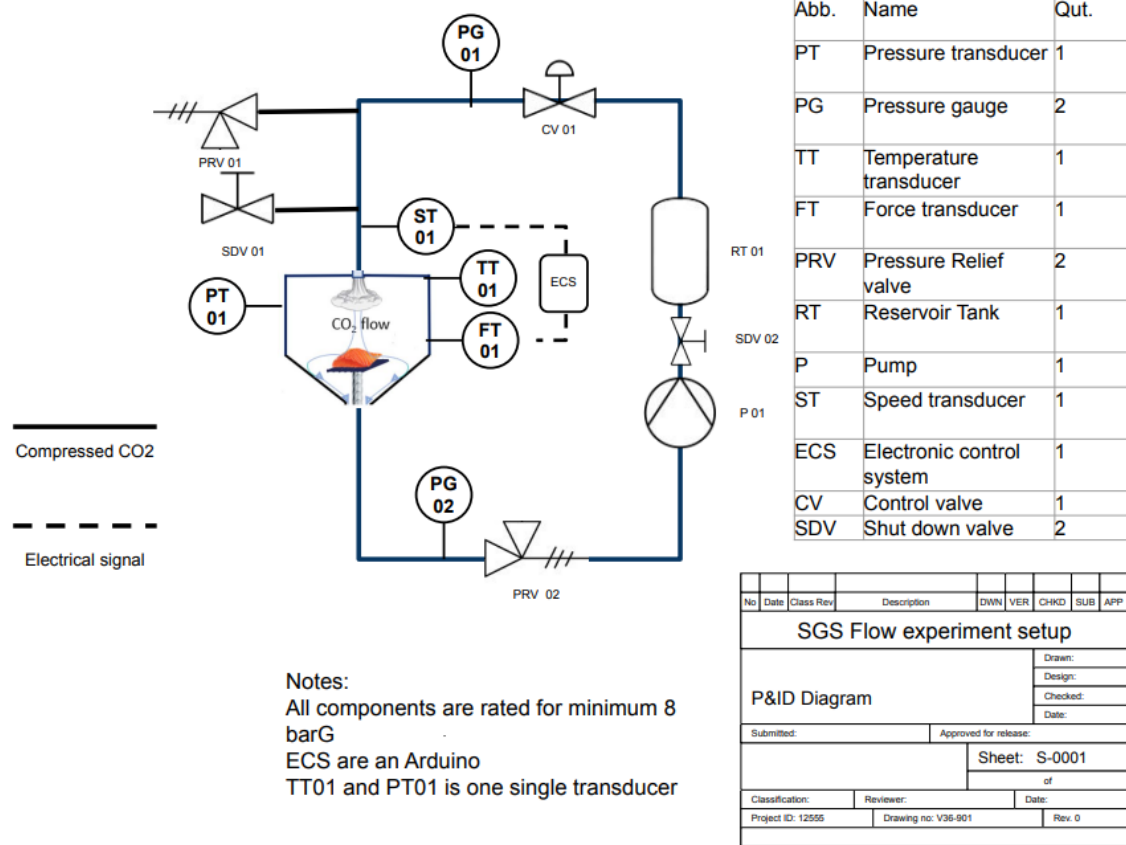
Figure 14: A P&ID of the circulation concept, showing all the components needed for the setup

The concept consists of CO_2 added to the setup through SDV01, shown in the P&ID in Figure 14. This is then closed. To get the gas to flow around the system, a compressor is used to increase the pressure of the gas and stored in a reservoir tank (RT01). The control valve (CV01) is set to the desired salmon experiment pressure and controls a constant downstream pressure, regardless of the compressor pressure, yielding this design parameter some design freedom. To have flow in the system, a pressure relief valve (PRV02) set to a lower pressure than CV01, and is used to create a pressure difference and thus get flow. The flow speed is proportional to this difference in pressure, and the setup can be adjusted to get the desired experiment flow. This flow is controlled with a speed transducer. A concept with weight was added to see how the force on the sample changes as a function of the flow speed, i.e. the force transducer (FT01). Both of these were to be controlled by, e.g. an Arduino, the ECS.

In case of over-pressurisation, a PRV01 is added to vent CO_2 should the pressure be too high to protect the components. This is also where the CO_2 is exited when the experiment is over. A lager to measure pressure and temperature inside the chamber (PT01 and TT 01) is used, and is described in Section 5.1.2. Pressure gauges are added to see how the pressure difference is at the start and end of the chamber. This is also to adjust the CV01 and PRV02 accurately. Finally, two valves around the RT01 are placed to lock the pressure inside the RT01 should it be necessary. The development of this concept is described in the following sections.

3.5   Compressor vs fan

To investigate how to get the gas to flow constantly the concept of compressor vs fan was invest-igated. First maximum volumetric flow needed to be determined. The equation for this is:

$$\dot{V} = A \cdot v \tag{12}$$

where $\dot{V}$ is the volumetric flow rate, A is the cross-sectional area, and v is the flow velocity. With a max desired speed of 50m/s and the inside diameter of the 3-inch Tri-Clamp section being 2.87 inches as the flow area, a volumetric flow rate of $12.5 m^3$/min was determined. This is extremely high and no compressor was found to be able to deliver such high flow rates at our price points. The highest volumetric flow rate compressor that was found was 6.5 CFM which is equal to 0.18 m^3/min (Team 2023). A fan, however, could be able to produce high speeds. The specifics are detailed in the next section.

3.6   Fan

Fans have two working principles, centrifugal and axial, shown in Figure 15. Centrifugal is suitable for achieving high static pressures in a container, while axial is best for high flow rates (Paul's Fan Company 2019). Therefore, axial fans were investigated.
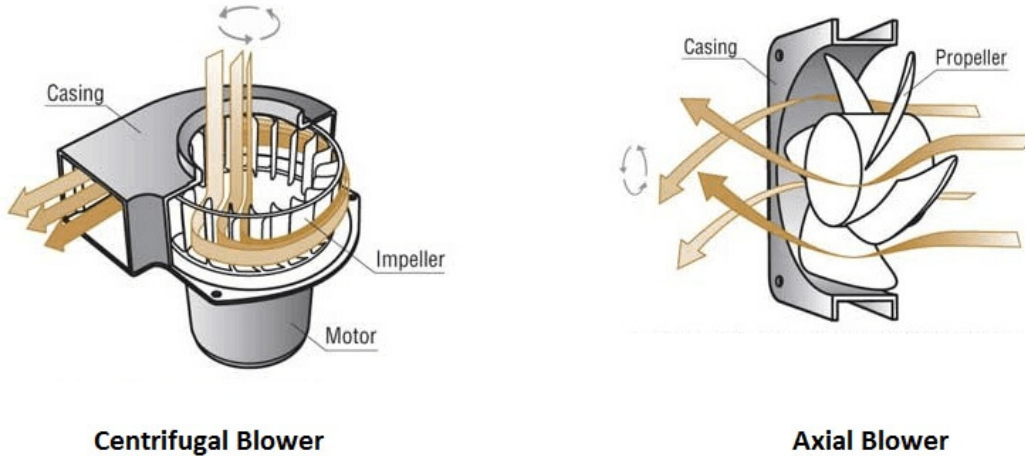
Figure 15:   Working   principles   of   centrifugal   and   axial   fans.   From https://vankool.com/blogs/everything-need-to-know-about-window-swamp-cooler/air-flow-of-centrifugal-blower-vs-axial-blower/

Fans are a complicated matter; typically, CFD is used to optimise the shape of the blade. In addition, knowing what PRM and power a fan needs to push CO_2 gas pressurised to 6 barG around at speeds up to 50m/s for a few hours is not straightforward. It was, however, calculated as an ideal RPM based on a few simplifications:

Firstly, one can assume that the average speed of the gas across the entire diameter of the fan is consistent with the average speed of the fan blade. This simplification overlooks friction and different speeds at different points on the blade.

Thus, calculating the average gas speed, using V_{avg} as the average speed and lies midway between the hub speed (essentially $0\,\mathrm{m/s}$ due to the hub's effective diameter of zero) and the tip speed V_{tip}, we have:

$$V_{avg} = \frac{V_{tip}}{2}$$

Given $V_{avg} = 50\,\mathrm{m/s}$, we deduce:

$$V_{tip} = 2 \times V_{avg} = 100\,\mathrm{m/s}$$

The relation between rpm (denoted as N) and the blade tip speed is:

$$V_{\text{tip}} = \pi \times d \times N$$

Here, d represents the fan's diameter, which is $0.073\,\text{m}$. Using $V_{\text{tip}} = 100\,\text{m/s}$, we can determine:

$$N = \frac{100}{\pi \times 0.073}$$

Solving this gives:

$$N \approx 26201\,\text{rpm}$$

Therefore, based on these assumptions, a fan of diameter 73mm would need to rotate at approximately $26,201\,\text{rpm}$ to propel the gas at $50\,\text{m/s}$. Because of these assumptions, i.e. known unknowns and unknown unknowns discussed in Section 6.5.1, it was decided that testing out different fans or motors in the lab was the best way to both learn about the physical properties of the fan and also try to converge on a solution quickly.

To rapidly test out different concepts a ventilation fan from Biltema, Sweden, rated for $187m^3/\text{h}$, was dismounted and tested. The fan was connected to a power supply fastened inside the pipe. More details on fastening in Section 3.10. This fan delivered the specified 12m/s; however, more speed was desired.

Figure 16: Final fan used in the experiment

A drone motor was borrowed and tested the next day. This was an X2814-9, Sunny Sky, USA, rated at 900 KV. KV is a value where the rpm is proportional to the supplied voltage times the KV, meaning a 12V power supply can make the fan spin at a theoretical 10800 RPM. When this was tested, the speed was around 18m/s. This could be adequate, but it was decided to use a fan that supplied the minimum theoretical RPM of 26000RPM. This fan was an ECO II Series 2207 2400KV from EMAX, USA, shown in Figure 16. This is the fan used in the experiment presented in Section 5. The ESC was placed inside the chamber in the tee to begin with but was moved outside of the chamber during the experiment due to heat generation described in Section 6.3.1.

3.7 Fan blades

Different fan blades were also tested. With the same motor in place, several fan blade designs were tested. The fan blades shown in Figure 17 were tested, including a 3D-printed one. By only changing out the fan blade, it was determined that the most important fan parameters were being smooth and having around a 45-degree angle of attack. It was also deemed that this was a rabbit hole of research and simulations and deemed outside the scope of this thesis. It was, therefore, decided to purchase a high-performance drone fan blade that was available with a high pitch of 3 inches, which means that the blade would move 3 inches after a full rotation. This looks arguably close enough to 45°with the approximations used.

Figure 17: Different motors with some of the different fan configurations tried. The fanblade on the right is a drone fan, and is what being used in the experiment

3.8 Flow Speed Transducer

To accurately measure flow speed, the integration of a transducer was essential. Three different concepts were considered: The first concept involved using a hot wire in the flow and monitoring the power required to maintain its temperature. While this method is simple and cost-effective with readily available components, a drawback emerged when researching how to calibrate the sensor. The sensor is made for air at standard atmospheric pressure. When applied to high-pressure CO_2, the altered thermal properties necessitated extensive sensor calibration.

The subsequent method considered was a laser Doppler anemometer. This device employs the Doppler effect in the medium to gauge flow velocity. Typically used in applications demanding consistently high accuracy, and these devices carry a significant price tag (RS Components 2023). Given the constraints of this thesis, procuring a high-end commercial device for flow measurement was deemed unsuitable.

The final approach determined flow speed directly via differential pressure, where the flow speed is directly proportional to the change in dynamic pressure. To separate dynamic from static pressure, a differential sensor is used. This relationship is represented by the equation (ToolBox 2023):

$$V = \sqrt{\frac{2\Delta P}{\rho}} \tag{13}$$

In this equation, ΔP represents the variance between static and dynamic pressure, while ρ signifies the density of CO_2. By referencing the system's temperature and pressure conditions, the CO_2 density, ρ, can be calculated. This allows the sensor to be precisely calibrated externally. Once validated, flow speed can be deduced from the differential pressure and density data.

In response, a design featuring a pitot tube within the extended Tri-Clamp pipe was conceived and prepped for welding, similar to pitot tubes for aeroplanes. The design included a small curved pipe to be welded inside the primary pipe, accompanied by a static and differential pipe connecting to both the chamber and the sensor, shown in Figure 18. The challenge lay in finding a sensor that could operate effectively within these pressure parameters, ensuring accuracy, and withstanding the difference between the internal sensor pressure and the external atmospheric pressure. A sensor that can be used is an MPX5100DP sensor from NPX, USA. However, just as welding was about to begin, an alternative, more straightforward design was identified. This design placed the sensor within the tee, enabling it to measure static pressure. The differential port was rerouted using a flexible tube inside the flow in the pipe, ensuring minimal disruption and flexibility in terms of adjustments and resolving the challenge posed by significant internal and external pressure differences in the sensor.

Because of time constraints, this sensor is not implemented into the final setup used for the experiments conducted in this thesis; however, this concept will be implemented for later publications.

The flow speed used in this thesis is determined by pre-measuring the fan speed by using an anemometer inside the extra tee section while sealing the chamber with a plastic bag to avoid outside air increasing flow speed.
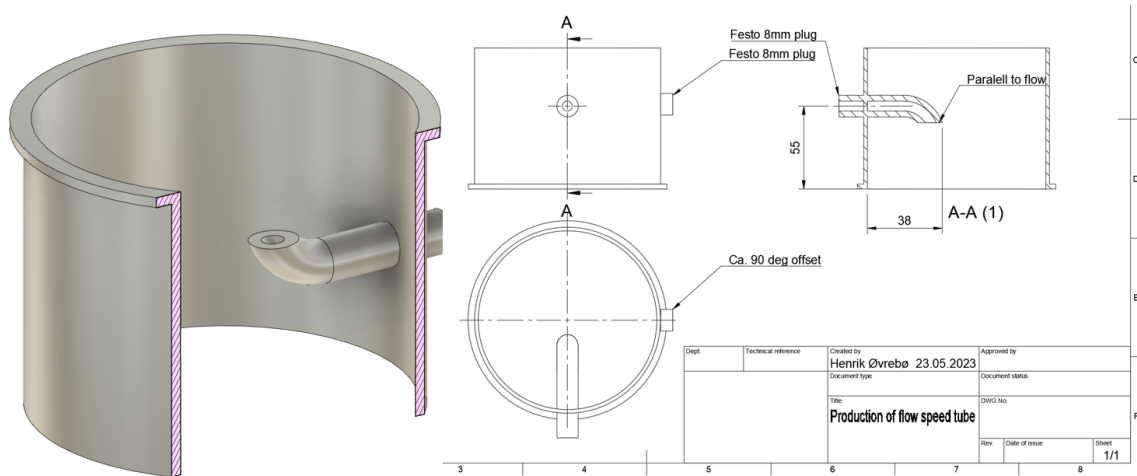
Figure 18: The concept sent to welding. However, after waiting for production to start for two weeks, the concept was changed

3.9 Festo fittings

Quick-release Festo connections were used to rapidly test the circulating concept with rapidly interchangeable pneumatics before a more permanent setup was made. These push-in fittings are made for pneumatic systems, allowing for easy and tool-free connection or disconnection of tubing, shown in Figure 19. They provide secure and leak-free connections, with a design that uses a collet mechanism and an O-ring for sealing. These fittings come in various sizes and configurations.

Figure 19: An 8 mm Festo connector with 1/4-inch tapered threads

3.10 Mounting of components

An essential aspect of this thesis is mounting all the different components. This section goes into detail about how the different designs were made. All of these components were 3D-printed.

3.10.1 General fastening to chamber

All the subsequent components were fastened to the chamber by removing the inside part up to the O-ring shape of the gaskets and replacing this with a 1 mm thick 3D-printed structure. The gaskets used in this thesis are shown in Figure 20. Different thicknesses were rapidly tested by 3D printing, and it was decided that a 1 mm thick ring would be securely fastened without compromising the chamber's sealing capabilities. The subsequent structures are modelled onto this chamber fastener.

Figure 20: The FDA-approved food-safe gasket from Dr. Component, USA in EPDM

3.10.2 Fan holder

The baseline for a fan holder is the way the fan manufacturer has placed the fastening screws. Based on this, a 5 mm centre fastening plate was made in the fan diameter. With different fans being tested, different designs were made, as seen in Figure 21.
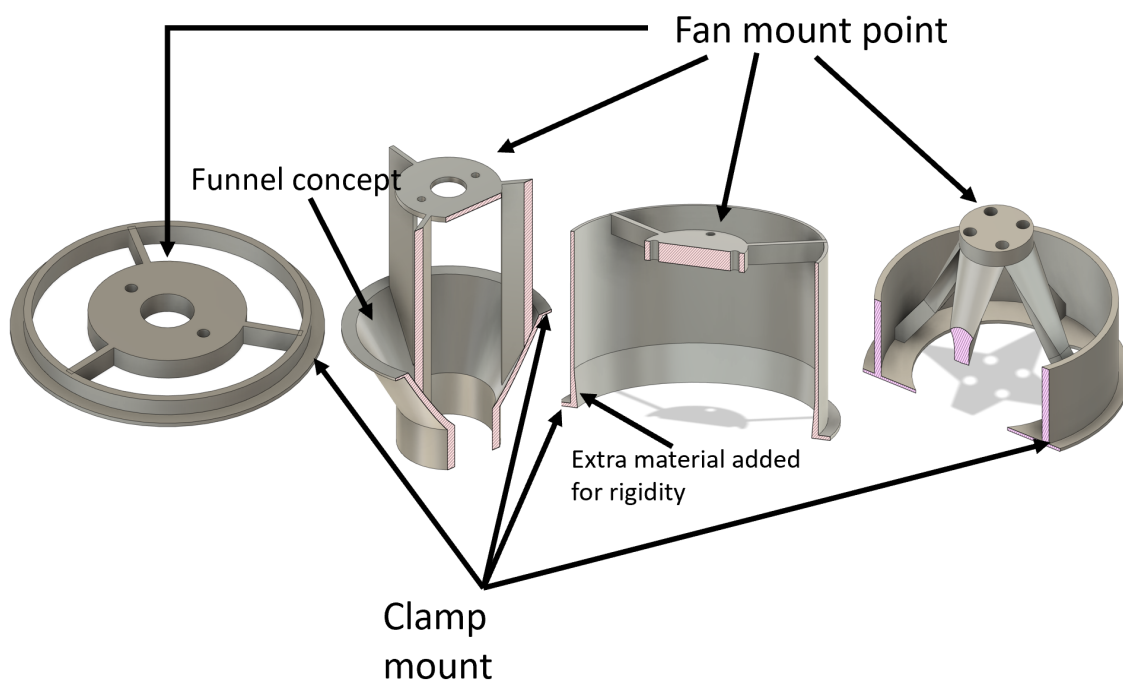
Figure 21: The different fan mount designs tried for the different motors and placement needs. Design number two from the left has a funnel after the blade to explore the design of narrowing the flow

The main idea is that the centre fastening plate is connected to the chamber fastener through 3-4 arms. These arms were rapidly tested, and the end design had four rectangular arms, with each side being 5mm. These arms were lofted to the entire surface of the centre fastening plate and were angeled so that the overhang was no issue and it could be 3D-printed in one piece. A centring ring was also incorporated to fasten the fan even better by dissipating any forces and vibrations into the pipe instead of the chamber fastener.

Depending on where the fan blade was required, the centre fastening plate was offset away from the plane of the chamber fastener. Since the last design was decided to be in the top of the tee, the centre fastener was required to be offset down the pipe to have room for the wires to be connected out the side of the tee while not getting tangled in the blade. This placement was chosen to have room for other components in the adjacent fastening section.

A fan funnel was also made, as seen in Figure 21. This was, however, not used for the reasons explained in Section 3.10.4

3.10.3   Wall in extra tee section to minimise turbulence

Since the placement of the fan was on the top of the tee, gas could flow inside the extra section of the tee and become turbulent. To remove this problem, a cover was designed, 3D-printed and mounted inside the extra tee section, shown in Figure 22. A small slit on the top was made for the wires leading to the motor.
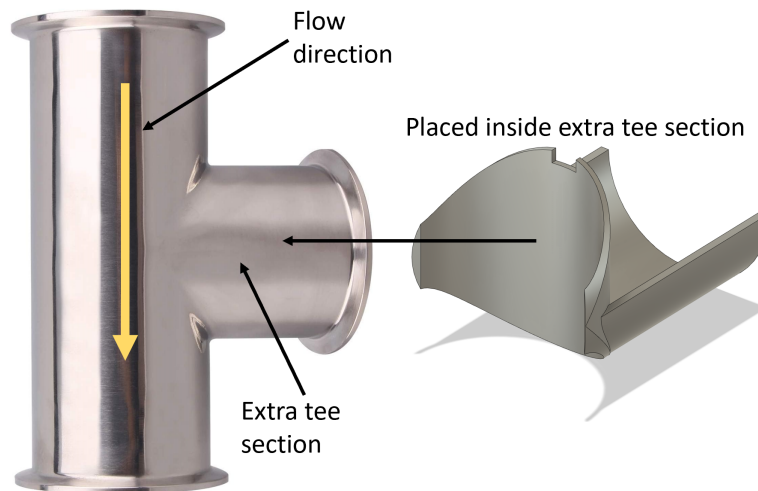
Figure 22: The designed pipe cover with a slit in the top for wires. The curves are exactly the inside radius of the 3-inch pipe

3.10.4   Mounting of movable orifice and pipes with narrower diameter

Because the scope of this thesis is also to make a setup to try to validate a simulation, it was desired to change both pipe diameters and have different orifice areas to spray CO_2 on the fish.

The movable orifice area is fastened like the pipe fastener in the 6-inch plate with screws on the inside to move the orifice up and down. The orifice itself is interchangeable with 3D-printed designs, shown in Figure 23.
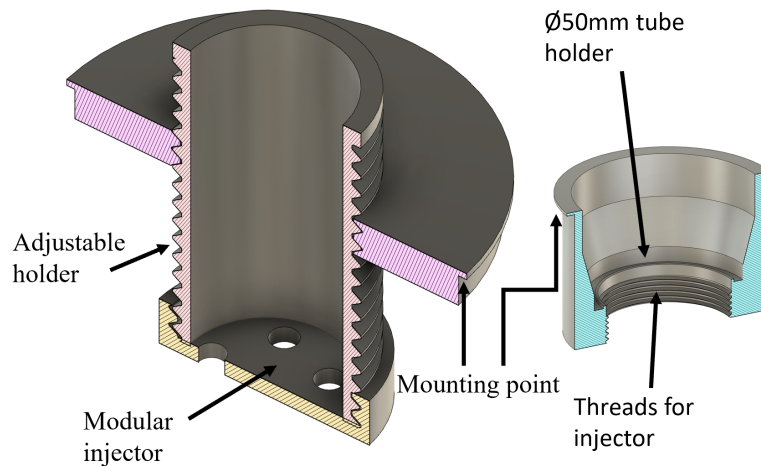
Figure 23: The adjustable orifice nozzle holder design. The design to the right was made to narrow the pipe flow to, e.g. 50mm by making a bottom holder with a ridge to hold a pipe with a smaller diameter than the 3-inch pipe

To incorporate different sizes of orifice area, a funnel at the top and fastening on the bottom is made. The pipe of a desired diameter is placed inside the slot, securing it from moving in the fastening plane and down in the chamber. A funnel, like the funnel in Figure 21, is made with the same slot on the top of the pipe to prevent the pipe from going up.

Although this modular design of fastening different diameter pipes inside the chamber was designed, it was decided not to test this in the experiments conducted in this thesis because of time constraints for experimentation. Therefore, the pipe with an inner diameter of 73mm is used. This concept is, however, to be implemented in future experiments and publications.

3.11   Pressure Testing

When working with high pressures and CO_2, safety is a vital aspect. Therefore the chamber was tested rigorously in terms of maximum pressure and leakage. The goal was to ensure a safe and effective environment, especially considering CO_2 can cause suffocation and fainting.

When the chamber and pneumatics were assembled, pressure tests were conducted to ascertain the system's safety. The first safety test was filling the chamber with water, then pressurising it to 8 barG using compressed air. Water was used to see major leaks quickly, and because it is incompressible, it was safer than using only compressed air (NiGen 2022). This test successfully certified the chamber's safety for handling pressures up to 8 barG. However, in this thesis, the chamber was operated at a maximum of 2 barG.

Subsequent pressure tests were carried out only with compressed air. The next test was a leak test over the time of an experiment. A successful test over two hours was done where no pressure reduction was seen at 6 barG.

Having completed this test with the unmodified setup, the incorporation of wires through the chamber to the electronics inside was necessary. For this problem, there were two solutions, either buy a connector to put wires through the chamber or drill holes and fill the hole and wires with sealing material Tec7. At this moment in the development process, speed was an important aspect because ordering a component would mean the electronics could not be tested inside for 1-2 weeks. Local stores only had connectors rated for IP67, which does not meet the requirements. Tec7 has a pressure resistance of 1.2 MPa, and the maximum pressure for this system was 0.8Mpa, so this should solve the problem. After a few days, a quote from an American company providing connectors suitable for this application came with a price of 90 $. However, since the speedy route was decided, the chamber was quickly ready for new pressure testing.
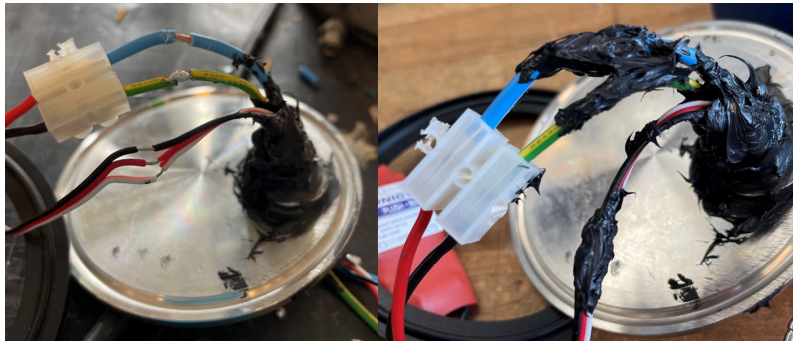
Figure 24: Leaking wires being stripped, separated and filled with Tec7. For the second Tec7 application, soapy water was used to make the application look more appealing

The modifications made before this test was drilling two holes for wire routing to the motor and scale. Wires were threaded through a Ø3mm hole in the 3-inch end cap in the tee and the bottom 6-inch end cap. These wires and holes were filled with Tec7. Tec 7 has a set time of 24h/6mm; this was deemed a sufficient set time. However, minor leaks were observed in the applied area, arguably because the sealant had not achieved full strength. After a reapplication and waiting three days, this area was sealed. There was still some leakage from gas escaping through the wires. This was solved by stripping the wires in one area and resealing them with an additional application of Tec7, shown in Figure 24. After this, airtightness was successfully restored, and a 3 barG pressure test affirmed that the chamber was sealed.

3.12 Electronics development

As the concept had different requirements for electronic components, it was decided that the electronic control system was prototyped with an Arduino. As described in Section 3.6, a fan was to be used to make the CO_2 flow, a weight was to be incorporated at the placement of the salmon and a flow sensor was needed. These were developed in parallel before everything was integrated. The finished electronics and their specifics are presented in Section 5.

Figure 25: Electronic speed controller used. This sends 5VDC back to the arduino

3.12.1 Electronics for motor

After initial tests with a desktop power supply, a 12V LiPo battery was used to power the brushless DC motors (BDCM). Unlike a regular DC motor that can be connected directly to DC power, a BDCM needs an electronic speed controller (ESC) to transform the DC to a Pulse-width modula-

tion (PWM) signal to operate the BDCM. The ESC is shown in Figure 25. Upon validating the idea, it was determined to utilise a 12V portable power supply. This decision was driven by the desire to avoid dependency on battery charging. Additionally, the lack of space within the system meant that the battery would have to be placed externally, further justifying the choice.

3.12.2 Scale combined with sample placement stand

Based on the initial experiment concept presented in Section 2.5, a sample placement stand, shown in Figure 27 for the experiment sample was modified to include a weight scale, shown in Figure 26. The stand was developed with a combination of a funnel and a stand. Both are 3D printed in one piece. In order to incorporate a weight in the stand, one of the arms was widened to 10mm, the size of the force gauge. This was offset with a stand, and on the other end, a 3D-printed sample placing stand was mounted with a slight offset. The two offsets are made in such a way that they transfer the forces correctly to the stand.

The sensor was calibrated using analogue values from the Arduino based on changes in resistance, and this calibration value was used to determine the actual weight in grams. To develop the scale, a tutorial was followed (Al-Mutlaq 2023). After some calibration issues, it was successfully implemented.
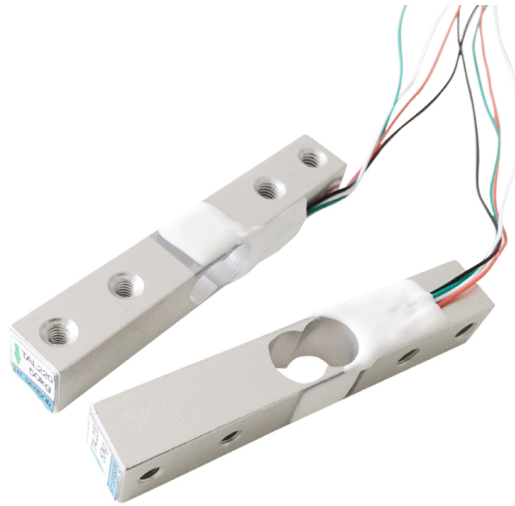
Figure 26: The TAL sensor bar

When testing with thin circulation tubes, it was discovered that the static pressure built up in the lower parts of the chamber due to the fan moving gas and the exit pipe being too small for that amount of gas; the scale showed a negative reading proportional to the speed of the fan. Therefore, the scale data is not included in the experiment done in this thesis but will be used for the next experiment using the new circulation pipes described in Section 3.16 and Figure 46.
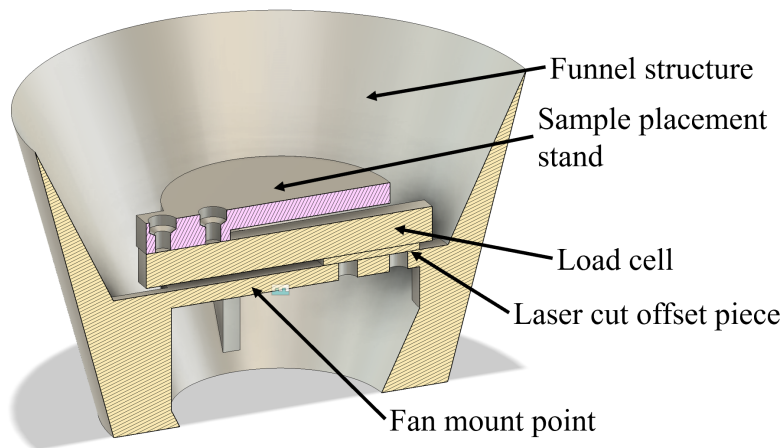
Figure 27: The final stand design with the weight sensor

3.13 CO$_2$ safety

Working with carbon dioxide (CO$_2$) in confined spaces, such as inside an industrial fridge, presents inherent safety challenges. If there are system leaks, the CO$_2$ can build up to dangerous levels and one can faint by suffocation. Up to this point, all tests was done with compressed air. It is important to analyse the hazards when working with different gases.

The primary way to mitigate this was to do rigorous leak testing with compressed air as described in Section 3.11 and vent all CO$_2$ after experiment completion out a window. In addition, an extra safety mechanism was incorporated, which is a CO$_2$ sensor to be worn by anyone who works up close with the chamber when CO$_2$ is in the system. During the experiments, the sensor showed no notable increase of % CO$_2$. There was, however, a slight increase when there were two people inside the fridge assembling the system, coming from exhaled CO$_2$. Therefore, it was concluded that these safety issues were handled safely with this experiment.

3.14 Temperature problems during full system test

When performing the first complete system test with the max speed of the fan at 3 barG, the chamber became very hot. The temperature measured after one hour was 39 °C while the ambient temperature was 23 °C. It was assumed this came from the ESC, and the ESC was moved outside the chamber.

To meet the temperature requirement, the entire setup is placed inside an industrial fridge to pre-cool and when the experiment is running.

Another measure to minimise heat inside the chamber was to purchase a SodaStream canister to supply pre-cooled CO$_2$ to the chamber, ensuring low temperatures. Because of time constraints, this was the setup that was used for the experiments in this thesis.

3.15 CO$_2$ measuring concept

When researching how to measure the CO$_2$ dissolution for an SGS process, a new concept of measuring CO$_2$ was developed. This will be developed further after this thesis.

The current way to analyse SGS samples is based on the same method of analysing MAP samples by indirectly measuring the CO$_2$, as described in Section 2.3 and 4.3. This unexplored concept focuses on measuring the CO$_2$ directly using a CO$_2$ sensor. The concept is based on the fact that gases want to create an equilibrium between a gas dissolved in, e.g. soda and the partial pressure

of the gas surrounding it. This is described by Henry's law in Equation 2. Instead of letting the sample reach equilibrium inside a sealed container and then measuring this indirectly, one can use, e.g. a commercial vacuum machine used in sous vide cooking to reduce the partial pressure of CO_2 to zero and store the gas evacuated in a flexible container like a balloon. All the CO_2 will not release immediately, so this is to be done several times until the bag does not inflate due to CO_2 escaping the sample. Then inside the balloon, a CO_2 sensor is placed to measure the CO_2 directly. In theory, all the CO_2 inside the balloon is from SGS and the surrounding air that was in the bag the first time it was sealed. Therefore, a comparative sample must be used to normalise these values. Issues with this concept are that one is relying on the accuracy of the CO_2 sensor, and you could introduce more CO_2 each time the bag is resealed to remove CO_2. One is, however, not relying on three machines that could introduce measurement errors while also only measuring the CO_2 indirectly. This concept will be developed further after this thesis.

3.16 Development of larger circulation pipes

As mentioned, small pneumatic 8 mm tubes were used to test the setup. With an inside diameter of 6 mm, there is not much space for the gas to circulate. Therefore, larger diameter circulation pipes are needed. However, due to time constraints, it was not time to finish these larger pipes and do the experiment for this thesis. Therefore, the experiment was done with the 8 mm tubes in this thesis. As of the delivery of this thesis, the larger pipes of 38 mm are finished and will be used in a future publication.

Using the criterium in Equation 3 and Equation 11 in a 6 mm pipe gives a mass flow rate of $0.3924 m^3/$min. Using this number and the same equation in the 73 mm section yields a max speed of 1.56m/s. The speed used in the experiment was 6-10 m/s, so this assumption of the speed of sound is wrong but still provides valuable insights into why the diameter of the circulation pipes needs to increase. Doing the same calculations with a circulation pipe of 38mm gives much more attractive numbers. The reason we get a higher flow speed in the experiment is both due to measurement errors and that the fan is both creating high pressure at the start of the circulation pipe and low pressure at the end, creating conditions for a higher volumetric flow transfer than what is assumed. There is, however, no experimental data to compare 6mm with 38mm regarding volumetric flow in this thesis.

4 Preparations and method

This chapter will cover the preparation and method for the experiment setup. It will also present the equipment and methods used to conduct the experiments.

4.1 Static chamber

The comparative experiments conducted in this thesis need a static chamber to be used as a baseline to compare the SGS experiment. This section presents the static chamber.
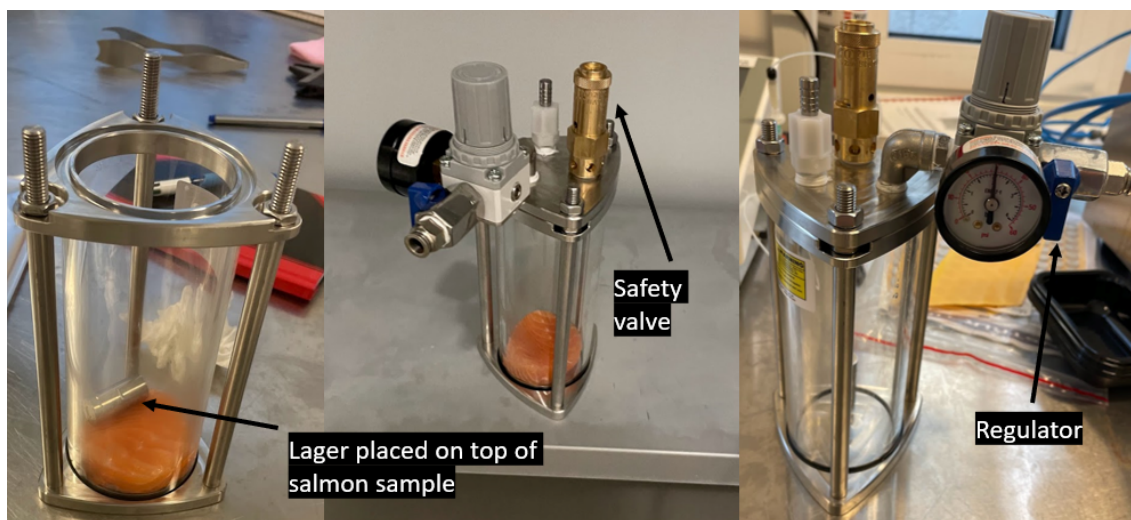
Figure 28: The static chamber 500ML-CTG from SR-TEK, UK; used in this experiment

The static pressure chamber 500ML-CTG from SR-TEK, UK, is a glass cylinder with an inner diameter of 65mm shown in Figure 28. Two 8 mm thick stainless steel end caps keep the pressure. The end caps are fastened with three long screws going from one end plate to another. On each screw, there are four bolts, two for each side. On one side, one bolt holds the centring plate of the glass, and the second presses the end cap down in the o-ring. This bolt layout is all equal on both sides and every screw.

In the top-end cap, there are two instruments of importance. One is a pressure safety valve, both acting as a safety valve such that the pressure inside the chamber does not exceed the maximum rated pressure of the vessel, which is 4 barG, while also being the point where the gas is evacuated both before and after the experiment. Next to it is a regulator valve with a gauge to regulate the desired pressure inside the vessel while the vessel is connected to an 8 mm quick-release connector to an external CO_2 supply.

4.2 Salmon cutter

A steel salmon cutter with an inner diameter of 65mm has been machined to perform the subsequent experiments and is shown in Figure 29. The cutter has an outer chamfer down to a sharp edge to cut equal sizes of salmon pieces. Another ring has also been machined with the same inner diameter but with a height of 20mm to guide the cut of each piece to the same height. This is the first step in an SGS experiment. After this, each piece is weighed and logged before the experiment starts.
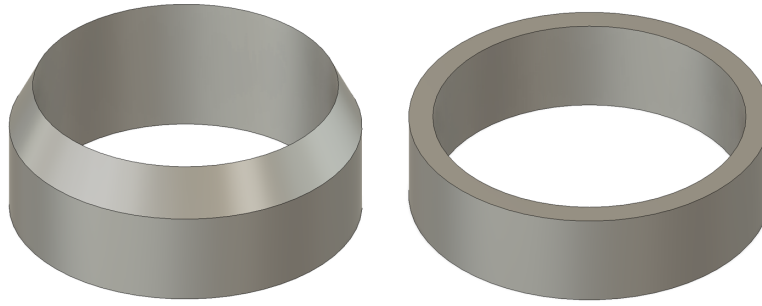
Figure 29: Salmon cutter and guide

4.3 Comparative experiment design

The following section describes the comparative experiment for both static and flow chambers. Where it is explicitly stated, the method differs.

Atlantic salmon was transported to NTNU, Trondheim, right after being slaughtered at a slaughterhouse nearby. The salmon was transported on ice in polystyrene (EPS) boxes. When arriving at NTNU (around 3 hours after slaughter), the salmon used had no signs of rigour mortis. The fish was immediately scaled and filleted. The fillets were cut as described in Section 4.2. 9 pieces started on ice in the styrofoam box, shown in Figure 30, while two samples were used for each SGS experiment.

Figure 30: Cut salmon samples in the styrofoam box on ice, waiting for the next experiment

All equipment surfaces were cleaned with soapy water, and parts close to electronics were cleaned with isopropyl alcohol before being prechilled to the experiment temperature of 3 ℃ the day before the experiment. When the experiment commences, a weighed piece of salmon is placed in the chamber bone side up, i.e. the surface that was just cut. The O-ring/gaskets are inspected for any debris or water present before the chambers are sealed with a wrench. An outside tank

fills the static chamber with CO_2, while the flow chamber gets prechilled CO_2 from a SodaStream canister. The valves controlling pressure inside the tanks are slowly opened while the gauges are observed. When the pressure hits the desired pressure, the relief valves are opened just enough for some hissing to occur. This is the gas leaving the chambers. This step ensures the chamber has 100% CO_2 and not some mixture of CO_2 and air. This is done for 2 minutes while venting the CO_2 out a window with a CO_2 sensor on the person doing the experiment. The CO_2 sensor was close by the entirety of the experiment. The CO_2 sensor is an Aspida Portable Gas Monitor from Analox, UK, which monitors CO_2 and O2. When this is complete, the experiment is considered started. The static chamber is placed in the industrial fridge together with the flow chamber at the desired temperature, which for this experiment was 3 °C. The flow chamber's fan is turned on at a speed of 6m/s. The experiment runs for one hour before the chambers are evacuated and opened.
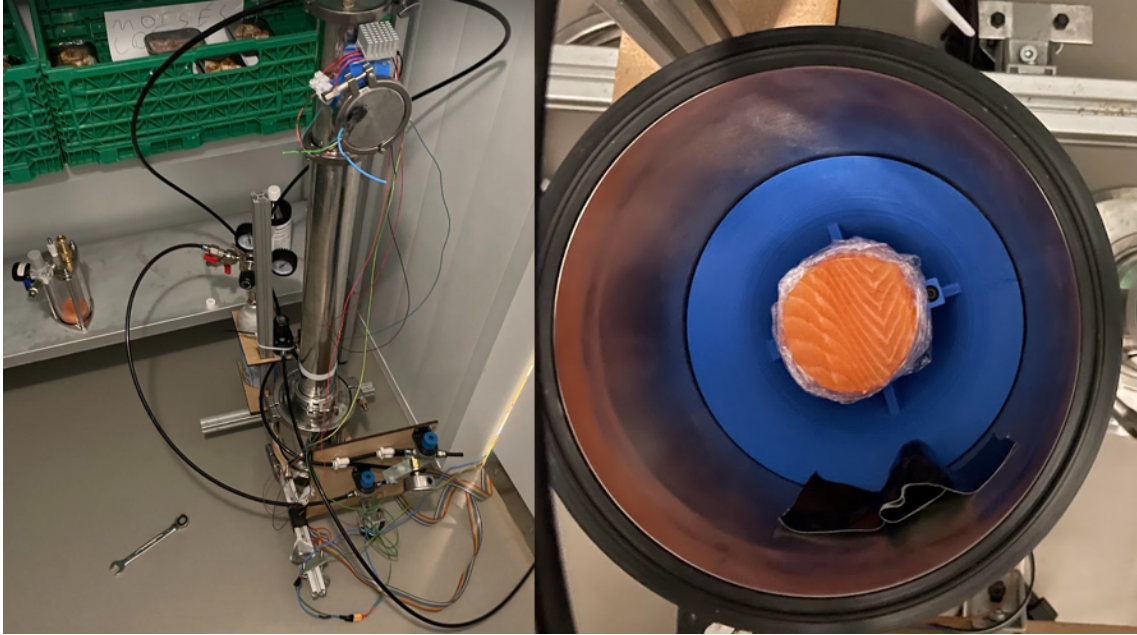
Figure 31: Static and flow chamber in fridge

4.3.1 Packaging of the samples

When each experiment was concluded, the two samples, together with one control sample from the styrofoam box, were repacked into 230 ml semi-rigid crystalline polyethylene terephthalate trays (C2125-1A, Færch Plast, Denmark) using a machine for packing and sealing trays (TL250, Webomatic, Germany). The trays are shown in Figure 32. The samples are numbered, e.g. 2.2, where the first number indicates the experiment: 1 is flow, 2 is static, and 3 is the control. The second number indicates the replication number, i.e. if it is the first, second or third replicated experiment. E.g., 2.2 is the second static sample.

Figure 32: Sample being weighed in tray

The air inside the packages was evacuated before being flushed with food-grade CO_2 (60%) and N2 (40%), using a MAP Mix 900 gas mixer (Dansensor, Denmark). The headspace gas composition was analysed using a Checkmate 9900 oxygen and carbon dioxide analyser (PBI-Dansensor, Denmark), shown in Figure 33. Gas composition measurements were conducted in empty trays immediately after packaging and in all trays at the end of the storage period (189 hours). Each time three samples were packed, three additional empty trays were packed to measure the average CO_2 content. The average CO_2 content measured was 61.7 % with a standard deviation of $\pm$ 0.3%.

Figure 33: Sample being analyzed by the CO_2 analyzer

4.3.2 Method of CO_2 analysis

To analyse the dissolution of CO_2 in the samples, a gravimetric method based on the procedure outlined by B. T. Rotabakk et al. 2007 and modified by Abel et al. 2018 was done (A. N. Jakobsen et al. 2022).

The change in CO_2 concentration (mg CO_2/kg) in the samples was analysed at regular intervals. This was done by immersing the packaged trays with the salmon samples underwater and gauging the buoyancy force using a texture analyser (Stable Micro System Ltd, TA-XT plus, Godalming, UK), thus calculating a package headspace.

Figure 34: Submerger

The trays were submerged at a controlled rate of 2 mm/s until submerged. The trays were held underwater for 20 seconds to attain stability. Buoyancy force measurements were taken in the last 10 seconds at 1-second intervals, totalling ten measurements. The average of these measurements was used for subsequent analysis, with all readings adjusted to account for the actual atmospheric pressure.

Analysis of this data with Equation 1 yields the results outlined in Section 5.

4.4 Quantitative sensory analysis experiment

Following the method described in Section 4.3 for the flow chamber, a quantitative, blind, tasting experiment was conducted (Ruiz-Capillas and Herrero 2021). This experiment was done at Trolllabs, and the SGS procedure was therefore done at room temperature, around 23 °C.

The freshest available Salmon from Salma, Bømlo, Norway, was purchased on the day of the experiment, placed in the flow chamber, and followed the procedure in Section 4.3. For this experiment, three samples were used. One sample was unprocessed as a control; one piece was

treated with SGS at 3 barG for 30 minutes, while the last was treated with SGS for 1 hour. The control sample was placed next to the setup to experience the same temperature as the other samples. The flow fan was turned on at 10 m/s. The tasting commenced immediately after the last sample was finished to experience the direct effect of CO_2 on salmon. The salmon was tasted raw. six volunteers got a plate divided into three with the three samples marked A, B and C, as not to say what was done with the different pieces. They were not primed in any way other than that a sensory score below 5 was unacceptable for eating. This rejection level is similar to the method deployed in B. Rotabakk et al. 2008. The participants were encouraged to both write open thoughts about the flavour and overall thoughts while afterwards giving open feedback in an open discussion. This was to gain interesting feedback on the experience rather than the actual flavour because the flavour does not represent an SGS product to be sold in a supermarket since the CO_2 fizz would normalize inside a packet.
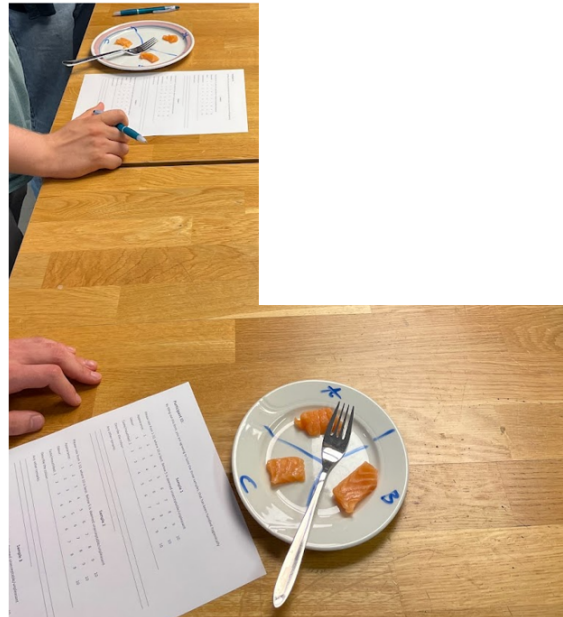
Figure 35: The sensory experiment

5   Results

This chapter will present the final flow chamber design results and experiment data. First, the final flow chamber design will be presented. Second, the comparative experiment data, including dissolution of CO_2 in the samples, temperature and pressure data, and lastly, quantitative sensory analysis experiment data will be presented.

5.1   Flow chamber presentation

This section describes the flow chamber shown in Figure 36. The Figure shows an overview of all the components, while the proceeding sections go into detail about each subsystem. First, the Tri-Clamp assembly is presented before the pneumatics and the P&ID for the system. Lastly, the electronics are presented.
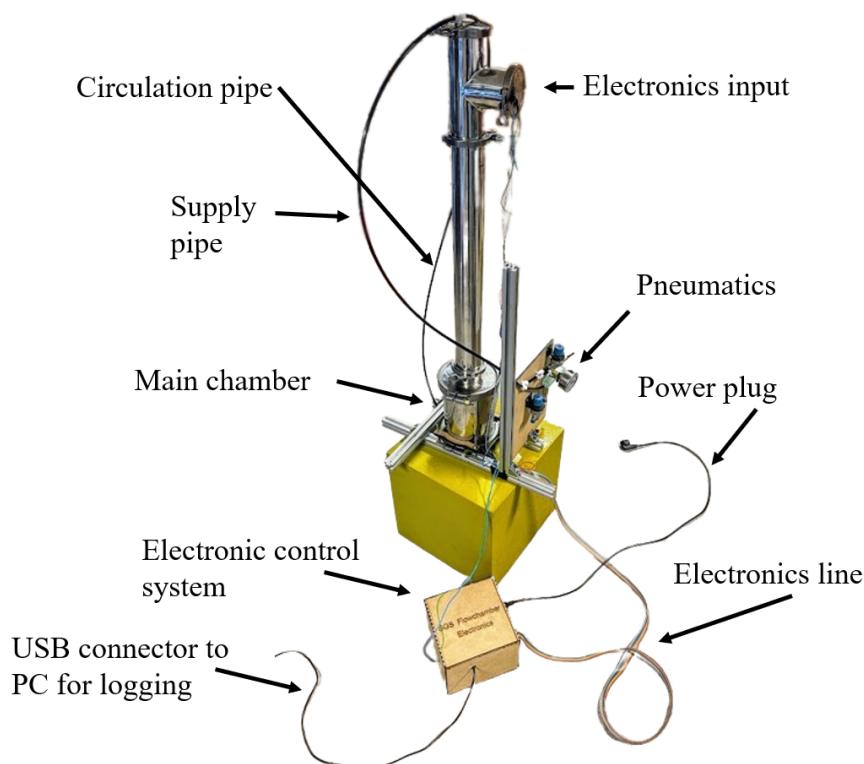
Figure 36: Overview of the flow system. All electronics outside the chamber are connected inside the electronic control system box, which is placed outside the fridge during the experiment. This picture does not show the SodaStream canister

The flow chamber is a steel construction based on several Tri-Clamp parts able to withstand 10 barG, as discussed in the prototyping chapter, and shown in Figure 37. The chamber is built around a main chamber. This is a 6-inch diameter and 8-inch long Tri-Clamp pipe with end caps. The top-end cap narrows down to a 3-inch ferrule. This 3-inch connector is connected to a 60-cm-long pipe. This pipe is subsequently connected to a 3-inch tee section to more easily incorporate different components due to difficulties in incorporating the flexibility and modularity of components in a 3-inch pipe. The Tee ends with a 3-inch end cap. All sections are sealed with a food-safe (FDA approved: 177.2600) gasket made from the rubber-type EPDM and standard Tri-Clamp clamp. The exception is the 6-inch pipe, which has high-pressure clamps due to the comparably lower pressure certification of standard clamps when the pipe diameter increases (Hygienic Stainless Steel 2023).

Figure 37: Overview of only the Tri-Clamp components used in the assembly

5.1.1 Pneumatics

This subsection goes into detail about the pneumatics used for the setup. Figure 38 shows all the components used to handle the gas between the lines. The gas supply lines are connected together.
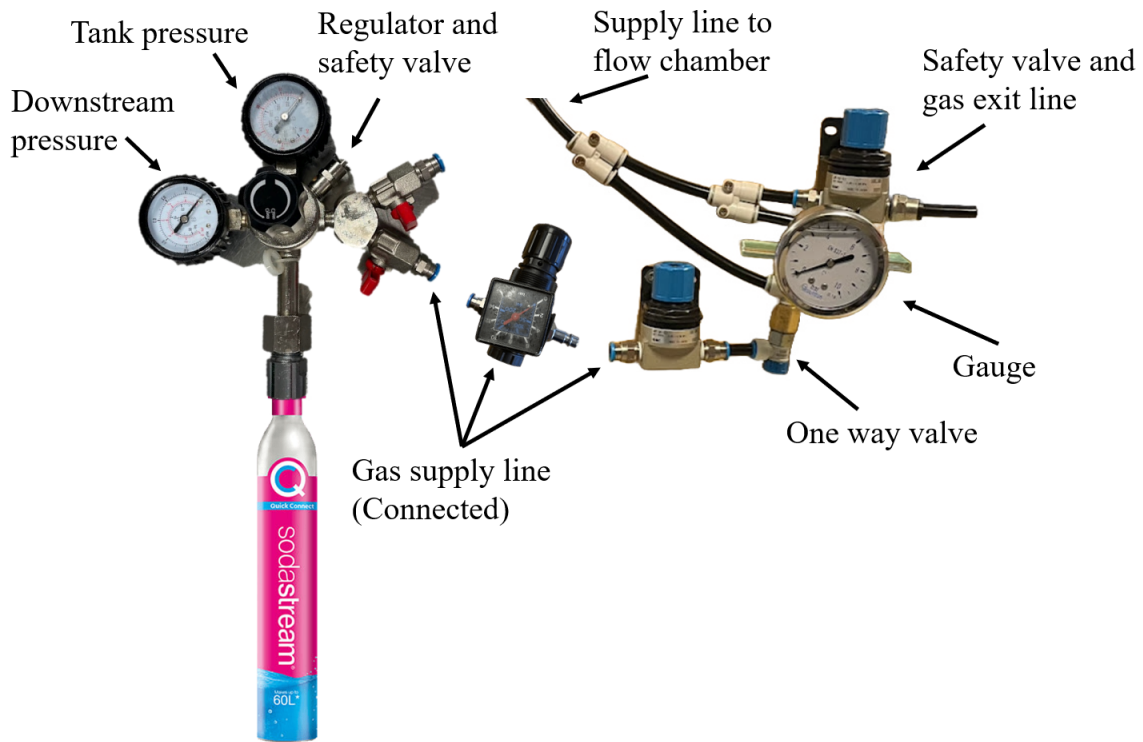
Figure 38: The overview of the pneumatic components

The modifications made to the off-the-shelf Tri-Clamp components mentioned in Section 5.1 are that each end plate has added connectors to add 8mm Festo quick connectors to attach tubes of CO_2. The connectors are fastened with 1/4-inch R and thread tape, meaning the threads are BSP tapered for a good seal in a pressure system. The threads in the cap were subsequently made with a straight BSP 1/4-inch tap. Tubes connect the bottom connector to the top, while a line split is incorporated into the circulation pipe to supply CO_2 to the system, both for filling and after filling, should the pressure reduce due to the absorption of CO_2 in the salmon. The supply valve is an R72G-2GK-RMN valve from Norgren, UK, with a spring that opens if the downstream pressure is too low, while the pressure relief valve (PRV) from SMC, USA is the opposite, where it opens should the upstream pressure become too high. Because of hysteresis in the spring, there needs to be a sufficient pressure drop/increase for the adjustment to be made. The PRV is set to its maximum 6.9 barG. This relief valve is connected to a long 8mm tube to exit the gas through a window in an emergency, during air flushing of the system and after experiment completion. A gauge is also implemented in the line to look at the pressure inside the tank. The details of the components in the process are shown in Figure 39.

The two valves are next to each other because the SMC (blue) valve is used for testing with compressed air, while the R72G (black) valve regulates according to downstream pressure and is used during experiments.
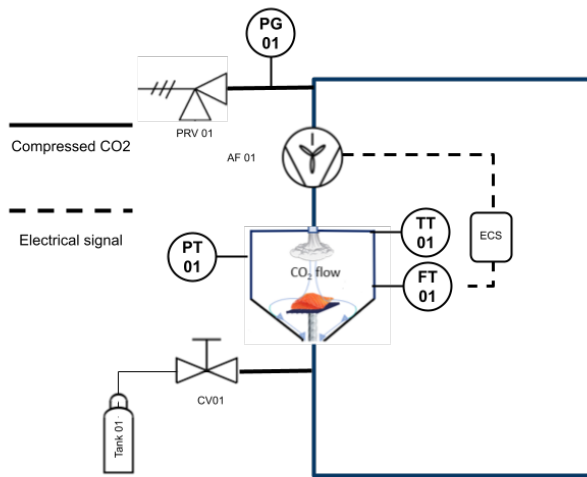
Abb.	Name	Qut.
PT	Pressure transducer	1
PG	Pressure gauge	1
TT	Temperature transducer	1
FT	Force transducer	1
PRV	Pressure Relief valve	1
ECS	Electronic control system	1
CV	Control valve	1
Tank	Sodastream 130L tank	1

Notes:
All components are rated for 7.9 barG
ECS are an Arduino
TT01 and PT01 is one single transducer

Figure 39: P&ID of the system. This shows all the components and how they are placed relative to each other. PT and TT are one component. The pressure rating of the system is 6.9 because that is the max rating of PRV01

5.1.2 Electronics

To gather data from the experiments, several sensors were integrated. This subsection describes each one. The motor, electronic speed controller, force transducer and amplifier schematic is shown in Figure 40.
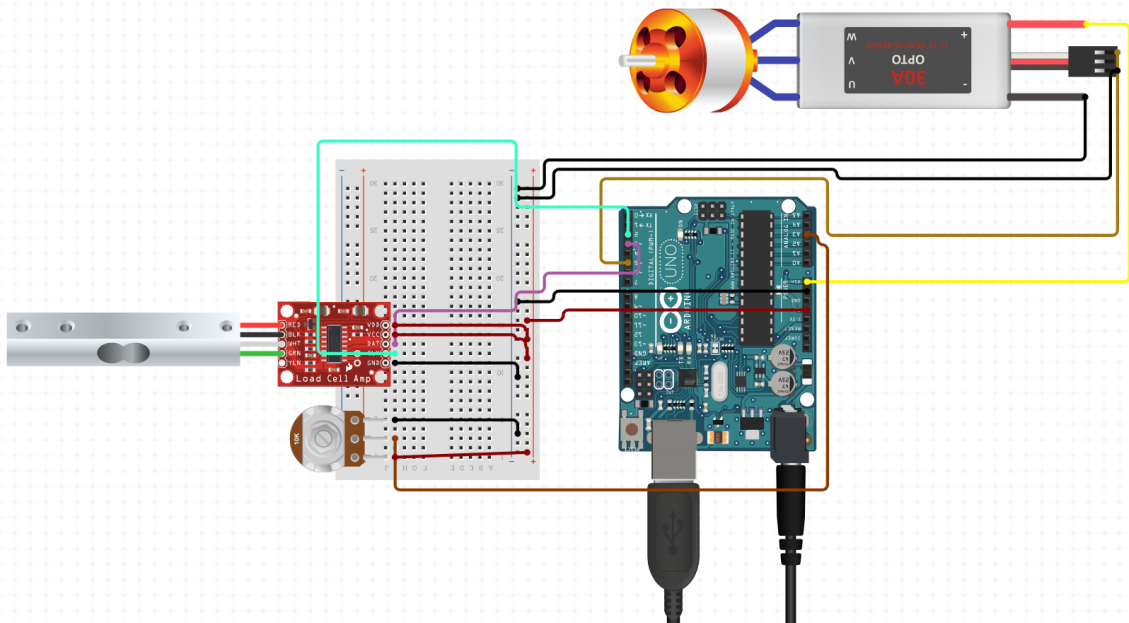
Figure 40: Schematic of the electronics. The power supply is connected directly to the ESC and not to the Arduino, but that has no practical difference

- Temperature and pressure sensor

  - An EBI 11 Series (Ebro, Germany) lager was used to log temperature and pressure during the experiments. This lager has a temperature accuracy of ± 0.1 °C and a pressure sensitivity of ± 20 mbar. This was placed inside the camber next to the salmon piece to see how the parameters changed during the experiment.

- Weight sensor

  - At the placement of the salmon, a weight sensor was integrated. This was to see how the force on the salmon changed as a function of the wind speed produced by the fan. The sensor was made from a TAL220 parallel beam load cell (HTC-sensor, China) connected to a Load Cell Amplifier, HX711 (AVIA semiconductor, China). This was needed to amplify the small change in resistance coming from the strain gauges embedded in the parallel beam load cell. This was then connected to the digital port of the Arduino. Because this sensor had negative readings when the fan was turned on because of static pressure build-up, the scale data is not used in the Results.

- Fan from a brushless DC motor

  - To push the CO_2 around the system, an EMAX ECO II Series 2207 2400KV brushless DC motor (EMAX, USA) was used. This produces 2400RPM for each volt increase, giving a large range of speeds. An ESC controls the brushless DC motor to modify the DC current to pulses given to the motor to drive it. To variate the fan speed, a potentiometer is added to the circuit.

- 12V power supply

  - To power the Arduino and fan during the experiment, a 12V power supply was used. This is easily plugged into the wall and supplies all the needed power required for the experiments. The power supply is connected to the ESC, which supplies the motor while also returning 5V to the Arduino as power.

5.2 Comparison experiment

This section presents the calculated dissolution of CO_2, together with the data collected with the pressure and temperature lager.

5.2.1 Dissolution of CO_2

Figure 41 shows the amount of dissolved CO_2 in MAP over the sampling time after the SGS experiment. The dissolution that happens after packing is from MAP. It is this the dissolution numbers refer to. Dissolution from SGS is dissolution from the experiment, meaning the lower the dissolved value [ppm] is, the more CO_2 has dissolved from SGS.
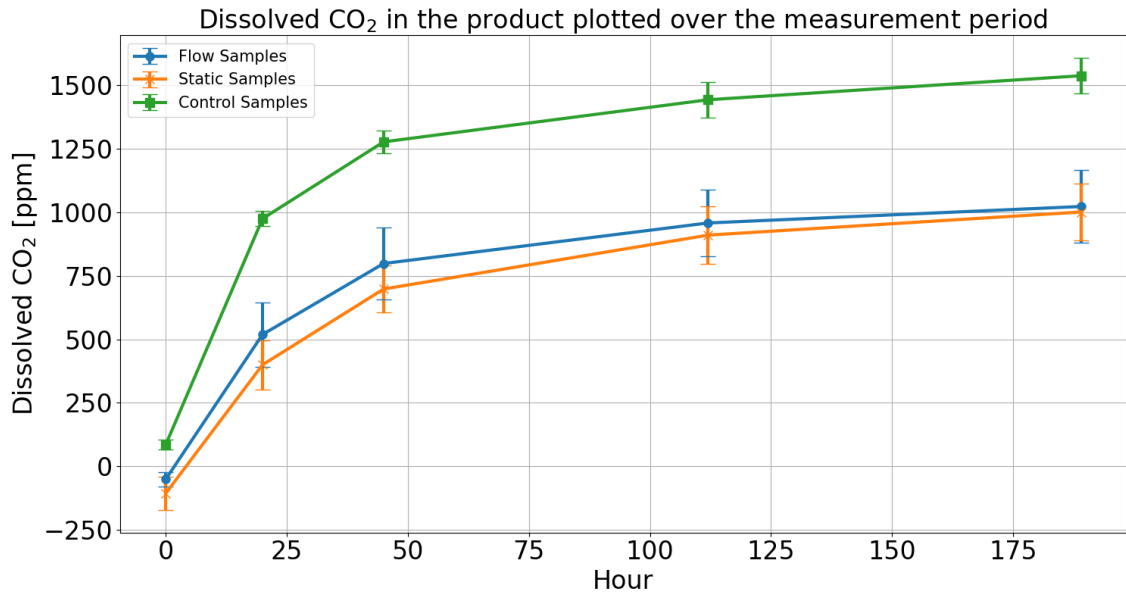
Figure 41: The plot shows how the changes in CO_2 are over time from right after the SGS experiment until 189 hours after packing

Dissolved CO_2 was calculated as described in Section 2.3 and 4.3. The first sample was taken at hour 0, the subsequent measurement was taken at hour 20, and the third and fourth samples were taken at hour 45 and 189, respectively.

The control sample shows a much higher dissolution of CO_2 than the static and flow samples. The flow samples have slightly higher dissolved CO_2 in the beginning, which plateaus at almost equal value at hour 189. The error bars indicate the standard deviation. The standard deviation is much higher for SGS samples than that for the control sample.

5.2.2 Pressure and temperature data

This subsection shows the lager data from experiments 1.1, 2.2 and 3.1. The y-axis is fixed to compare the relative values between the experiments. The start and end of the experiments are included to see any effects like high lager temperatures affecting the measurements.
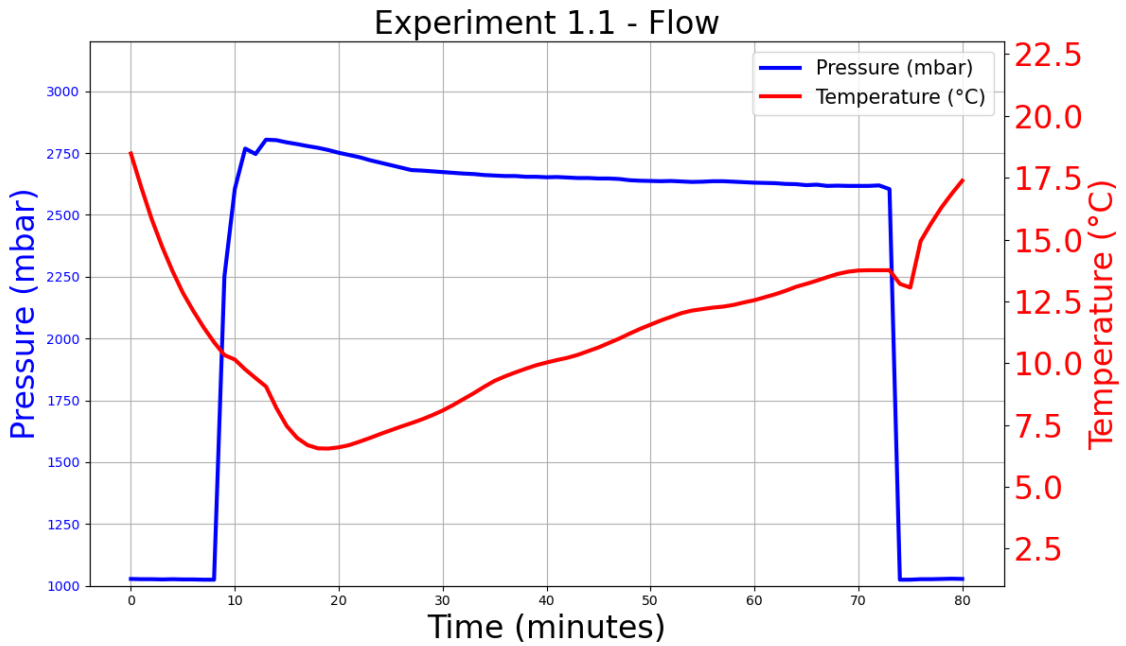
Figure 42: Temperature (Red) and pressure (Blue) plotted over the first flow experiment period gathered from the EBI lager

Experiment 1.1 was the first flow experiment. Here, the setup was prechilled overnight. The temperature for the flow experiments drops faster compared to the static one. The temperature subsequently steadily increases. The lager sits in the chamber for 8 minutes before the experiment starts.

The pressure is increased to 2 barG, and the little dip at the start is the flushing of the system. The pressure drops to 2600mbarA towards the end.
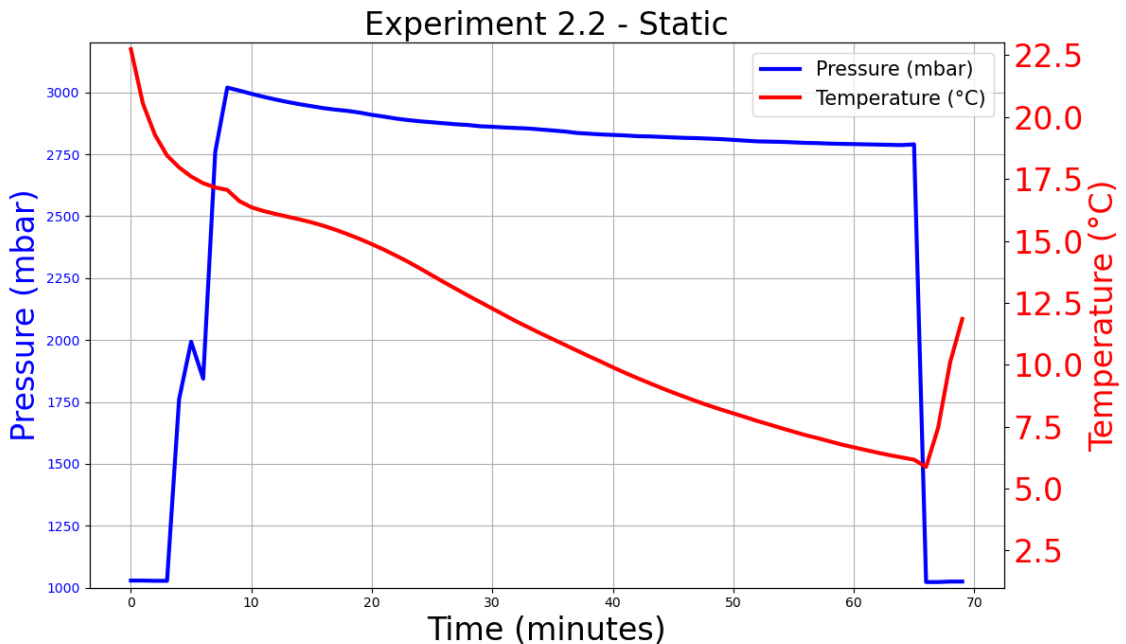
Figure 43: Temperature (Red) and pressure (Blue) plotted over the second static experiment period gathered from the EBI lager

Experiment 2.2 in Figure 43 shows the data from the second static experiment. The temperature slowly decreases while the pressure drops to 2800mbarA
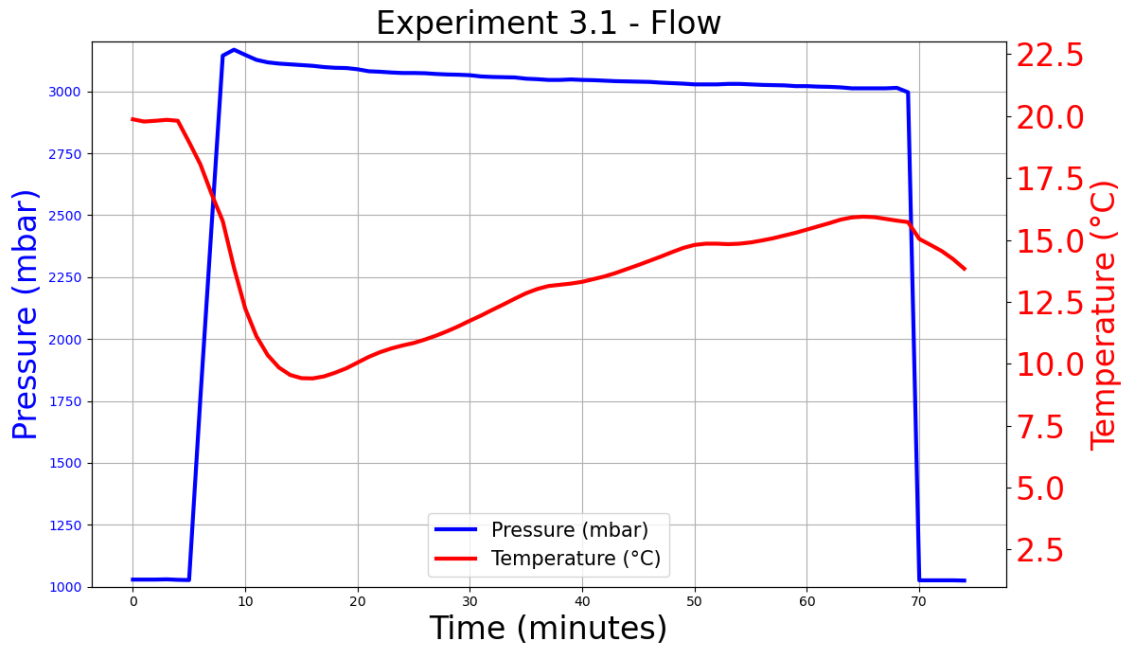
Figure 44: Temperature (Red) and pressure (Blue) plotted over the third flow experiment period gathered from the EBI lager

Figure 44 shows the last flow experiment. Here, the pressure in the chamber is higher than 2barG, steadily dropping. The temperature drops to 10 degrees C and steadily increases. The lowest temperature here is higher than for experiment 1.1. In this experiment, the experiment starts quickly after the lager is placed.

	1.1	2.2	1.3
Avg pressure [mbarA]	2671.2	2856.2	3052.5
% change from 2.2	-6.9%	0.0%	6.4%
Avg temperature [deg C]	10.2	11.1	13.0
% change from 2.2	-8.2%	0.0%	14.9%
Total dissolved CO_2 after SGS	1154.6	1139.1	788.3
% change from 2.2	1.3%	0.0%	-44.5%

Table 1: Data table

Table 1 shows the calculated average values from the three experiments. The data's first two minutes and the last minute are removed to remove the flushing period and potential errors. The relative difference for experiments 1.3 and 3.3 relative to 2.2 is also calculated in %. Comparing 1.1 and 2.2, the dissolved CO_2 from MAP is higher in 1.1. The temperature is, on average, < 1 °C lower in 1.1, while 2.2 have higher pressure. Sample 3.1 has around 200 ppm more dissolved CO_2 from SGS, compared to 2.2, giving a dissolved difference of 44.5%. The pressure and temperature are 200 mbarA and 2 °C higher, respectively, in 1.3 compared to 2.2.

Experiment	Start	End	Total absorption (End+Start)
1.1	-21,72	1176,34	1154.62
1.2	-87,87	1059,97	972.10
1.3	-43,82	832,11	788.29
Average absorption			971.67

Table 2: Start and end values for PPM dissolved CO_2 in the three flow experiments. The bottom line is the average of the total between the start and end of each experiment

Experiment	Start	End	Total absorption (End+Start)
2.1	-168,68	950,12	781.44
2.2	-15,96	1155,01	1139.05
2.3	-135,29	898,00	762.71
Average absorption			894.40

Table 3: Start and end values for PPM dissolved CO_2 in the three static experiments. The bottom line is the average of the total between the start and end of each experiment

Table 2 and 3 shows the starting values, ending values, and the total absorption for PPM dissolved CO_2 for the flow and static experiment. The total absorption is calculated by adding the negative starting values to the end values. The three flow experiments have higher dissolved CO_2 from MAP on average compared to the static experiment.

5.3 Quantitative sensory analysis experiment

This section presents the data and the general feedback collected in the sensory analysis experiment.
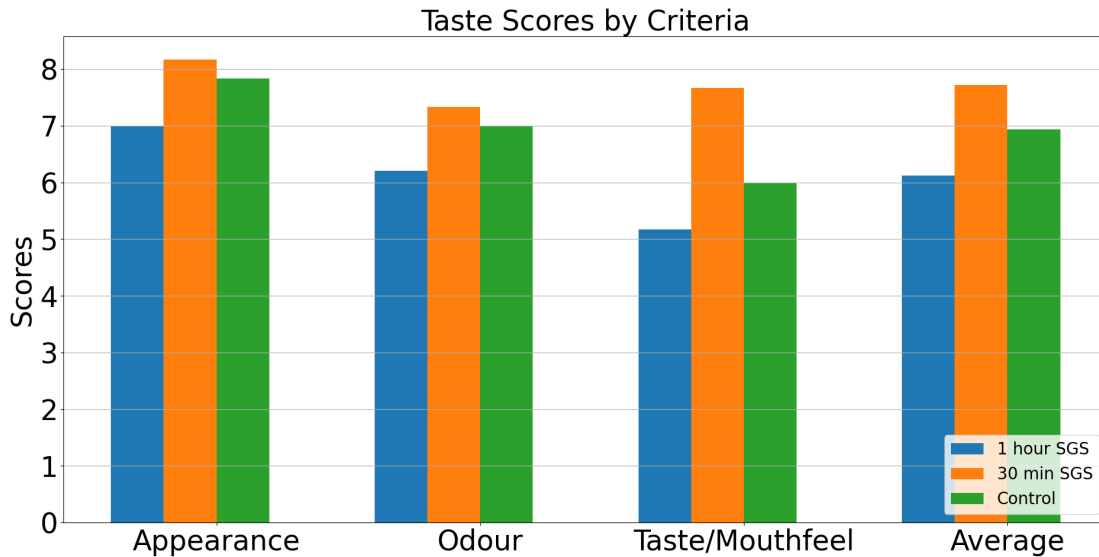
Figure 45: Participants' response in the sensory analysis experiment

Figure 45 shows the average score from 1 to 10 for the three criteria: appearance, odour and taste/mouthfeel. The average of these scores is also presented.

The 1-hour SGS scored worst overall, while the 30-minute SGS scored better than the control in all categories. There was not much difference in odour; however, for taste/mouthfeel, there were relatively large differences.

6 Discussion

This section discusses the results and data and subsequently suggests design improvements based on the comparative and sensory experiments. This section also discusses the prototyping and the overarching design challenges that were discovered through the developments done in this thesis.

6.1 Comparison experiment

The total absorption is calculated by adding the negative starting values to the end values. This is done to compensate for the fact that the amount of gas in the headspace increases as soon as the sample is packed because CO_2 desorbs from the sample to the headspace. This could be because the sample's surface is so saturated with CO_2 that the gas wants to equalize to the headspace. However, when the gas in the surface has the time to dissolve deeper into the product, the gas can again dissolve into the product's surface. This continues until the whole sample is saturated. It is the opposite effect for the control sample, which rapidly dissolves CO_2 because nothing is dissolved in the surface.

6.1.1 Difference between flow and static

The flow and static samples have very similar dissolution curves. Figure 41, Table 2 and 3 shows different levels of dissolved CO_2 for the static and flow experiments when the measurement period starts at t=0. Higher desorption of CO_2 at this time for the static sample indicates a greater concentration difference between the surface and headspace. The higher CO_2 concentration on the surface of the static sample could be due to the lower temperature at which the static experiment is conducted compared to the flow experiment. This is because Henry's constant is different at different temperatures, and thus the maximum concentration in Equation 2 is different. However, since the two samples plateaus at the same level, the two experiment's samples had arguably similar amounts of total CO_2 dissolved in the samples when the measurement period started.

Research also suggests that when fat content increases, the solubility also increases as more fat becomes available as a liquid to dissolve into (M. Jakobsen and Bertelsen 2004). This increased dissolution happens above 2 °C for high-fat products and below 2 °C for low-fat products. It could also be interesting to identify whether salmon should be processed at a higher temperature than 1 °C. However, the temperatures used in this thesis are way over this and thus, the difference can not be investigated.

6.2 Experiment setup

As shown in Figure 42, 43 and 44, the temperature and pressure conditions (experiment parameters) differed for each experiment. This is not good and shows itself in the error bars in Figure 41. The error bars are the standard deviation of the samples. The error bars for SGS samples are much larger than the control samples. This comes from the fact that each experiment had different temperature and pressure conditions, contributing to the different dissolution of CO_2. However, some intrinsic measurement deviations are shown in the error bars for the control sample. In addition, the experiment parameters are different for the flow vs static experiments. This means there is much uncertainty regarding what parameter affects the dissolution of CO_2. However, because of previous research, there are some conclusions to be drawn from this.

As seen in Table 1, there are differences between experiments 1.1, 2.2 and 1.3. 1.1 have 6.9% lower pressure and arguably no difference in dissolved CO_2. Pressure has a much stronger effect on dissolution than temperature, as the perturbation plot in M. Jakobsen and Bertelsen 2004 suggests. On the other hand, 1.3 has 6.4% higher pressure than 2.2 while having 44.5% higher dissolution from SGS. Had experiment 1.1 been conducted at a similar temperature and pressure as 2.2, one could predict that the dissolved CO_2 would be greater in 1.1 than in 2.2, like in 1.3. However, since there is only temperature and pressure data on those three experiments, it is hard

to conclude definitively. However, this shows there is potential for the flowing SGS technology to perform better than the static experiment when one compensates for the different experiment characteristics.

In addition, there is higher total average absorption from SGS in the static experiments than in the flow seen in Table 3 and 2. This is coming from high dissolution from experiments 2.1 and 2.3. However, looking past the conclusion of their similarities is hard when there is no temperature and pressure data to compensate for. Therefore, it is only possible to compensate for experiments 1.1, 2.2 and 1.3.

Based on the data in the results, there is arguably no difference in CO_2 dissolution between the flow and static experiment. We know that decreased temperature and increased pressure affect the dissolution positively. Since the flow setup experienced higher temperatures and lower pressures than the static ones, we can conclude that the flow setup provides better SGS absorption if improvements to the setup are made. This needs to be verified with more experiments and testing.

6.3   Experiment improvement

For the flow setup, there are other ongoing developments and lessons learned. This section describes improvements to the design, experiment and procedures.

6.3.1   Heat generation

Based on the data in Section 5, the most pressing issue is the heat generation in the flow system. This is arguably because of the fan. New tests with other fans should be done to determine the amount of heat generated for the experiment. In addition, larger circulation pipes are now implemented into the system as discussed in Section 3.16 and 7 and shown in Figure 46. This could also ease the strain on the fan. The sensory experiment was run with the fan at 10m/s, but due to increased temperature, this was reduced to 6 m/s, and the ESC was moved outside the chamber without signs of improvement. In addition, even though the fridge temperature was set to 3 °C, the regulator was very insensitive; therefore, the cooling system sometimes did not start until it reached 7 degrees, and then the temperature dropped to 1 °C. A better fridge should, therefore, be used for the next experiments.

If significant heat is still generated in the system, more improvements need to be made. One concept is to develop a heat exchanger on the top of the pipe, after the fan, to cool down the gas. This can be supplied with a heat reservoir of a 3D-printed "bucket" around the pipe filled with ice water to cool the system. Another solution is to water-cool the fan. This, however, can be hard due to the large difference in pressure outside and inside the tank. This system would need to have welded pipes and a large bucket outside with a pump supplying fresh water. If the water should be pressurized inside the tank, then the water reservoir also needs to be pressurized, which there is no room for. Through the experiments conducted, it is evident that the system cannot rely on the cooling of the fridge to keep things cold. The fridge should only maintain the temperature, not working on cooling other parts.

6.3.2   Pressure reading improvements

Before the experiments, it was assumed that equal pressures would be achieved by reading the two gauges and putting them on 2 barG. However, as the data in Figure 42, 43 and 44 shows, there needs to be a better way to get comparative pressure readings. Therefore, there is a need for the setup to have comparable measurements between the experiments, which are done simultaneously. Therefore, separate sensors should be incorporated into the two setups with live viewing in order to duplicate/replicate the experiments. The lager used can be a good indicator and calibration method.

In addition, it is observed from Figure 42 and 44 that the pressure in the flow experiments does not stay stable as it is designed to do. The reason for this is discovered in Figure 31 as the supply gas is connected with the wrong valve, which is sensitive to changes in upstream pressure and not downstream pressure. Thus, when the pressure drops, the valve does not supply more CO_2. To avoid this, a more rigorous testing procedure must be incorporated, and the right-designed valve must be used.

The PRV being rated for a maximum of 6.9 barG is because the price difference between a valve like this and another that can handle 10 barG was too much to justify the purchase when the experiments conducted in this thesis require a maximum 2 barG. If, however, it is wanted to do experiments at a higher pressure, it is simply possible to purchase and swap out this valve with another one.

6.3.3 CO_2 tank

To remove the need for the setup to cool the gas, a SodaStream canister was used as discussed in Section 3.14. Because of uncertainty regarding whether there was enough gas for both flow and static experiments, the flow was conducted with precooled CO_2, and the static one was conducted with outside CO_2 gas. It was also assumed that the gas would get colder quicker than it actually did because previous experiments had. However, this experiment was done on a hot summer day instead of early spring, as in the previous experiments. As seen in the experiment data, the comparative experiments had different temperature conditions; therefore, comparing the two experiments is harder.

For the next experiments, one backup canister should be available, and both should get pre-cooled CO_2.

6.4 Tasting experiment

The tasting experiment was conducted to iron out any final issues before the comparative experiment with the setup while also getting some data on the taste of an SGS-treated salmon.

Through the feedback received from the participants, it was clear that taste and mouthfeel changed drastically compared to each other. Therefore, it is suggested for future tasting experiments that the two sensory criteria are to be separate. The tasting experiment shows that the sample that was treated with SGS for 30 minutes was preferred over the control sample. This could be due to the different cuts of salmon, but the feedback showed that it was firmer and fresher tasting. The control sample was sitting out for one hour while the other samples were in a bacteriostatic environment, and thus the off-taste would not have time to set. It still shows a trend of SGS-treated samples being better than samples not treated with SGS.

The one-hour sample scored considerably worse than the other two samples. The reason is arguably that it came straight from an SGS chamber and therefore had a fizzy and tingling sensation in addition to an acidic taste. One participant preferred the one-hour SGS sample, describing it as a pleasant acidity that he liked. He said that he normally takes lemon juice and soy sauce on his sashimi, and this is similar to the acid coming from the lemon. Therefore, it may also have culinary implications as a treatment for new and exciting flavours. However, it is important to note that the actual taste of a product treated with SGS on commercial shelves will not be similar to the taste of salmon right after it has been in the chamber because the CO_2 will desorb out and mellow in flavour. We will, therefore, not see sparkling salmon on store shelves any time soon.

6.5 Prototyping

Regarding the prototyping that was done, there are some reflections related to design fixation and equipment choice.

6.5.1 Fixation on machining camber instead of Tri-Clamps

The main issue arising from the prototype development was that much of the time of this thesis was spent designing a chamber to be machined. In the end, this design was not needed and underscores the importance for a product developer to not fall into the error of design fixation (Jansson and Smith 1991). This could come from the fact that it was defined a goal of FEA of the chamber and machining from the start. Therefore, some goals should be defined looser to make the product development more flexible. However, having some goals to work out from is also nice. In addition, I could have thought of the idea to research larger diameter Tri-clamps; however, this was not done due to design fixation and no obvious large dimensions presenting themselves to me. The unknown unknowns at the beginning, like needing a circulation concept, fan research and heat generation problems, are problems that underscore the importance of having the ability to be "agile" and flexible when designing physical prototypes rapidly, like the Huner Gather model suggests (Steinert and Leifer 2012).

6.5.2 Fan vs Compressor

From the discussion made in Section 3.5 on whether to use a fan or compressor to circulate, the conclusion seems very short and easy. However, a few weeks were used to research and talk to people regarding how to use a compressor before the fan solution emerged. This was also probably some design fixation coming from the original concept of using an external CO_2 supply where the flow comes from differential pressure. Because this concept revolved around a pressure difference, it seemed obvious that a circulation concept needed a compressor to incorporate flowing CO_2 into the system. However, for this system, it is a faulty premise that it is possible to make a continuous circulation system able to operate for one hour or more. This would need a tank of a minimum of 12 tonnes of CO_2 and a deposit tank to put it into if one does not compress the gas into the main chamber. This, however, would be slow with compressors available in the market (Team 2023). It is, therefore, better to use a fan for continuous flow. However, one concept emerging from this design work is to rethink the entire setup and use a discrete flow system to remove the limitations a continuous system has. This will be presented in Section 7.3.

6.5.3 Prototyping vs simulation

This setup was designed with constraints from a simulation setup. This helped this thesis move along quickly in the beginning; however, when conflicting design choices were discovered, limitations required more complex solutions and testing before an adequate solution emerged. An example of this is the requirement of a pipe diameter of Ø 65mm and a fan speed of 50m/s. To achieve these two requirements means using an extremely large fan area or a powerful fan. A powerful fan produces more heat than the system and fridge are able to cool, and thus a complex optimization problem has emerged, which originally was outside the scope of this thesis. Had the Ø65 mm constraint just been a suggestion, the pipe could have been way narrower and high flow speeds could have been achieved with a low-power fan. Therefore, it is suggested that such prototyping comes before and during the development of the simulation and not after the simulation is finished set up.

7 Future work

7.1 Improvements to the flow setup underway

As discussed, there are lessons learned and ongoing developments of the setup as this thesis is being written. This section will summarise this, describe what has been done since the experiments were conducted and describe future research avenues.

7.1.1 Improvements that are finished

This subsection describes all the changes that were made after the experiment was conducted.
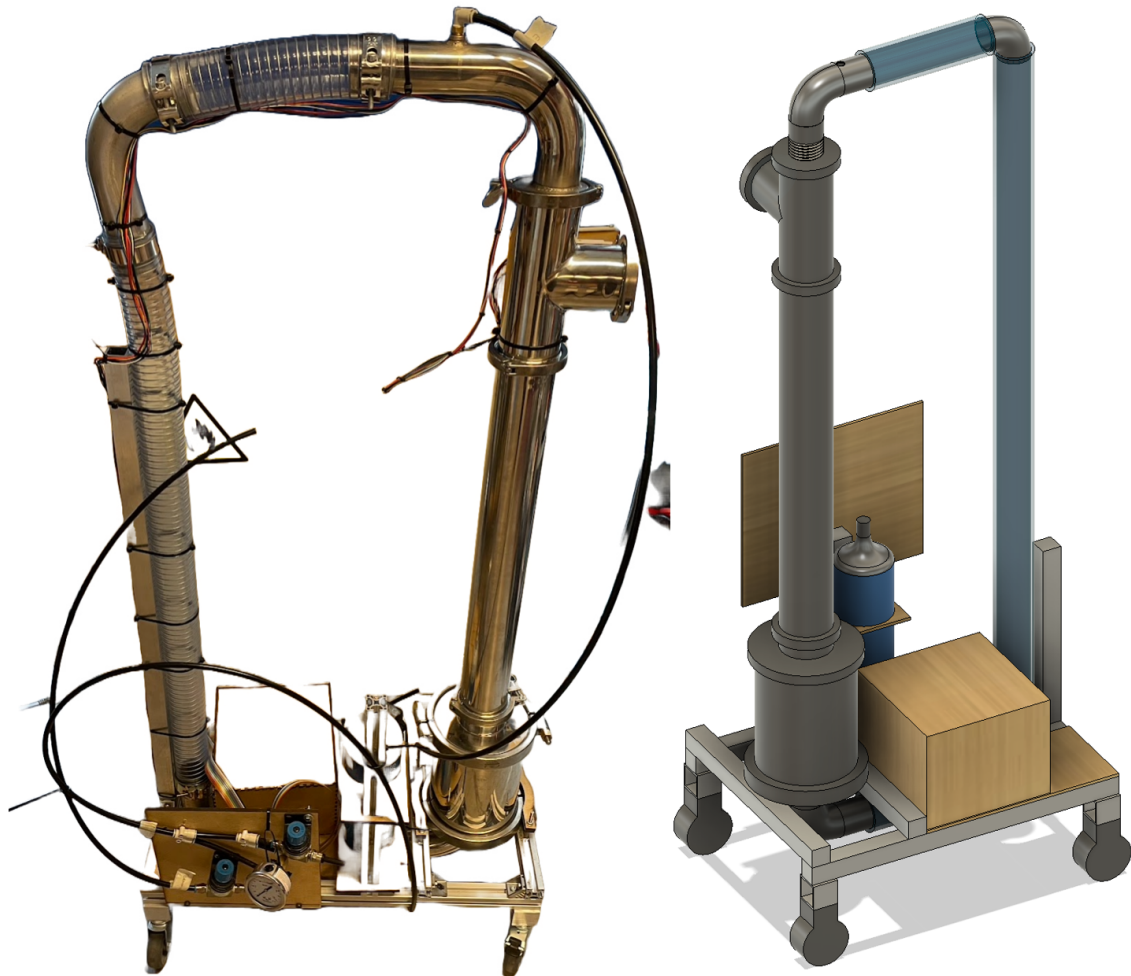
Figure 46: New new setup as of the finishing of this thesis. The small pneumatic tubes are replaced with larger 38 mm tubes, and the electronics are made easier to handle

- Larger diameter circulation pipes

  As the setup used for the experiments in this thesis was more for testing, larger diameter pipes have been made and implemented into the system, shown in Figure 46. Two 90-degree stainless steel angles have been welded on the two end caps at either end of the setup and connected through a set of circulation pipes made from reinforced PVC pipes rated at 7 barG. The connection point is clamped and filled with Tec7, sealing the chamber.

- Improved wiring

The wiring done during the prototyping was done as an agile method. Because changes in the setup while prototyping, like the number of wires required for a component, would change suddenly, the wiring was done easily and modular with a screw terminal. Pins were used in the beginning; however, when the setup was moved or disassembled, the pins had a tendency to fall out. Instead of having the screw terminal dangling in the setup, a screw terminal holder was 3D-printed and mounted next to the entry of the wires, shown in Figure 47. A box connecting the wires to different sections of the setup was also implemented, making the setup more accessible and easier to error search.
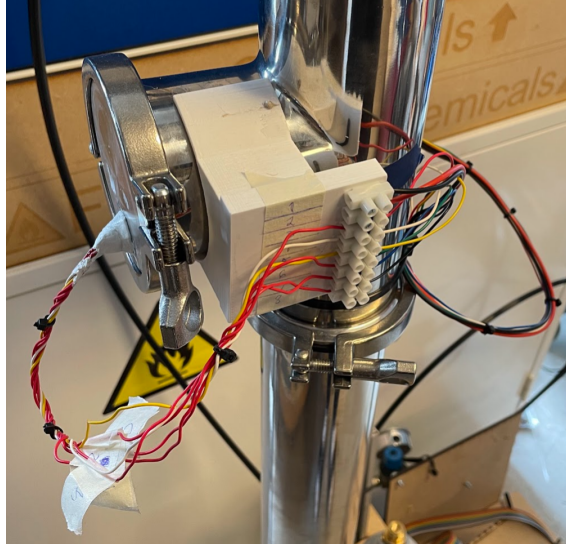
Figure 47: Connector for the wires that are stripped to the pipes in a practical way. Wires are also connected with 3D-printed holder

- Implementation of the injection nozzle

  The orifice point mount was also finished, designed and 3Dprinted. The mount is mounted like the other components; however, it is mounted in the top part of the 6-inch pipe because then no space of 73 mm would be used for the mounting structure. The design is a screw being able to move up and down to assess different orifice points while the nozzle itself is interchangeable to different designs.

7.1.2 Improvements to be done

This subsection describes all the changes that are going to be made after this thesis is finished.

- Design for incorporating differential sensor

  The differential sensor should be incorporated to the setup. A sensor like the MPX5100DP can be placed in the extra side of the tee to read the static pressure in the system there, while a pipe is connected to the flow port and guided downstream the fan and mounted to the side of the flow pipe.

- Live sensor integration of pressure and temperature sensor

  With the wires incorporated in the system, a pressure and temperature sensor should be implemented in the system for live reading of the experiment characteristics.

- Find a solution for the heat generation problem

  As discussed in Section 6.3.1 the heat generated by the fan is a problem. Any fan generates heat, especially if there is resistance or more viscous fluid, e.g. gas at higher pressure. Therefore, it should be investigated if a lower power, high rpm fan should be bought together with the concept of a heat exchanger.

When these improvements have been done, and tests are done to verify, then the author will do more experiments for future publications.

7.2 Next experiment

When the setup is improved, and one can replicate the experiments easily, then new experiments will be conducted with even more samples to make the findings significant.

The next experiment does not differ very much from the methods used in this thesis. However, there are some key differences. For starters, the pressure and temperature must be equal when the experiment starts. This will be done with live, digital readings from the setups. Both static and flow setups will get CO_2 from a prechilled CO_2 canister. It will also be tried to use a better fridge which is better at maintaining the specified temperature.

The final development done, new experiment data and this thesis will culminate in paper submitted to Design 2024 and Journal of Food Engineering. The draft of their abstracts are given in Section 8.

7.3 Discrete flow concept

The main principle surrounding the flow setup is to use flowing CO_2 to induce a higher total pressure on the surface of a sample by increasing the dynamic pressure. Much of the previous research on SGS has mostly been done in a pressure range of 2-3 barG and up to 6 bars. Therefore, higher pressures should be explored with a flow setup that has higher velocities for one moment and then high-pressure static the next. Then, one can combine both high flows and pressures in a realistic environment. This is a flow setup with flow in discrete steps.

One can use the same layout as shown in Figure 14, with circulation and a compressor; however, since a compressor has a max flow of 6.5 CFM, then one uses the reservoir tank effectively. The valve to the reservoir tank is closed until max desired pressure is gained, and then the valve is opened, spraying CO_2 into the chamber. When the pressures are equalized, the valve is closed, and the cycle repeats. This concept could also be realistic for industrial processing lines, where research can be put into how many cycles and at which pressures are one getting the most effective SGS.

8 Abstracts to be published

This chapter presents draft abstracts to be submitted in two papers. Paper one is a design paper to be submitted to Design 2024 on the 15th of November, 2023. The second paper will go into more detail about food science and the experiment data and will be submitted to the Journal of Food Engineering on the 31st of October, 2023.

8.1 Paper to be submitted to Design 2024

Sustainability issues are important for design stakeholders. Food safety is crucial for human health and a significant contributor to climate change. This paper presents a modular, low-cost processing line setup to be used for testing and further research of Soluble Gas Stabilisation (SGS). SGS dissolves bacteriostatic CO_2 into a food product to increase shelf life. The intention of making such a setup with off-the-shelf brewing equipment, 3D-printed components and cheap electronics was to create a low-cost early prototype validation of the viability of a food science technology outside the limited lab experiments, such that the experiments could easily be replicated and used in further research. By developing this setup, many lessons are learned, and in turn, more resources can be used on the next setup to improve efficiency. These results may help future researchers develop and discover new concepts to more effectively dissolve CO_2 into food products without destroying the sensory qualities while also suggesting this kind of prototyping can help in all aspects of food processing equipment to make the food sector more sustainable.

8.2 Paper to be submitted to Journal of Food Engineering

Food safety is important for humans and a significant contributor to climate change. Food waste and packaging usage are problems in today's industry. A potential technology to reduce food waste and use less packaging material is the implementation of Soluble Gas Stabilisation (SGS). SGS is a development of Modified Atmosphere Packaging (MAP) in stores today, where bacteriostatic CO_2 is dissolved into a food product to increase shelf life. Lab-scale, early-phase research has been done to verify the microbiological effectiveness of SGS. However, the research is limited to the biological aspect and does not explore the real-world implications and optimization this technology has the potential to become. E.g, MAP achieves bacteriostatic properties after a few days, and lab-scale SGS achieves this after a few hours; while no research has tried to use as little time as possible, e.g. 5 minutes at high pressures. Therefore this paper presents a continuous pressurized flow setup that is used for experiments that have never been done before. The experiment conducted in this paper is a comparison with existing static experiments with a control sample. The experiments suggest that a setup like this achieves bacteriostatic properties more rapidly than current static SGS experiments, pathing the way for more research to lift the technology to industry adaptation. This conclusion is based on data on the CO_2 dissolution, flow speed, dynamic force on the sample, temperature and pressure data. Through the use of a flexible and modular setup, more research and data are being generated than limited static experiments, also showing the need to develop new setups to test new food science technology. This paper concludes that the flow chamber design may help researchers develop and optimize a way for the SGS technology to be widely adopted in the food processing industry and make new advancements in SGS technology.

9   Conclusion

In conclusion, this thesis presents a relatively low-cost rapidly developed test setup to enable research into the practical viability of the Soluble Gas Stabilization (SGS) technology. The aim was to develop a pressure chamber able to produce continuous flow on a food sample, to potentially increase knowledge of SGS in food science.

The experiments conducted in this thesis suggest that there is potential for such a flexible and modular setup, while also underscoring the need to develop the setup further to a point where replicability is consistent. This conclusion is based on data of the CO_2 dissolution, temperature and pressure data. The final setup developments needed were also proposed.

The intention of making such a setup with off-the-shelf brewing equipment, 3D-printed components and cheap electronics was to make a low-cost early prototype validation of the viability of this technology outside the limited lab experiments, such that the experiments could easily be replicated and used in further research. By developing this setup, many lessons are learned and in turn, more resources can be used on the next setup to improve efficiency.

These results may help future researchers develop and discover new concepts to more effectively dissolve CO_2 into food products without destroying the sensory qualities.

Bibliography

Abel, Nanna et al. (Jan. 2018). 'The influence of lipid composition, storage temperature, and modified atmospheric gas combinations on the solubility of CO2 in a seafood model product'. In: *Journal of Food Engineering* 216, pp. 151–158. ISSN: 0260-8774. DOI: 10.1016/j.jfoodeng.2017.08.020. URL: https://www.sciencedirect.com/science/article/pii/S0260877417303576 (visited on 22nd Aug. 2023).

Atuonwu, James and Savvas Tassou (Jan. 2021). 'Decarbonisation of food manufacturing by the electrification of heat: A review of developments, technology options and future directions'. In: *Trends in Food Science & Technology* 107, pp. 168–182. ISSN: 0924-2244. DOI: 10.1016/j.tifs.2020.10.011. URL: https://www.sciencedirect.com/science/article/pii/S0924224420306348 (visited on 15th Aug. 2023).

Blakistone, Barbara A. (Dec. 2012). *Principles and Applications of Modified Atmosphere Packaging of Foods*. en. Google-Books-ID: MXAQBwAAQBAJ. Springer Science & Business Media. ISBN: 978-1-4615-6097-5.

Boler, D.D. and D.R. Woerner (Oct. 2017). 'What is meat? A perspective from the American Meat Science Association'. en. In: *Animal Frontiers* 7.4, pp. 8–11. ISSN: 2160-6056, 2160-6064. DOI: 10.2527/af.2017.0436. URL: https://academic.oup.com/af/article/7/4/8/4775089 (visited on 15th Aug. 2023).

Brennan, Linda et al. (Jan. 2021). 'The role of packaging in fighting food waste: A systematised review of consumer perceptions of packaging'. In: *Journal of Cleaner Production* 281, p. 125276. ISSN: 0959-6526. DOI: 10.1016/j.jclepro.2020.125276. URL: https://www.sciencedirect.com/science/article/pii/S0959652620353208 (visited on 15th Aug. 2023).

Cervoni, Barbie (Sept. 2022). *Salmon Nutrition Facts and Health Benefits*. en. Section: Verywell. URL: https://www.verywellfit.com/salmon-nutrition-facts-calories-and-health-benefits-4106641 (visited on 17th Aug. 2023).

Collins, Jack A., Henry R. Busby and George H. Staab (2010). *Mechanical Design of Machine Elements and Machines: A Failure Prevention Perspective, 2nd Edition — Wiley*. en-us. URL: https://www.wiley.com/en-us/Mechanical+Design+of+Machine+Elements+and+Machines%3A+A+Failure+Prevention+Perspective%2C+2nd+Edition-p-9780470413036 (visited on 21st Aug. 2023).

Dang, Tem Thi, Tone Mari Rode and Dagbjørn Skipnes (Sept. 2020). *Independent and combined effects of high pressure, microwave, soluble gas stabilization, modified atmosphere and vacuum packaging on microbiological and physicochemical shelf life of precooked chicken breast slices - ScienceDirect*. URL: https://doi.org/10.1016/j.jfoodeng.2020.110352 (visited on 20th Aug. 2023).

Ebert, Edward and Kemal Aganovic (2022). 'Current Technology Readiness Levels (TRL) of Non-thermal Technologies and Research Gaps for Improved Process Control and Integration into Existing Production Lines'. en. In: *Nonthermal Processing in Agri-Food-Bio Sciences: Sustainability and Future Goals*. Ed. by Anet Režek Jambrak. Food Engineering Series. Cham: Springer International Publishing, pp. 511–540. ISBN: 978-3-030-92415-7. DOI: 10.1007/978-3-030-92415-7_15. URL: https://doi.org/10.1007/978-3-030-92415-7_15 (visited on 15th Aug. 2023).

Ellingsen, H., J. O. Olaussen and I. B. Utne (May 2009). 'Environmental analysis of the Norwegian fishery and aquaculture industry—A preliminary study focusing on farmed salmon'. In: *Marine Policy* 33.3, pp. 479–488. ISSN: 0308-597X. DOI: 10.1016/j.marpol.2008.11.003. URL: https://www.sciencedirect.com/science/article/pii/S0308597X08001553 (visited on 15th Aug. 2023).

EN1092 Flange standard (2023).

Engineering ToolBox (2023). *Metric Steel Bolts - Grades and Property Classes*. URL: https://www.engineeringtoolbox.com/steel-bolts-metric-grades-d_1428.html (visited on 21st Aug. 2023).

Esmaeilian, Sara (2023). 'Concept development of soluble gas stabilization (SGS) technology for seafood - unpublished doctoral dissertation (in preparation)'. PhD thesis. Norwegian University of Science and Technology, Trondheim.

Esmaeilian, Sara et al. (Dec. 2021). 'The use of soluble gas stabilization technology on food – A review'. en. In: *Trends in Food Science & Technology* 118, pp. 154–166. ISSN: 0924-2244. DOI: 10.1016/j.tifs.2021.09.015. URL: https://www.sciencedirect.com/science/article/pii/S0924224421005392 (visited on 3rd Aug. 2023).

Fremery, Donald de and Morris F. Pool (1960). 'BIOCHEMISTRY OF CHICKEN MUSCLE AS RELATED TO RIGOR MORTIS AND TENDERIZATIONa'. en. In: *Journal of Food Science* 25.1. _eprint: https://onlinelibrary.wiley.com/doi/pdf/10.1111/j.1365-2621.1960.tb17938.x, pp. 73–87. ISSN: 1750-3841. DOI: 10.1111/j.1365-2621.1960.tb17938.x. URL: https://onlinelibrary.wiley.com/doi/abs/10.1111/j.1365-2621.1960.tb17938.x (visited on 16th Aug. 2023).

Fusieger, Andressa et al. (May 2023). 'Bactericidal and bacteriostatic effects of sodium polyphosphate emulsifying salts on selected targets in processed cheese'. In: *Food Control* 147, p. 109580. ISSN: 0956-7135. DOI: 10.1016/j.foodcont.2022.109580. URL: https://www.sciencedirect.com/science/article/pii/S0956713522007733 (visited on 20th Aug. 2023).

Giovannoni, Elena and Giacomo Fabietti (2013). 'What Is Sustainability? A Review of the Concept and Its Applications'. en. In: *Integrated Reporting: Concepts and Cases that Redefine Corporate Accountability*. Ed. by Cristiano Busco et al. Cham: Springer International Publishing, pp. 21–40. ISBN: 978-3-319-02168-3. DOI: 10.1007/978-3-319-02168-3_2. URL: https://doi.org/10.1007/978-3-319-02168-3_2 (visited on 15th Aug. 2023).

Heide, Morten (2020). 'Økt konsum av sjømat i Norge'. no. In.

High Vac Depot staff (Dec. 2020). *KF Or CF — Which Should I Use?* en-US. URL: https://highvacdepot.com/2020/12/11/kf-or-cf-which-should-i-use/ (visited on 1st Sept. 2023).

Hygienic Stainless Steel (2023). *Tri-clamp pressure rating standard EN4825*.

Iqbal, Jamshed, Zeashan Hameed Khan and Azfar Khalid (May 2017). 'Prospects of robotics in food industry'. en. In: *Food Science and Technology* 37. Publisher: Sociedade Brasileira de Ciência e Tecnologia de Alimentos, pp. 159–165. ISSN: 0101-2061, 1678-457X. DOI: 10.1590/1678-457X.14616. URL: https://www.scielo.br/j/cta/a/g8Vvv8rW7D7rsfwctx9gmvc/?lang=en (visited on 16th Aug. 2023).

Jakobsen, Anita Nordeng et al. (2022). 'Application of soluble gas stabilization technology on ready-to-eat pre-rigor filleted Atlantic salmon (Salmo salar L.)' en. In: *Journal of Food Science* 87.6. _eprint: https://onlinelibrary.wiley.com/doi/pdf/10.1111/1750-3841.16164, pp. 2377–2390. ISSN: 1750-3841. DOI: 10.1111/1750-3841.16164. URL: https://onlinelibrary.wiley.com/doi/abs/10.1111/1750-3841.16164 (visited on 3rd Aug. 2023).

Jakobsen, Marianne and Grete Bertelsen (Dec. 2004). 'Predicting the amount of carbon dioxide absorbed in meat'. In: *Meat Science* 68.4, pp. 603–610. ISSN: 0309-1740. DOI: 10.1016/j.meatsci.2004.05.012. URL: https://www.sciencedirect.com/science/article/pii/S0309174004001378 (visited on 18th Aug. 2023).

Jansson, David G. and Steven M. Smith (Jan. 1991). 'Design fixation'. In: *Design Studies* 12.1, pp. 3–11. ISSN: 0142-694X. DOI: 10.1016/0142-694X(91)90003-F. URL: https://www.sciencedirect.com/science/article/pii/0142694X9190003F (visited on 3rd Sept. 2023).

Jensen, Bent-Are and Rachel Mutter (Dec. 2022). *There is a new ranking of the world's 15 largest farmed salmon producers*. en. Section: salmon. URL: https://www.intrafish.com/salmon/there-is-a-new-ranking-of-the-worlds-15-largest-farmed-salmon-producers/2-1-1371739 (visited on 16th Aug. 2023).

Knorr, Dietrich, Mary Ann Augustin and Brijesh Tiwari (2020). 'Advancing the Role of Food Processing for Improved Integration in Sustainable Food Chains'. In: *Frontiers in Nutrition* 7. ISSN: 2296-861X. URL: https://www.frontiersin.org/articles/10.3389/fnut.2020.00034 (visited on 15th Aug. 2023).

Lambert, Smith and Karen (Mar. 1991). 'Shelf life extension and microbiological safety of fresh meat – a review'. In.

Lima, Marieli et al. (Nov. 2014). 'Application of CO 2 in Perna perna Mussel: Evaluation of Absorption Mechanism During Soluble Gas Stabilization (SGS) Process'. In: *Food Engineering Reviews* 6. DOI: 10.1007/s12393-014-9103-x.

Lima, Marieli de et al. (May 2021). 'Investigation of soluble gas stabilization combined with modified atmosphere packaging on the shelf life of cooked blue mussels (Mytilus edulis)'. en. In: *Research, Society and Development* 10.6. Number: 6, e4310615463–e4310615463. ISSN: 2525-3409. DOI: 10.33448/rsd-v10i6.15463. URL: https://rsdjournal.org/index.php/rsd/article/view/15463 (visited on 21st May 2023).

Matweb (2023). *316L Stainless Steel*. URL: https://asm.matweb.com/search/SpecificMaterial.asp?bassnum=mq316q (visited on 29th Aug. 2023).

McMillin, Kenneth W. (Sept. 2008). 'Where is MAP Going? A review and future potential of modified atmosphere packaging for meat'. In: *Meat Science*. 54th International Congress of Meat Science and Technology (54th ICoMST), 10-15August 2008, Cape Town, South Africa

80.1, pp. 43–65. ISSN: 0309-1740. DOI: 10.1016/j.meatsci.2008.05.028. URL: https://www.sciencedirect.com/science/article/pii/S0309174008001691 (visited on 16th Aug. 2023).

Megawatsoft (2023). *CO2 Tables Calculator*. URL: https://www.carbon-dioxide-properties.com/co2tablesweb.aspx (visited on 1st Sept. 2023).

Monforti, Fabio et al. (May 2015). *Energy use in the EU food sector: State of play and opportunities for improvement*. DOI: 10.2790/158316.

Murcek, Roman et al. (May 2021). 'Development of a quartz crystal sensor system to monitor local soil removal during cleaning in closed food processing lines'. In: *Food and Bioproducts Processing* 127, pp. 282–287. ISSN: 0960-3085. DOI: 10.1016/j.fbp.2021.03.011. URL: https://www.sciencedirect.com/science/article/pii/S0960308521000559 (visited on 16th Aug. 2023).

Al-Mutlaq, Sarah (2023). *Load Cell Amplifier HX711 Breakout Hookup Guide - SparkFun Learn*. URL: https://learn.sparkfun.com/tutorials/load-cell-amplifier-hx711-breakout-hookup-guide (visited on 1st Sept. 2023).

Myers, Richard A. (May 1985). 'Modified atmosphere package and process'. US4515266A. URL: https://patents.google.com/patent/US4515266A/en?q=(%22modified+atmosphere+packaging%22)&oq=%22modified+atmosphere+packaging%22&sort=old (visited on 3rd Aug. 2023).

Nations, United (2017). *World population projected to reach 9.8 billion in 2050, and 11.2 billion in 2100*. en. Publisher: United Nations. URL: https://www.un.org/en/desa/world-population-projected-reach-98-billion-2050-and-112-billion-2100 (visited on 15th Aug. 2023).

Al-Nehlawi, A. et al. (May 2013). 'Effect of high carbon dioxide atmosphere packaging and soluble gas stabilization pre-treatment on the shelf-life and quality of chicken drumsticks'. In: *Meat Science* 94.1, pp. 1–8. ISSN: 0309-1740. DOI: 10.1016/j.meatsci.2012.12.008. URL: https://www.sciencedirect.com/science/article/pii/S0309174012004342 (visited on 15th Aug. 2023).

NiGen (May 2022). *How To Pressure Test a Gas Line — Requirements, Tips & More*. en-US. URL: https://nigen.com/gas-line-pressure-testing-requirements-tips/ (visited on 6th Aug. 2023).

Novatech (2023). *Tec7 - TECHNICAL DATA SHEET*.

Olabi, A. G. et al. (Feb. 2023). 'Micromobility: Progress, benefits, challenges, policy and regulations, energy sources and storage, and its role in achieving sustainable development goals'. In: *International Journal of Thermofluids* 17, p. 100292. ISSN: 2666-2027. DOI: 10.1016/j.ijft.2023.100292. URL: https://www.sciencedirect.com/science/article/pii/S2666202723000125 (visited on 15th Aug. 2023).

Olatunde, Oladipupo Odunayo and Soottawat Benjakul (2018). 'Natural Preservatives for Extending the Shelf-Life of Seafood: A Revisit'. en. In: *Comprehensive Reviews in Food Science and Food Safety* 17.6. _eprint: https://onlinelibrary.wiley.com/doi/pdf/10.1111/1541-4337.12390, pp. 1595–1612. ISSN: 1541-4337. DOI: 10.1111/1541-4337.12390. URL: https://onlinelibrary.wiley.com/doi/abs/10.1111/1541-4337.12390 (visited on 15th Aug. 2023).

Øvrebø, Henrik H. et al. (July 2023). 'CREATING AN OPEN-SOURCE, LOW-COST COMPOSITE FEEDER DESIGN TO IMPROVE FILAMENT QUALITY OF HIGH-PERFORMANCE MATERIALS TO BE USED IN FUSED FILAMENT FABRICATION (FFF)'. en. In: *Proceedings of the Design Society* 3, pp. 1097–1106. ISSN: 2732-527X. DOI: 10.1017/pds.2023.110. URL: https://www.cambridge.org/core/journals/proceedings-of-the-design-society/article/creating-an-opensource-lowcost-composite-feeder-design-to-improve-filament-quality-of-highperformance-materials-to-be-used-in-fused-filament-fabrication-fff/B3789EB72618A3CF91F4B6B932600898 (visited on 1st Sept. 2023).

Pankey, G. A. and L. D. Sabath (Mar. 2004). 'Clinical Relevance of Bacteriostatic versus Bactericidal Mechanisms of Action in the Treatment of Gram-Positive Bacterial Infections'. In: *Clinical Infectious Diseases* 38.6, pp. 864–870. ISSN: 1058-4838. DOI: 10.1086/381972. URL: https://doi.org/10.1086/381972 (visited on 17th Aug. 2023).

Paul's Fan Company (Nov. 2019). *The Difference Between an Axial and Radial Fan*. en-US. URL: https://paulsfans.com/blog/difference-axial-radial-fan/ (visited on 20th Aug. 2023).

Poyatos-Racionero, Elisa et al. (Jan. 2018). 'Recent advances on intelligent packaging as tools to reduce food waste'. In: *Journal of Cleaner Production* 172, pp. 3398–3409. ISSN: 0959-6526. DOI: 10.1016/j.jclepro.2017.11.075. URL: https://www.sciencedirect.com/science/article/pii/S095965261732735X (visited on 15th Aug. 2023).

Reisch, Lucia, Ulrike Eberle and Sylvia Lorek (Oct. 2013). 'Sustainable food consumption: an overview of contemporary issues and policies'. In: *Sustainability: Science, Practice and Policy* 9.2. Publisher: Taylor & Francis _eprint: https://doi.org/10.1080/15487733.2013.11908111, pp. 7–

25. ISSN: null. DOI: 10.1080/15487733.2013.11908111. URL: https://doi.org/10.1080/15487733.2013.11908111 (visited on 15th Aug. 2023).

Robertson, Gordon L. (Sept. 2005). *Food Packaging: Principles and Practice, Second Edition.* 2nd ed. Boca Raton: CRC Press. ISBN: 978-0-429-13289-6. DOI: 10.1201/9781420056150.

Rotabakk, B. T., O. I. Lekang and M. Sivertsvik (Sept. 2007). 'Volumetric method to determine carbon dioxide solubility and absorption rate in foods packaged in flexible or semi rigid package'. In: *Journal of Food Engineering* 82.1, pp. 43–50. ISSN: 0260-8774. DOI: 10.1016/j.jfoodeng.2007.01.013. URL: https://www.sciencedirect.com/science/article/pii/S0260877407000593 (visited on 18th Aug. 2023).

Rotabakk, B.T., S. Birkeland and M. Sivertsvik (Apr. 2008). *Enhancement of Modified Atmosphere Packaged Farmed Atlantic Halibut (Hippoglossus Hippoglossus) Fillet Quality by Soluble Gas Stabilization - B.T. Rotabakk, S. Birkeland, O.I. Lekang, M. Sivertsvik, 2008.* URL: https://journals.sagepub.com/doi/abs/10.1177/1082013208092051?casa_token=lVNiJvmqZqcAAAAA:Ni3U9EgmYQ9TraIh3sFxWyiYehzCO2MKLB5JThmttjxaYSNMcr2xFj6VMM7WawQm2stJDkjKznE (visited on 20th Aug. 2023).

Rotabakk, Bjørn T. et al. (2006). 'Effect of Modified Atmosphere Packaging and Soluble Gas Stabilization on the Shelf Life of Skinless Chicken Breast Fillets'. en. In: *Journal of Food Science* 71.2. _eprint: https://onlinelibrary.wiley.com/doi/pdf/10.1111/j.1365-2621.2006.tb08915.x, S124–S131. ISSN: 1750-3841. DOI: 10.1111/j.1365-2621.2006.tb08915.x. URL: https://onlinelibrary.wiley.com/doi/abs/10.1111/j.1365-2621.2006.tb08915.x (visited on 20th Aug. 2023).

RS Components (2023). *7ME6520-3MC13-2AA1 — Siemens SITRANS F M Series Electromagnetic In-line Flow Sensor Fitting for Liquid, 0 m/s Min, 10 m/s Max — RS.* URL: https://no.rs-online.com/web/p/flow-sensors/8044051?cm_mmc=NO-PLA-DS3A-_-google-_-CSS_NO_EN_Pmax_Test-_-_-8044051&matchtype=&gclid=Cj0KCQjwl8anBhCFARIsAKbbpyRWSVOJGNTe7KwzhTZSdcw83qVESgwcB&gclsrc=aw.ds (visited on 1st Sept. 2023).

Ruggerio, Carlos Alberto (Sept. 2021). 'Sustainability and sustainable development: A review of principles and definitions'. In: *Science of The Total Environment* 786, p. 147481. ISSN: 0048-9697. DOI: 10.1016/j.scitotenv.2021.147481. URL: https://www.sciencedirect.com/science/article/pii/S0048969721025523 (visited on 15th Aug. 2023).

Ruiz-Capillas, Claudia and Ana M. Herrero (Mar. 2021). 'Sensory Analysis and Consumer Research in New Product Development'. In: *Foods* 10.3, p. 582. ISSN: 2304-8158. DOI: 10.3390/foods10030582. URL: https://www.ncbi.nlm.nih.gov/pmc/articles/PMC8001375/ (visited on 4th Sept. 2023).

Sciencedirect (2023). *Salmo Salar - an overview — ScienceDirect Topics.* URL: https://www.sciencedirect.com/topics/agricultural-and-biological-sciences/salmo-salar (visited on 20th Aug. 2023).

Sivertsvik, M. and S. Birkeland (Oct. 2006). 'Effects of Soluble Gas Stabilisation, Modified Atmosphere, Gas to Product Volume Ratio and Storage on the Microbiological and Sensory Characteristics of Ready-to-Eat Shrimp (Pandalus borealis)'. en. In: *Food Science and Technology International* 12.5. Publisher: SAGE Publications Ltd STM, pp. 445–454. ISSN: 1082-0132. DOI: 10.1177/1082013206070171. URL: https://doi.org/10.1177/1082013206070171 (visited on 15th Aug. 2023).

Sivertsvik, Morten and Jens Stoumann Jensen (Oct. 2005). 'Solubility and absorption rate of carbon dioxide into non-respiring foods. Part 3: Cooked meat products'. In: *Journal of Food Engineering* 70.4, pp. 499–505. ISSN: 0260-8774. DOI: 10.1016/j.jfoodeng.2004.10.005. URL: https://www.sciencedirect.com/science/article/pii/S0260877404004984 (visited on 15th Aug. 2023).

Skaug, Martin (Jan. 2023). *Norway's seafood exports worth NOK 151.4 billion in 2022.* en. URL: https://en.seafood.no/news-and-media/news-archive/norways-seafood-exports-worth-nok-151.4-billion-in-2022/ (visited on 16th Aug. 2023).

Solidworks (2020). *Distributed Coupling for Pins and Bolts - 2020 - What's New in SOLIDWORKS.* URL: https://help.solidworks.com/2020/English/WhatsNew/c_distributed_coupling_connectors.htm (visited on 5th Aug. 2023).

Steinert, Martin and Larry Leifer (Jan. 2012). ''Finding One's Way': Re-Discovering a Hunter-Gatherer Model based on Wayfaring'. In: *International Journal of Engineering Education* 28, pp. 251–252.

Stenmarck, Åsa et al. (Mar. 2016). *Estimates of European food waste levels.*

Team, Linquip (June 2023). *The 12 Highest CFM Air Compressors in 2023 — Linquip*. en-US. Section: Compressor. URL: https://www.linquip.com/blog/the-12-highest-cfm-air-compressors-in-2023/ (visited on 14th Aug. 2023).

Thielemann, Jens T (Nov. 2014). *Pinbone removal in pre-rigor salmon*. en. URL: https://www.sintef.no/en/projects/2009/pinbone-removal-in-pre-rigor-salmon/ (visited on 8th Aug. 2023).

ToolBox, Engineering (2023). *Pitot Tubes*. URL: https://www.engineeringtoolbox.com/pitot-tubes-d_612.html (visited on 29th Aug. 2023).

Trelleborg (2023). *O-Ring Calculator — Trelleborg Sealing Solutions*. URL: https://www.trelleborg.com/en/seals/resources/design-support-and-engineering-tools/o-ring-calculator (visited on 4th Aug. 2023).

U.S. Department of Agriculture (Apr. 2019). *Farmed Atlantic Salmon - Nutrients - FoodData Central*. URL: https://fdc.nal.usda.gov/fdc-app.html#/food-details/175168/nutrients (visited on 17th Aug. 2023).

Wang, Lijun (Oct. 2014). 'Energy efficiency technologies for sustainable food processing'. en. In: *Energy Efficiency* 7.5, pp. 791–810. ISSN: 1570-6478. DOI: 10.1007/s12053-014-9256-8. URL: https://doi.org/10.1007/s12053-014-9256-8 (visited on 15th Aug. 2023).

Wieben, Emilie (2017). 'Food loss and waste and the linkage to global ecosystems'. In.

Willett, Walter et al. (Feb. 2019). 'Food in the Anthropocene: the EAT–Lancet Commission on healthy diets from sustainable food systems'. English. In: *The Lancet* 393.10170. Publisher: Elsevier, pp. 447–492. ISSN: 0140-6736, 1474-547X. DOI: 10.1016/S0140-6736(18)31788-4. URL: https://www.thelancet.com/journals/lancet/article/PIIS0140-6736(18)31788-4/fulltext (visited on 15th Aug. 2023).

Appendix

A   Bolts, lid and pipe thickness calculation

```python
import numpy as np
r=90#mm
p=1#MPa
SF=3
sigma_max = 205#MPa
A_m10=58#mm^2
sigma_bolt = 800#MPa


A_tank = r**2*np.pi #=A_lid


F_bolts = p*A_tank*2 #Because the pressure will act on the walls and the lid
F_gasket = 5000#N


F_bolts_gasket = F_bolts+F_gasket
F_bolt = A_m10*sigma_bolt
n_bolts = F_bolts_gasket*SF/F_bolt


print("This simplification requires minimum", np.round(n_bolts,0), "Bolts")



t_pipe = SF*(np.sqrt(3) *np.sqrt(np.pi**2 *p**2 *r**4 +
    196830000))/(2*np.pi*r*sigma_max)



print("Pipe should be minimum", np.round(t_pipe,2), "mm thick")
```

B   Experiment code for plotting

```python
import pandas as pd
import matplotlib.pyplot as plt

# Read the data
# Read the data without headers
data = pd.read_csv(r"C:\Users\Henrik\Desktop\Pythonplotting\Dissolved CO2 - All
    samples.txt", sep='\t', encoding='utf-16', header=None)

#data = pd.read_csv(r"C:\Users\Henrik\Desktop\Pythonplotting\Dissolved CO2 - All
    samples - adjusted to start at 0.txt", sep='\t', encoding='utf-16',
    header=None)
plt.figure(figsize=(15, 8))

# Plotting the dissolved CO2 for flow samples against the hour stamp
plt.errorbar(data.iloc[:, 2], data.iloc[:, 0], yerr=data.iloc[:, 1],
            label="Flow Samples", linestyle='-', marker='o', linewidth=3,
    capsize=7, markersize=8)

# Plotting the dissolved CO2 for static samples
plt.errorbar(data.iloc[:, 5], data.iloc[:, 3], yerr=data.iloc[:, 4],
            label="Static Samples", linestyle='-', marker='x', linewidth=3,
    capsize=7, markersize=8)

# Plotting the dissolved CO2 for control samples
```

```python
plt.errorbar(data.iloc[:, 8], data.iloc[:, 6], yerr=data.iloc[:, 7],
             label="Control Samples", linestyle='-', marker='s', linewidth=3,
 ↪  capsize=7, markersize=8)

plt.xlabel('Hour', fontsize=24)
plt.ylabel(r'Dissolved CO$_2$ [ppm]', fontsize=24)  # CO2 written with subscript
 ↪  notation
plt.title(r'Dissolved CO$_2$ in the product plotted over the measurement period',
 ↪  fontsize=24)  # CO2 written with subscript notation
plt.xticks(fontsize=24)  # Adjusting x-axis tick font size
plt.yticks(fontsize=24)  # Adjusting y-axis tick font size
plt.legend(fontsize=15)
plt.grid(True)
plt.tight_layout()
plt.show()
```

C   Sensory analysis data

```python
import pandas as pd
import numpy as np
import matplotlib.pyplot as plt

# Read the data without headers
data = pd.read_csv(r"C:\Users\Henrik\Desktop\Pythonplotting\Taste data.txt",
 ↪  sep='\t', header=None, encoding='utf-16')
values = data.values[0]  # Extract the single row of data

# Splitting data into experiment types
experiment_types = ['1 hour SGS', '30 min SGS', 'Control']
grouped_data = [values[i:i+4] for i in range(0, len(values), 4)]

# Defining labels for the bars
criteria = ['Appearance', 'Odour', 'Taste/Mouthfeel', 'Average']

bar_width = 0.2
positions = np.arange(len(criteria))

plt.figure(figsize=(15, 8))

for i, (experiment, scores) in enumerate(zip(experiment_types, grouped_data)):
    plt.bar(positions + i * bar_width, scores, width=bar_width, label=experiment)

plt.ylabel('Scores', fontsize=34)
plt.title('Taste Scores by Criteria', fontsize=34)
plt.xticks(positions + 1.5*bar_width, criteria, fontsize=34)
plt.yticks(fontsize=34)
plt.legend(fontsize=20, loc='lower right')
plt.tight_layout()
plt.grid(axis='y')
plt.show()
```

D Feedback SGS sensory experiment

Sample ID	1			2			3		
	Appearance	Odour	Taste/mouthfeel	Appearance	Odour	Taste/mouthfeel	Appearance	Odour	Taste/mouthfeel
1	10	5	8	7	5	7	8	4	9
2			3	10	10	8	6	10	3
3	7	8	6	7	7	6	7	7	6
4	3	3	3	6	5	8	8	6	7
5	8	7	5	10	8	8	10	8	5
6	7	8	6	9	9	9	8	7	6
Avg	7	6.2	5.166666667	8.16666667	7.333	7.666666667	7.83333333	7	6
Avg of avg	6.122222222			7.722222222			6.944444444		
Henrik	7	9	6	10	10	10	9	10	7

ID	Comments		
1	Light pink. White fat clearly visible. Looks wet, a sharp but suptle taste, almost acidic, but does not taste sour Mye fett ga muligens rart utseende ift de andre. Rar konsistens	Dark pink/orange, matt. Looks "dry". Stiff in texture, almost as it has been cooked. Identiskfarge. Antar denne er den ubehandlete	Pink, white stripes bearly visible. Looks damp not wt nor dry. More firm than 1, less firm than 2. God smak, saftig, men litt rar, oppsmuldret konsistens. Oppleves litt tørr ift sample 2. Identisk til de andre
2			
3	Normal. A bit less odour than the others maybe	Normal	Normal
4	Ville ikke valgt denne om jeg hadde hatt valget. Veldig matt. Veldig søt lukt. Mest fiskete smak av de 3. Var litt uttørket.	Matt	Minst matt. Litt syrlig
5	Pink/redish - less white stripes than the rest - other than that, looks normal. Acceptable, but funky/wiered after taste	Pink/redish, looks normal	Pink redish, looks normal
6	Not so good colour. More white than other. Tasted not so much	Good pink colour. Tasted more than the other samples	Not so pink as sample 2, but looked better than sample 1. Tasted not so much.

E Arduino code for the electronics

```
#include <Servo.h>

Servo ESC;     // create servo object to control the ESC

int potValue;  // value from the analog pin


#include "HX711.h"

#define calibration_factor 1702.19 //This value is obtained using the
↪   SparkFun_HX711_Calibration sketch

#define DOUT  2
#define CLK   3

HX711 scale;


void setup() {
  Serial.begin(9600);
  Serial.println("HX711 scale demo");
```

```
  scale.begin(DOUT, CLK);
  scale.set_scale(calibration_factor); //This value is obtained by using the
↪  SparkFun_HX711_Calibration sketch
  scale.tare(); //Assuming there is no weight on the scale at start up, reset the
↪  scale to 0

  Serial.println("Readings:");
  // Attach the ESC on pin 9
  ESC.attach(4,1000,2000); // (pin, min pulse width, max pulse width in
↪  microseconds)
}




void loop() {
  //Serial.print("Reading: ");
  Serial.print(scale.get_units(), 1); //scale.get_units() returns a float
  //Serial.print(" g"); //You can change this to kg but you'll need to refactor
↪  the calibration_factor
  Serial.println();
  potValue = analogRead(A0);    // reads the value of the potentiometer (value
↪  between 0 and 1023)
  //Serial.print(potValue);
  potValue = map(potValue, 0, 1023, 0, 180);   // scale it to use it with the
↪  servo library (value between 0 and 180)
  ESC.write(potValue);    // Send the signal to the ESC
}
```

F   Machined Flow chamber with 13 mm lid simulation

Simulation of Tank V4 ass

Date: mandag 17. april 2023
Designer: Solidworks
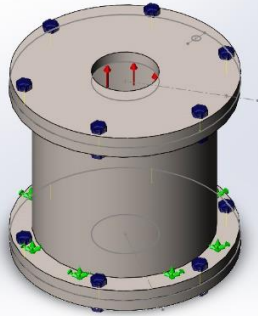**Study name:** Static 2
Analysis type: Static

Table of Contents

Description
No Data

Model Information
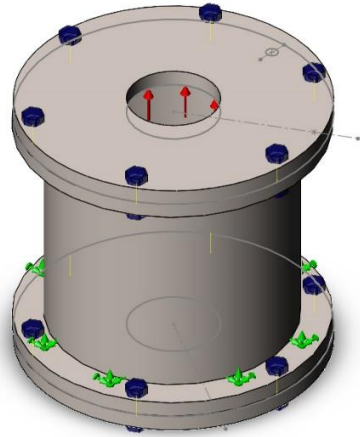
Model name: Tavn V4 ass
Current Configuration: Default

Solid Bodies

Document Name and Reference	Treated As	Volumetric Properties	Document Path/Date Modified
Boss-Extrude3	Solid Body	**Mass:4.80091 kg Volume:0.000598095 m^3 Density:8 027 kg/m^3 Weight:47.0489 N**	**C:\Users\Henrik\Desktop\ Masteroppgave\CAD\Solid works\Lid tank V3.SLDPRT** Apr 17 10:13:48 2023

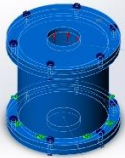|			
Boss-Extrude3	Solid Body	**Mass:4.80091 kg Volume:0.000598095 m^3 Density:8 027 kg/m^3 Weight:47.0489 N**	**C:\Users\Henrik\Desktop\ Masteroppgave\CAD\Solid works\Lid tank V3.SLDPRT** Apr 17 10:13:48 2023
Boss-Extrude3	Solid Body	**Mass:5.75399 kg Volume:0.00071683 m^3 Density:8 027 kg/m^3 Weight:56.3891 N**	**C:\Users\Henrik\Desktop\ Masteroppgave\CAD\Solid works\Tank V4.SLDPRT** Apr 17 10:14:11 2023

Study Properties

Study name	Static 2
Analysis type	Static
Mesh type	Solid Mesh
Thermal Effect:	On
Thermal option	Include temperature loads
Zero strain temperature	298 Kelvin
Include fluid pressure effects from SOLIDWORKS Flow Simulation	Off
Solver type	FFEPlus
Inplane Effect:	Off
Soft Spring:	Off
Inertial Relief:	Off
Incompatible bonding options	Automatic
Large displacement	Off
Compute free body forces	On
Friction	Off
Use Adaptive Method:	Off
Result folder	SOLIDWORKS document (C:\Users\Henrik\Desktop\Masteroppgave\CAD\Solidworks)

Units

Unit system:	SI (MKS)
Length/Displacement	mm
Temperature	Kelvin
Angular velocity	Rad/sec
Pressure/Stress	N/m^2
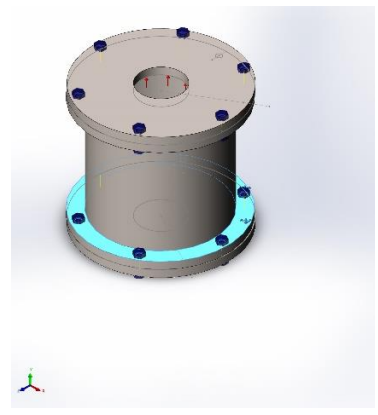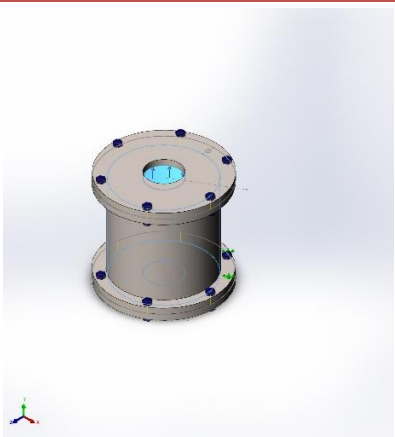
Material Properties

Model Reference	Properties	Components
	Name: AISI Type 316L stainless steel **Model type:** Linear Elastic Isotropic **Default failure criterion:** Max von Mises Stress **Yield strength:** 1.7e+08 N/m^2 **Tensile strength:** 4.85e+08 N/m^2 **Elastic modulus:** 2e+11 N/m^2 **Poisson's ratio:** 0.265 **Mass density:** 8 027 kg/m^3 **Shear modulus:** 8.2e+10 N/m^2 **Thermal expansion coefficient:** 1.65e-05 /Kelvin	SolidBody 1(Boss-Extrude3)(Lid tank V3-1), SolidBody 1(Boss-Extrude3)(Lid tank V3-2), SolidBody 1(Boss-Extrude3)(Tank V4-1)
Curve Data:N/A		

Loads and Fixtures
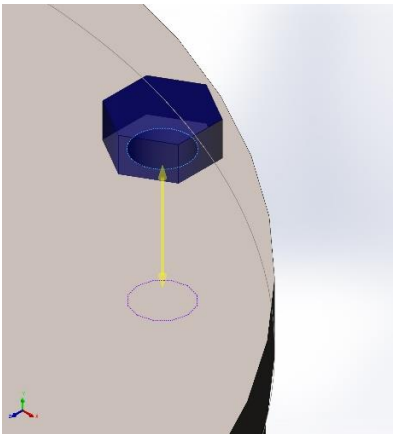
Fixture name	Fixture Image	Fixture Details
Fixed-1		**Entities:** 1 face(s) **Type:** Fixed Geometry

Resultant Forces

Components	X	Y	Z	Resultant
Reaction force(N)	-15.0125	-59 481.6	-9.13092	59 481.6
Reaction Moment(N.m)	0	0	0	0

Load name	Load Image	Load Details
Pressure-1		**Entities:** 3 face(s) **Type:** Normal to selected face **Value:** 1 **Units:** N/mm^2 (MPa) **Phase Angle:** 0 **Units:** deg
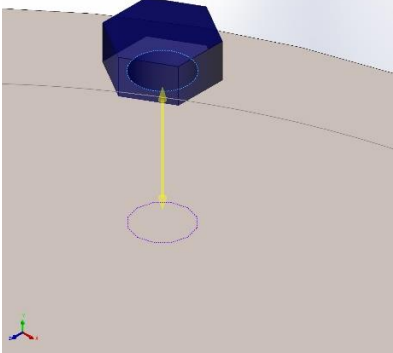
Connector Definitions

Pin/Bolt/Bearing Connector

Model Reference	Connector Details		Strength Details
 Counterbore with Nut-20	**Entities:** **Type:** **Connection Type:** **Head diameter:** **Nut diameter:** **Nominal shank diameter:** **Material name:** **Young's modulus:** **Poisson's ratio:** **Preload (Axial):** **Friction Factor (K):** **Tight Fit:**	2 edge(s) Bolt(Head/Nut diameter)(Counterbore) Distributed 15 mm 15 mm 10 mm Alloy Steel 2.1e+11 N/m^2 0.28 100 N 0.2 No	No Data

Connector Forces
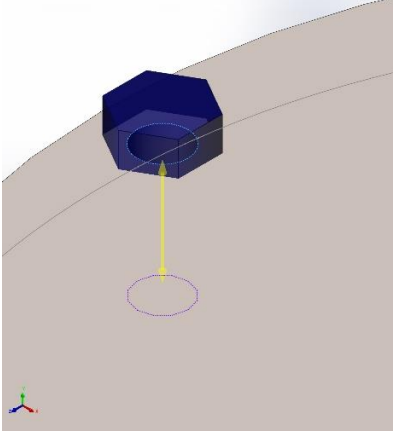
Type	X-Component	Y-Component	Z-Component	Resultant
Axial Force (N)	0	9 695.2	0	9 695.2
Shear Force (N)	-213.51	0	346.99	407.42
Bending moment (N.m)	-13.451	0	-8.5857	15.958

Model Reference	Connector Details		Strength Details
 Counterbore with Nut-21	**Entities:** **Type:** **Connection Type:** **Head diameter:** **Nut diameter:** **Nominal shank diameter:** **Material name:** **Young's modulus:** **Poisson's ratio:** **Preload (Axial):** **Friction Factor (K):** **Tight Fit:**	2 edge(s) Bolt(Head/Nut diameter)(Counterbore) Distributed 15 mm 15 mm 10 mm Alloy Steel 2.1e+11 N/m^2 0.28 100 N 0.2 No	No Data
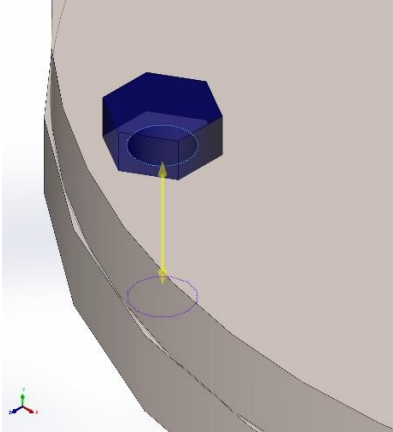
Connector Forces

Type	X-Component	Y-Component	Z-Component	Resultant
Axial Force (N)	0	9 506.9	0	9 506.9
Shear Force (N)	191.42	0	401.98	445.23
Bending moment (N.m)	-13.098	0	7.1988	14.946
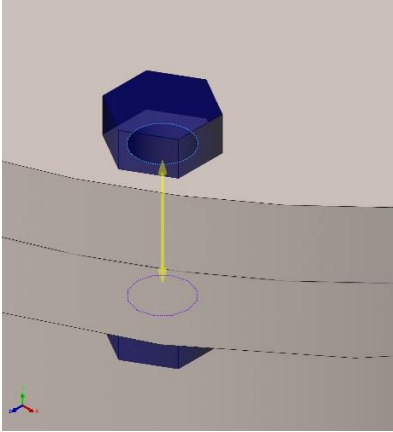
	Entities:	2 edge(s)	
	Type:	Bolt(Head/Nut diameter)(Counterbore)	No Data
	Connection Type:	Distributed	
	Head diameter:	15 mm	
	Nut diameter:	15 mm	
	Nominal shank diameter:	10 mm	
	Material name:	Alloy Steel	
	Young's modulus:	2.1e+11 N/m^2	
	Poisson's ratio:	0.28	
	Preload (Axial):	100 N	
	Friction Factor (K):	0.2	
Counterbore with Nut-22	Tight Fit:	No	

Connector Forces

Type	X-Component	Y-Component	Z-Component	Resultant
Axial Force (N)	0	9 158.9	0	9 158.9
Shear Force (N)	471.22	0	18.425	471.58
Bending moment (N.m)	-0.17197	0	14.652	14.653
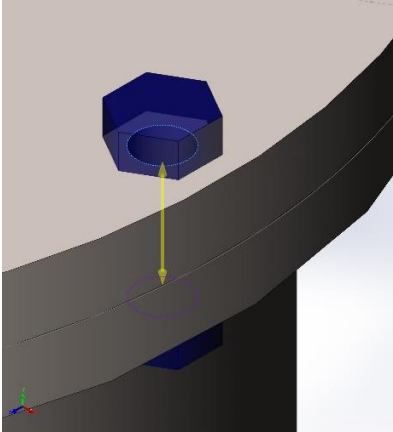
	Entities:	2 edge(s)	
	Type:	Bolt(Head/Nut diameter)(Counterbore)	No Data
	Connection Type:	Distributed	
	Head diameter:	15 mm	
	Nut diameter:	15 mm	
	Nominal shank diameter:	10 mm	
	Material name:	Alloy Steel	
	Young's modulus:	2.1e+11 N/m^2	
	Poisson's ratio:	0.28	
	Preload (Axial):	100 N	
	Friction Factor (K):	0.2	
Counterbore with Nut-23	Tight Fit:	No	

Connector Forces

Type	X-Component	Y-Component	Z-Component	Resultant
Axial Force (N)	0	9 284.1	0	9 284.1
Shear Force (N)	221.31	0	-416.48	471.62
Bending moment (N.m)	12.866	0	7.1313	14.71
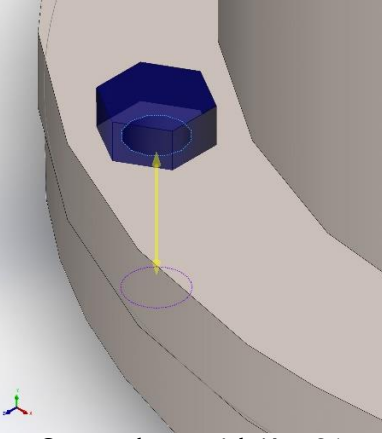
Counterbore with Nut-24

Entities:	2 edge(s)	
Type:	Bolt(Head/Nut diameter)(Counterbore)	No Data
Connection Type:	Distributed	
Head diameter:	15 mm	
Nut diameter:	15 mm	
Nominal shank diameter:	10 mm	
Material name:	Alloy Steel	
Young's modulus:	2.1e+11 N/m^2	
Poisson's ratio:	0.28	
Preload (Axial):	100 N	
Friction Factor (K):	0.2	
Tight Fit:	No	

Connector Forces

Type	X-Component	Y-Component	Z-Component	Resultant
Axial Force (N)	0	9 571	0	9 571
Shear Force (N)	-252.49	0	-366.75	445.25
Bending moment (N.m)	12.732	0	-7.9215	14.995
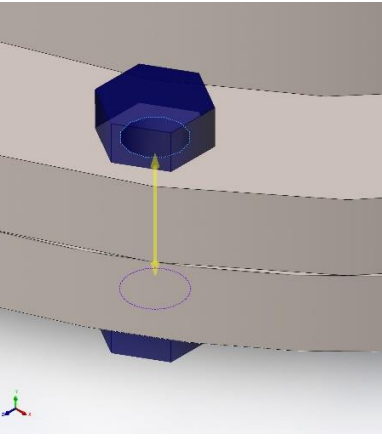
Counterbore with Nut-25

Entities:	2 edge(s)	
Type:	Bolt(Head/Nut diameter)(Counterbore)	No Data
Connection Type:	Distributed	
Head diameter:	15 mm	
Nut diameter:	15 mm	
Nominal shank diameter:	10 mm	
Material name:	Alloy Steel	
Young's modulus:	2.1e+11 N/m^2	
Poisson's ratio:	0.28	
Preload (Axial):	100 N	
Friction Factor (K):	0.2	
Tight Fit:	No	

Connector Forces

Type	X-Component	Y-Component	Z-Component	Resultant
Axial Force (N)	0	9 886.7	0	9 886.7
Shear Force (N)	-402.93	0	24.95	403.7
Bending moment (N.m)	-0.14453	0	-15.794	15.795

Counterbore with Nut-26

Entities:	2 edge(s)
Type:	Bolt(Head/Nut diameter)(Counterbore)
Connection Type:	Distributed
Head diameter:	15 mm
Nut diameter:	15 mm
Nominal shank diameter:	10 mm
Material name:	Alloy Steel
Young's modulus:	2.1e+11 N/m^2
Poisson's ratio:	0.28
Preload (Axial):	100 N
Friction Factor (K):	0.2
Tight Fit:	No

No Data

Connector Forces

Type	X-Component	Y-Component	Z-Component	Resultant
Axial Force (N)	0	8 085.5	0	8 085.5
Shear Force (N)	-268.74	0	460.26	532.98
Bending moment (N.m)	0.75836	0	0.45628	0.88504

Counterbore with Nut-27

Entities:	2 edge(s)
Type:	Bolt(Head/Nut diameter)(Counterbore)
Connection Type:	Distributed
Head diameter:	15 mm
Nut diameter:	15 mm
Nominal shank diameter:	10 mm
Material name:	Alloy Steel
Young's modulus:	2.1e+11 N/m^2
Poisson's ratio:	0.28
Preload (Axial):	100 N
Friction Factor (K):	0.2
Tight Fit:	No

No Data

Connector Forces

Type	X-Component	Y-Component	Z-Component	Resultant
Axial Force (N)	0	8 774.8	0	8 774.8
Shear Force (N)	262.36	0	452.64	523.18
Bending moment (N.m)	0.66191	0	-0.43392	0.79146
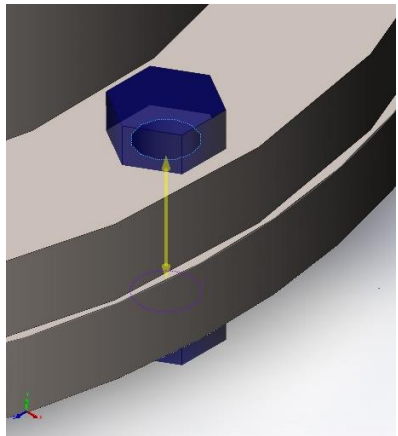
Counterbore with Nut-28

Entities:	2 edge(s)	
Type:	Bolt(Head/Nut diameter)(Counterbore)	
Connection Type:	Distributed	
Head diameter:	15 mm	
Nut diameter:	15 mm	
Nominal shank diameter:	10 mm	
Material name:	Alloy Steel	No Data
Young's modulus:	2.1e+11 N/m^2	
Poisson's ratio:	0.28	
Preload (Axial):	100 N	
Friction Factor (K):	0.2	
Tight Fit:	No	

Connector Forces

Type	X-Component	Y-Component	Z-Component	Resultant
Axial Force (N)	0	8 693.1	0	8 693.1
Shear Force (N)	523.71	0	0.2951	523.71
Bending moment (N.m)	-0.064048	0	-0.9533	0.95545

Counterbore with Nut-29

Entities:	2 edge(s)	
Type:	Bolt(Head/Nut diameter)(Counterbore)	
Connection Type:	Distributed	
Head diameter:	15 mm	
Nut diameter:	15 mm	
Nominal shank diameter:	10 mm	
Material name:	Alloy Steel	No Data
Young's modulus:	2.1e+11 N/m^2	
Poisson's ratio:	0.28	
Preload (Axial):	100 N	
Friction Factor (K):	0.2	
Tight Fit:	No	

Connector Forces

Type	X-Component	Y-Component	Z-Component	Resultant
Axial Force (N)	0	9 396.3	0	9 396.3
Shear Force (N)	265.73	0	-464.4	535.05
Bending moment (N.m)	-0.81647	0	-0.48741	0.95089

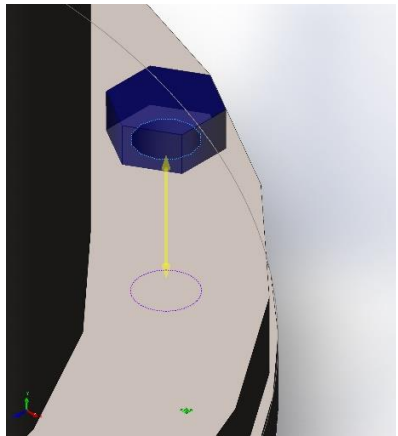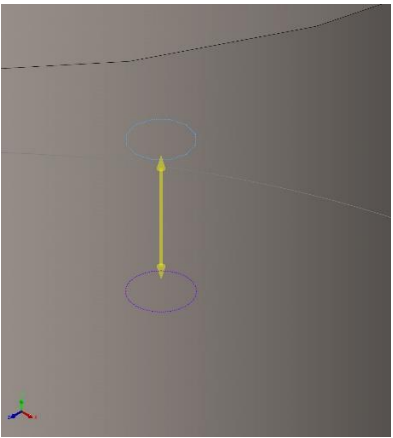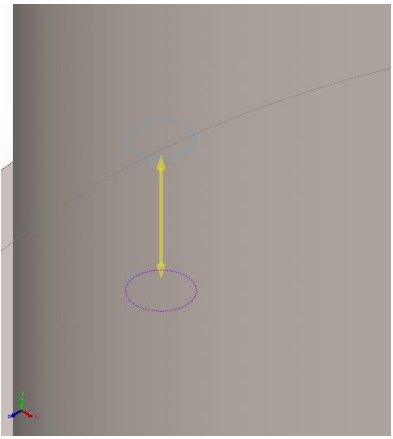|		
Counterbore with Nut-30	Entities: 2 edge(s) Type: Bolt(Head/Nut diameter)(Counterbore) Connection Type: Distributed Head diameter: 15 mm Nut diameter: 15 mm Nominal shank diameter: 10 mm Material name: Alloy Steel Young's modulus: 2.1e+11 N/m^2 Poisson's ratio: 0.28 Preload (Axial): 100 N Friction Factor (K): 0.2 Tight Fit: No	No Data

Connector Forces

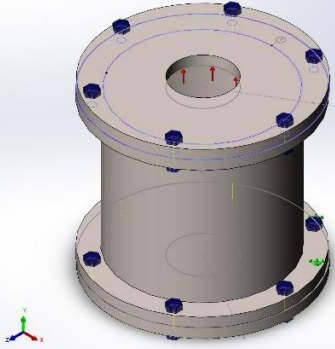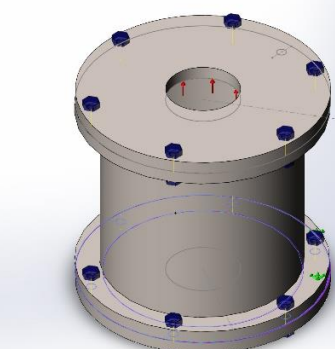| Type	X-Component	Y-Component	Z-Component	Resultant
Axial Force (N)	0	8 858.4	0	8 858.4
Shear Force (N)	-271.42	0	-436.8	514.26
Bending moment (N.m)	-0.90511	0	0.33408	0.9648

Counterbore with Nut-31	Entities: 2 edge(s) Type: Bolt(Head/Nut diameter)(Counterbore) Connection Type: Distributed Head diameter: 15 mm Nut diameter: 15 mm Nominal shank diameter: 10 mm Material name: Alloy Steel Young's modulus: 2.1e+11 N/m^2 Poisson's ratio: 0.28 Preload (Axial): 100 N Friction Factor (K): 0.2 Tight Fit: No	No Data

Connector Forces

Type	X-Component	Y-Component	Z-Component	Resultant
Axial Force (N)	0	8 321.9	0	8 321.9
Shear Force (N)	-525.93	0	-2.6698	525.93
Bending moment (N.m)	-0.16672	0	0.96243	0.97677

Contact Information

Contact	Contact Image	Contact Properties
Contact Set-3		**Type:** No Penetration contact pair **Entities:** 2 face(s) **Advanced:** Node to surface

Contact/Friction force

Components	X	Y	Z	Resultant
Contact Force(N)	0	2.4194E-11	0	2.4194E-11

Contact	Contact Image	Contact Properties
Contact Set-4		**Type:** No Penetration contact pair **Entities:** 2 face(s) **Advanced:** Node to surface

Contact/Friction force

Components	X	Y	Z	Resultant
Contact Force(N)	0	1.7735E-11	0	1.7735E-11

Mesh information

| Mesh type	Solid Mesh
Mesher Used:	Standard mesh
Automatic Transition:	Off
Include Mesh Auto Loops:	Off
Jacobian points for High quality mesh	16 Points
Element Size	7.99636 mm
Tolerance	0.399818 mm
Mesh Quality	High
Remesh failed parts with incompatible mesh	Off

Mesh information - Details

Total Nodes	71796
Total Elements	39203
Maximum Aspect Ratio	12.484
% of elements with Aspect Ratio < 3	74.6
Percentage of elements with Aspect Ratio > 10	0.00765
Percentage of distorted elements	0
Time to complete mesh(hh;mm;ss):	00:00:07
Computer name:	HENRIKSSURFACE

Model name: Tavn V4 ass
Study name: Static 2(-Default-)
Mesh type: Solid Mesh
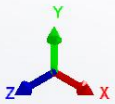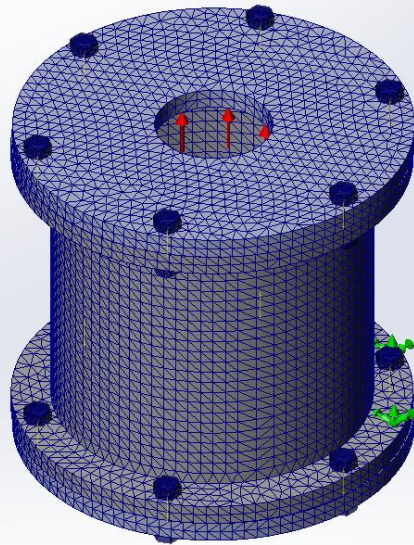
Sensor Details

No Data

Resultant Forces

Reaction forces

Selection set	Units	Sum X	Sum Y	Sum Z	Resultant
Entire Model	N	-15.0125	-59 481.6	-9.13092	59 481.6

Reaction Moments

Selection set	Units	Sum X	Sum Y	Sum Z	Resultant
Entire Model	N.m	0	0	0	0

Free body forces

Selection set	Units	Sum X	Sum Y	Sum Z	Resultant
Entire Model	N	-0.189856	-0.00778174	0.136099	0.233728

Free body moments

Selection set	Units	Sum X	Sum Y	Sum Z	Resultant
Entire Model	N.m	0	0	0	1e-33

Beams

No Data

Study Results

Name	Type	Min	Max
Stress1	VON: von Mises Stress	1.090e+05N/m^2 Node: 48051	1.813e+08N/m^2 Node: 67232

Model name: Tavn V4 ass
Study name: Static 2(-Default-)
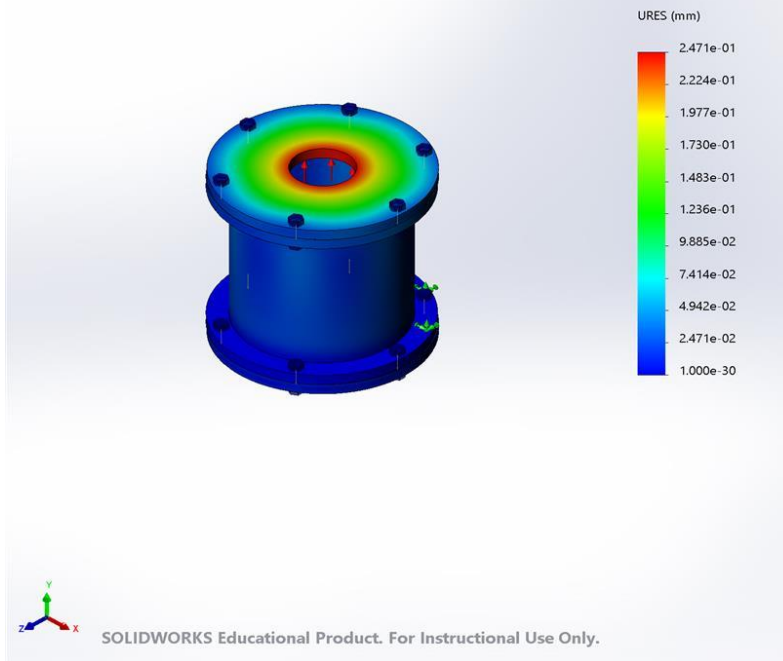Plot type: Static nodal stress Stress1

von Mises (N/m^2)

1.813e+08
1.631e+08
1.450e+08
1.269e+08
1.088e+08
9.068e+07
7.257e+07
5.445e+07
3.634e+07
1.822e+07
1.090e+05

Yield strength: 1.700e+08

SOLIDWORKS Educational Product. For Instructional Use Only.
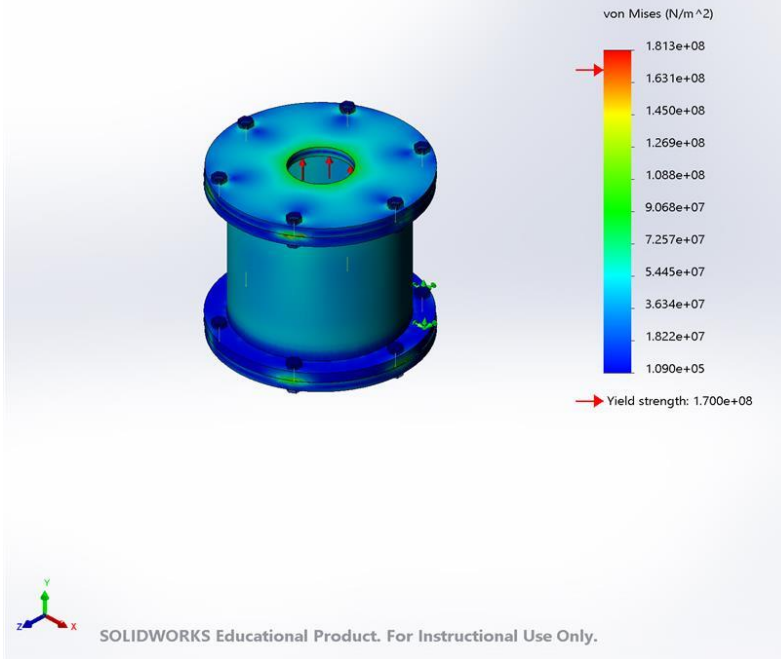
Tavn V4 ass-Static 2-Stress-Stress1

Name	Type	Min	Max
Displacement1	URES: Resultant Displacement	0.000e+00mm Node: 33853	2.471e-01mm Node: 17138

Tavn V4 ass-Static 2-Displacement-Displacement1

Name	Type	Min	Max
Strain1	ESTRN: Equivalent Strain	3.787e-07 Element: 35392	4.698e-04 Element: 12459

Model name: Tavn V4 ass
Study name: Static 2(-Default-)
Plot type: Static strain Strain1
Deformation scale: 1

ESTRN

4.698e-04
4.228e-04
3.759e-04
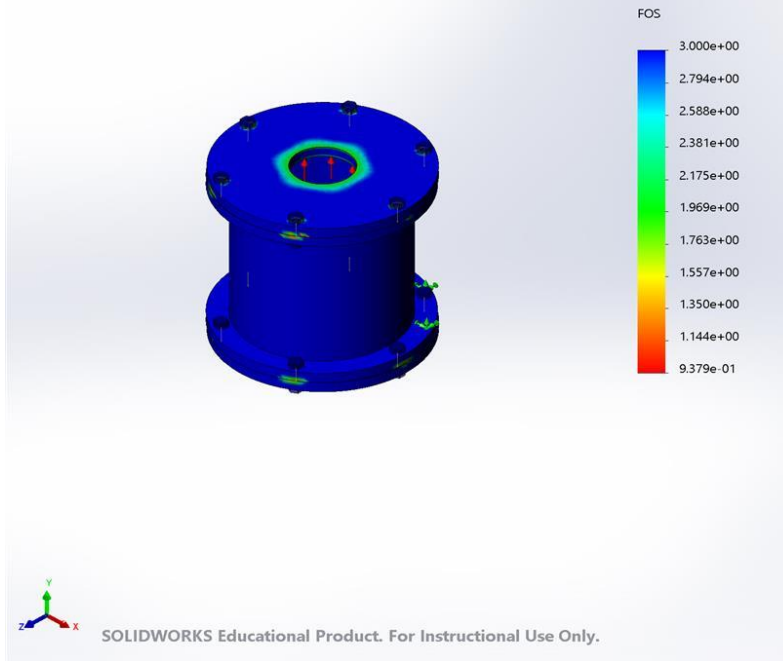3.290e-04
2.820e-04
2.351e-04
1.881e-04
1.412e-04
9.426e-05
4.732e-05
3.787e-07

SOLIDWORKS Educational Product. For Instructional Use Only.
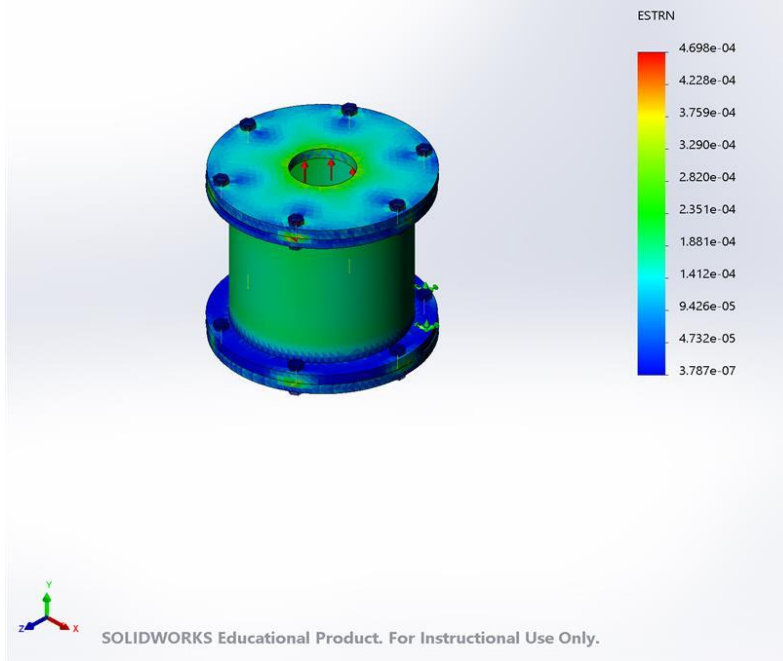
Tavn V4 ass-Static 2-Strain-Strain1

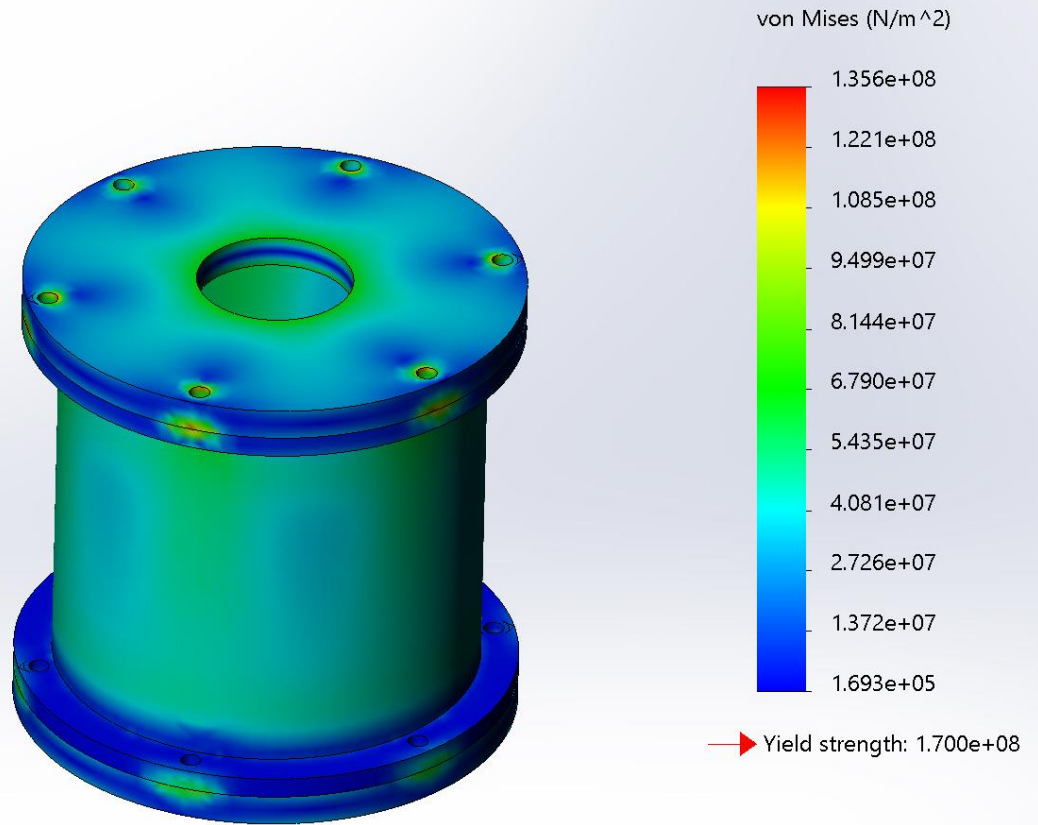| Name	Type	Min	Max
Factor of Safety1	Automatic	9.379e-01 Node: 67232	3.000e+00 Node: 5

Model name: Tavn V4 ass
Study name: Static 2(-Default-)
Plot type: Factor of Safety Factor of Safety1
Criterion : Automatic
Factor of safety distribution: Min FOS = 0.94

FOS

3.000e+00
2.794e+00
2.588e+00
2.381e+00
2.175e+00
1.969e+00
1.763e+00
1.557e+00
1.350e+00
1.144e+00
9.379e-01

Tavn V4 ass-Static 2-Factor of Safety-Factor of Safety1

Model name: Tavn V4 ass
Study name: Static 2(-Default-)
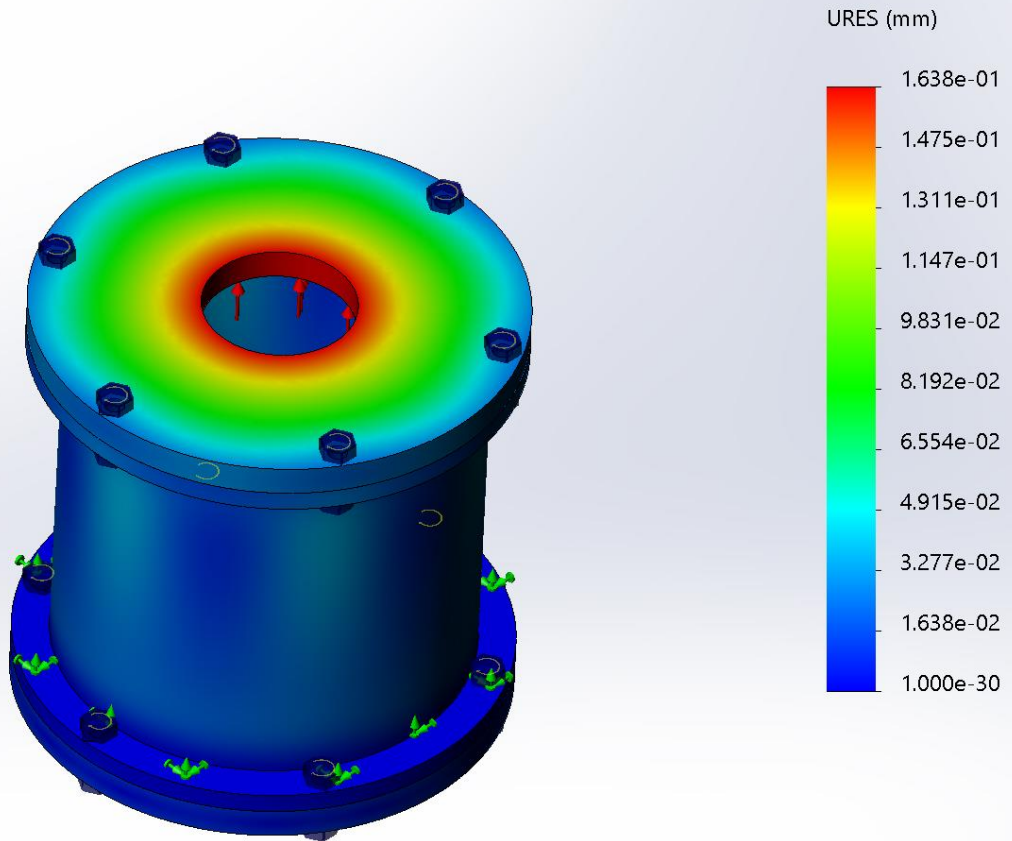Plot type: Static nodal stress Stress1

von Mises (N/m^2)

1.356e+08
1.221e+08
1.085e+08
9.499e+07
8.144e+07
6.790e+07
5.435e+07
4.081e+07
2.726e+07
1.372e+07
1.693e+05

→ Yield strength: 1.700e+08

Image-1

Model name: Tavn V4 ass
Study name: Static 2(-Default-)
Plot type: Static displacement Displacement1
Deformation scale: 1

URES (mm)

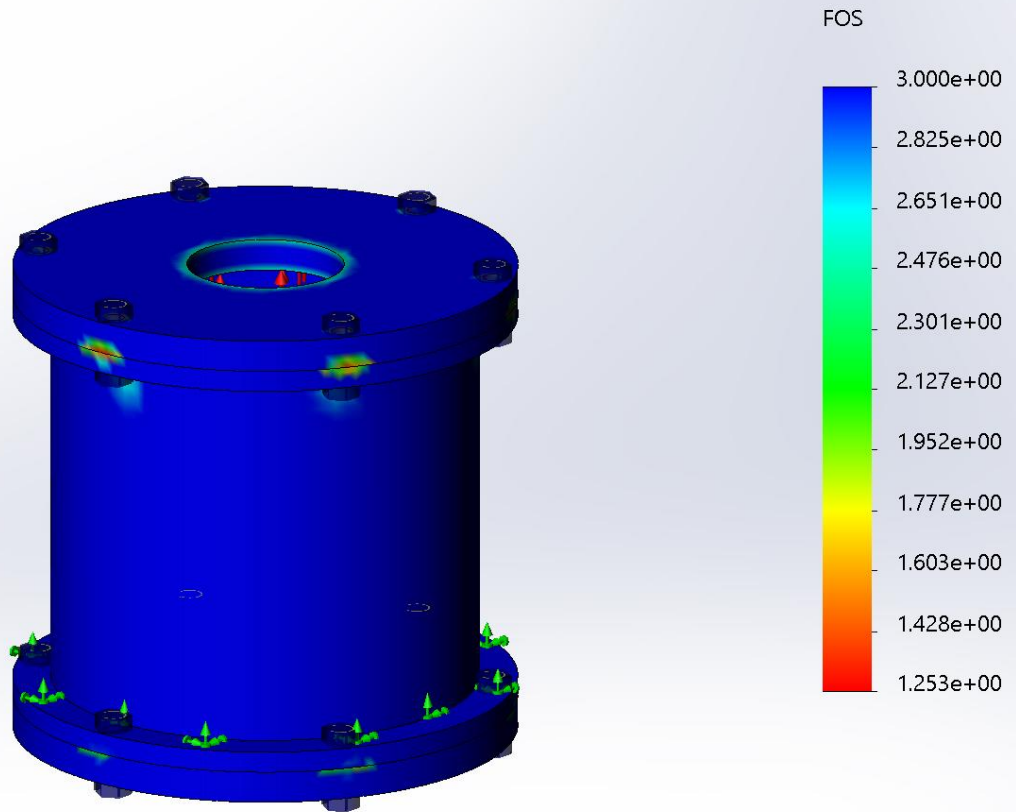1.638e-01
1.475e-01
1.311e-01
1.147e-01
9.831e-02
8.192e-02
6.554e-02
4.915e-02
3.277e-02
1.638e-02
1.000e-30

Image-2

Model name: Tavn V4 ass
Study name: Static 2(-Default-)
Plot type: Factor of Safety Factor of Safety1
Criterion : Automatic
Factor of safety distribution: Min FOS = 1.3

FOS

3.000e+00
2.825e+00
2.651e+00
2.476e+00
2.301e+00
2.127e+00
1.952e+00
1.777e+00
1.603e+00
1.428e+00
1.253e+00

Image-3

Conclusion